Single molecule force spectroscopy

AFM: lab on a tip

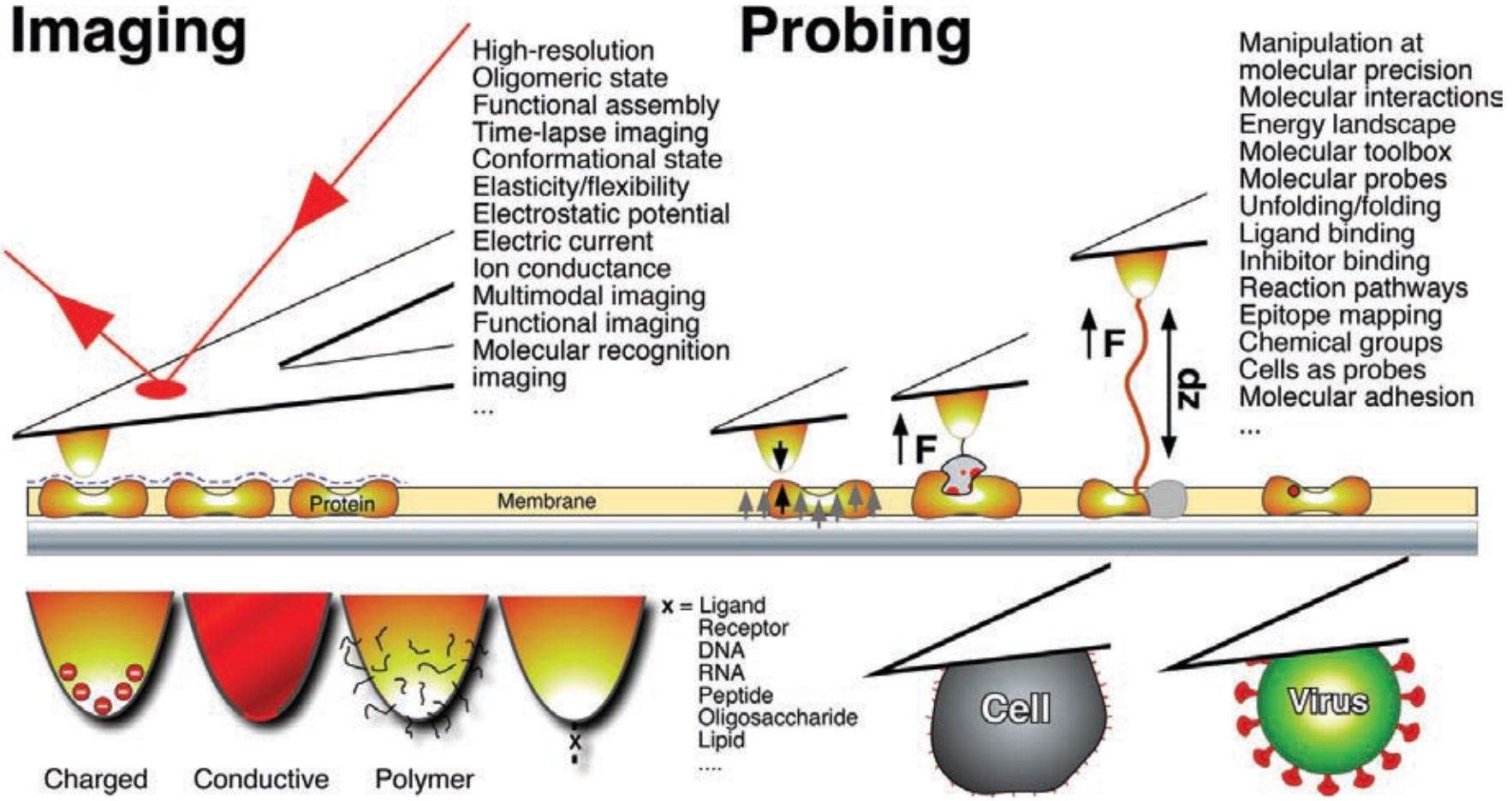

S. Scheuring, D. Muller, H. Stalhberg, H.-A. Engel, A. Engel, *Eur. Biophys. J.* **31**, 172 (2002)

Single molecule manipulation

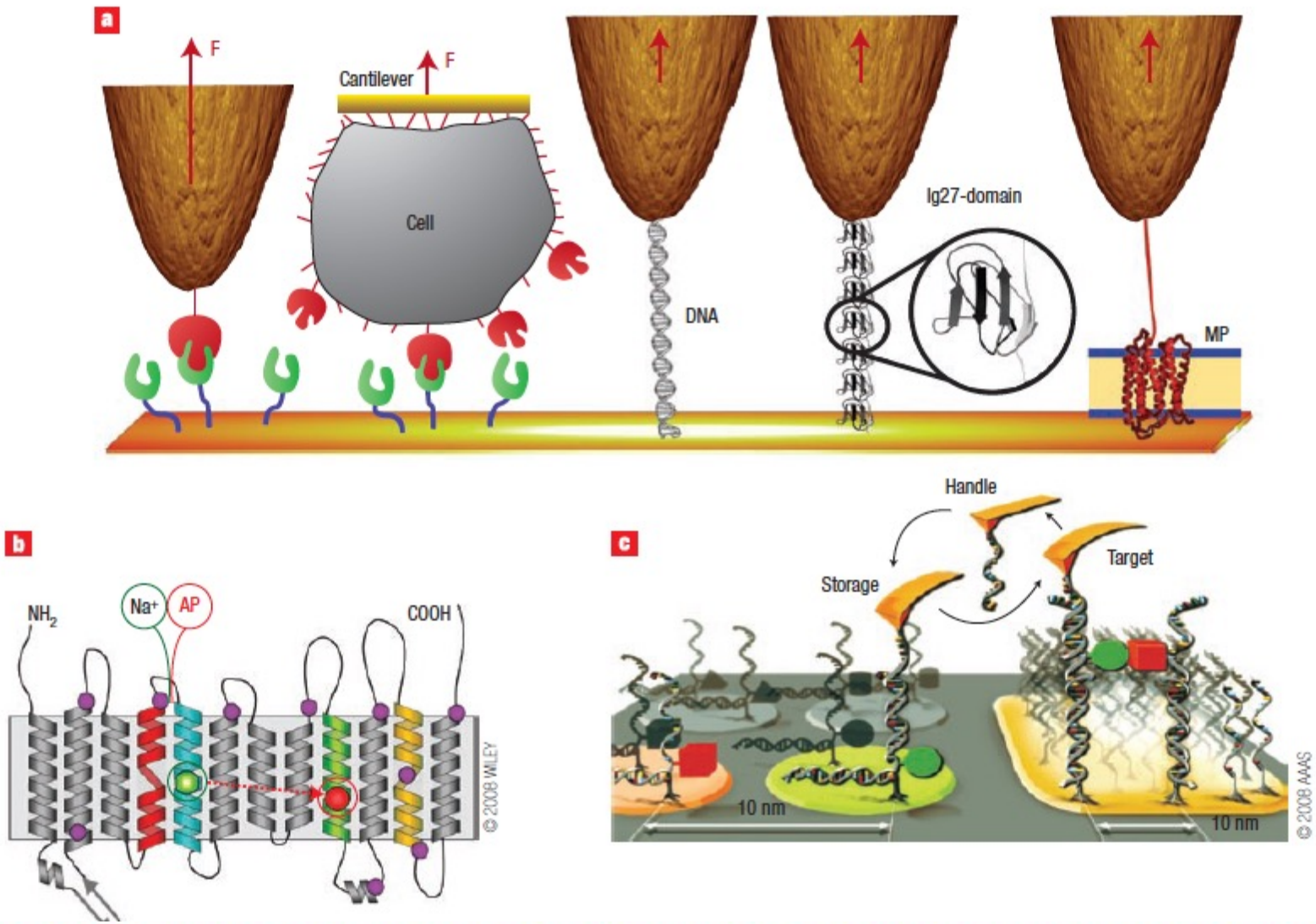

Figure 3 Single molecule manipulation, control and design. **a**, Applying AFM to probe interaction forces (F) of single biomolecules. These examples measure ligand–receptor interactions in their isolated form (left) and embedded in their cellular environment (probe replaced by a biological cell); stretching of a DNA molecule; unfolding of Ig27-titin; and unfolding of a membrane protein (MP). **b**, SMFS can detect and locate interactions (circles) on the structure of membrane proteins (here proton/sodium antiporter NhaA from *E. coli*). A ligand (Na^+ ion) or inhibitor (AP, 2-aminoperimidine) binding to the ligand-binding site (green circle) establishes different interactions activating (green circle) or deactivating (green and red circles) the antiporter (composed of 12 transmembrane helices). **c**, Single molecules can be mechanically assembled by picking up from discrete storage sites with a DNA oligomer at the AFM probe and depositing them at a target site with nanoscopic precision. Reproduced with permission from refs 52, 53 and 63.

Single molecule force spectroscopy

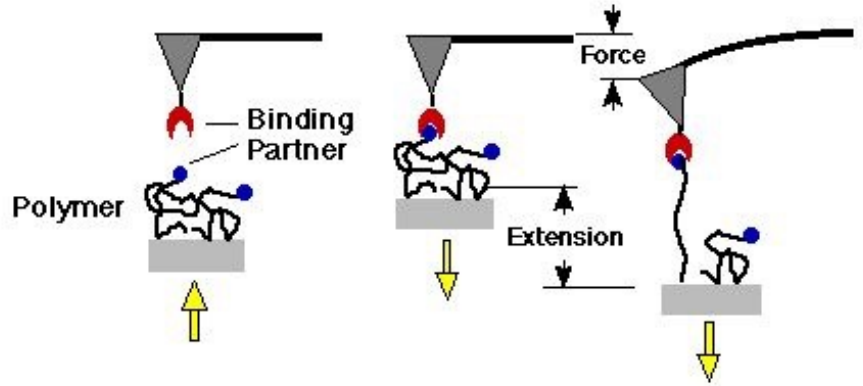

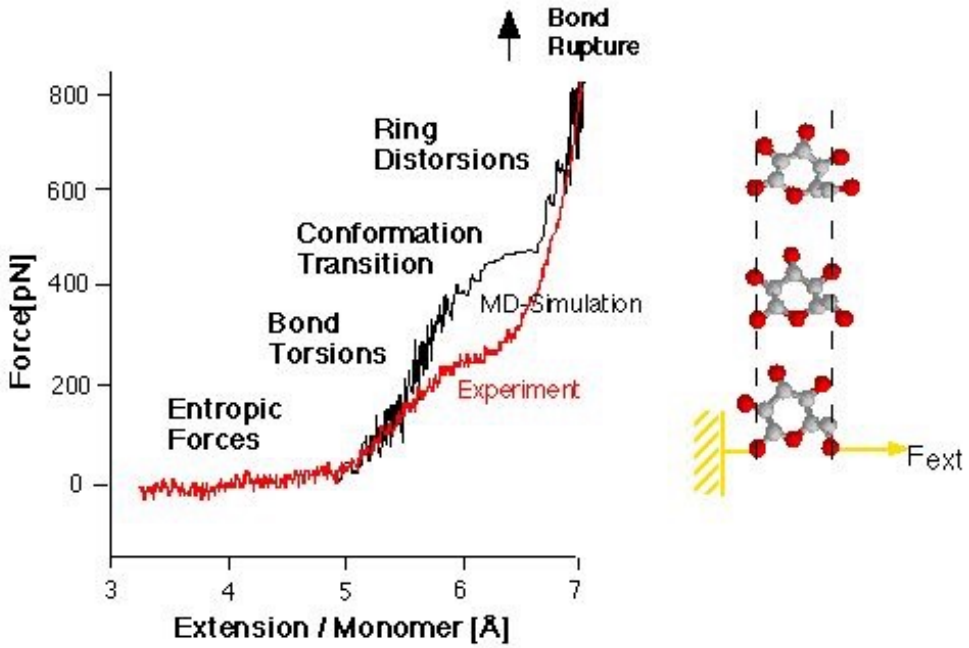

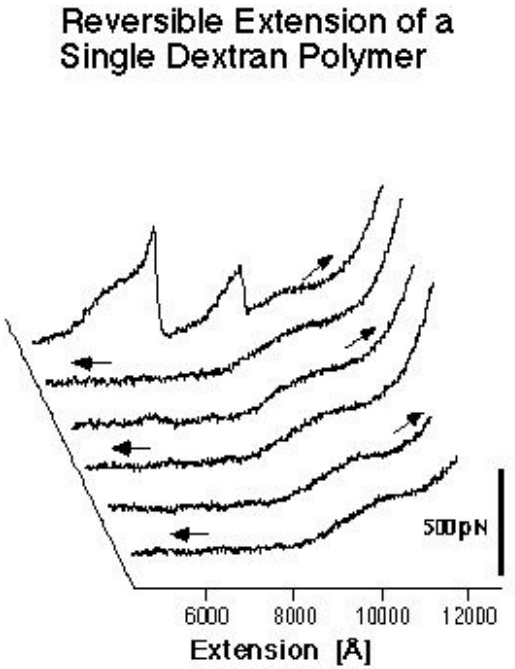

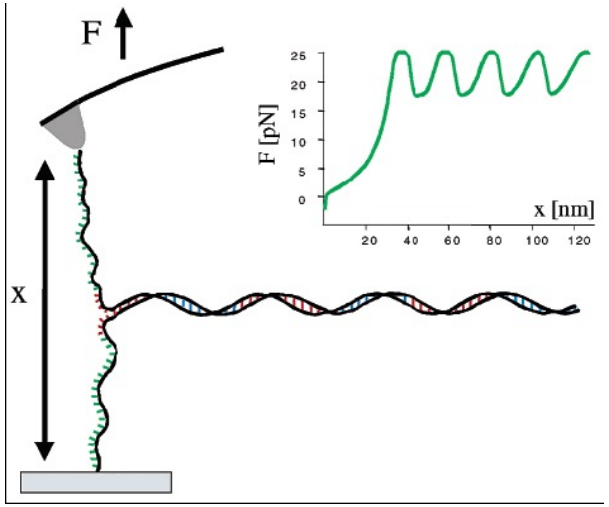

Single molecule manipulation

Single-molecule techniques analyze individual members in complex, heterogeneous populations, enabling to reveal the diversity of hidden molecular behaviors and rare events.

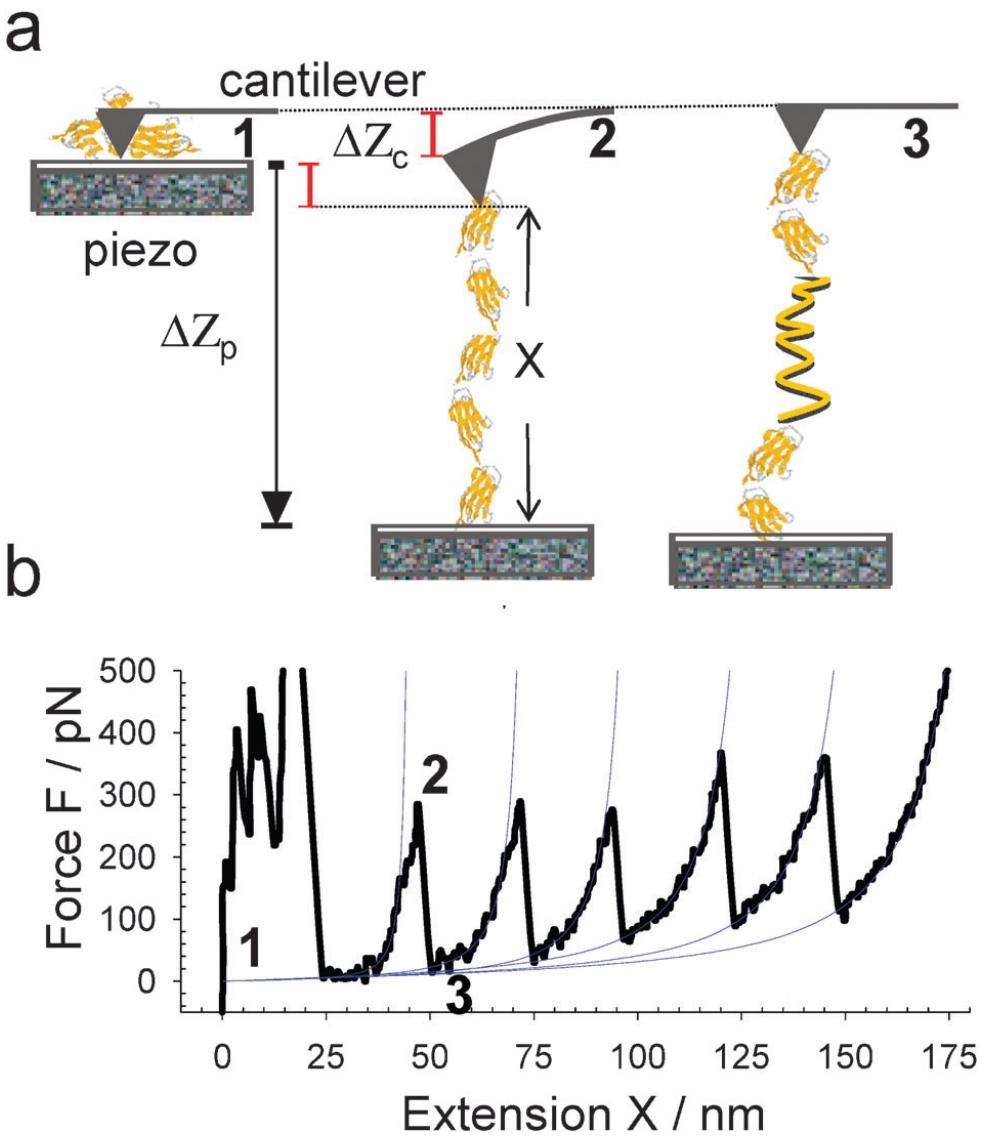

Single-molecule assays permit the direct measurement of the molecular elasticity of polysaccharides, proteins or nucleic acids, otherwise impossible, and the acceleration of certain molecular reactions, such as protein unfolding or ligand–receptor bond rupture.

$$X = \Delta Z_P - \Delta Z_c$$
$$F = k_c \Delta Z_c$$

P.E. Marszalek, Y. F. Dufrene
Chem. Soc. Rev., 2012, 41, 3523–3534

Single molecule manipulation

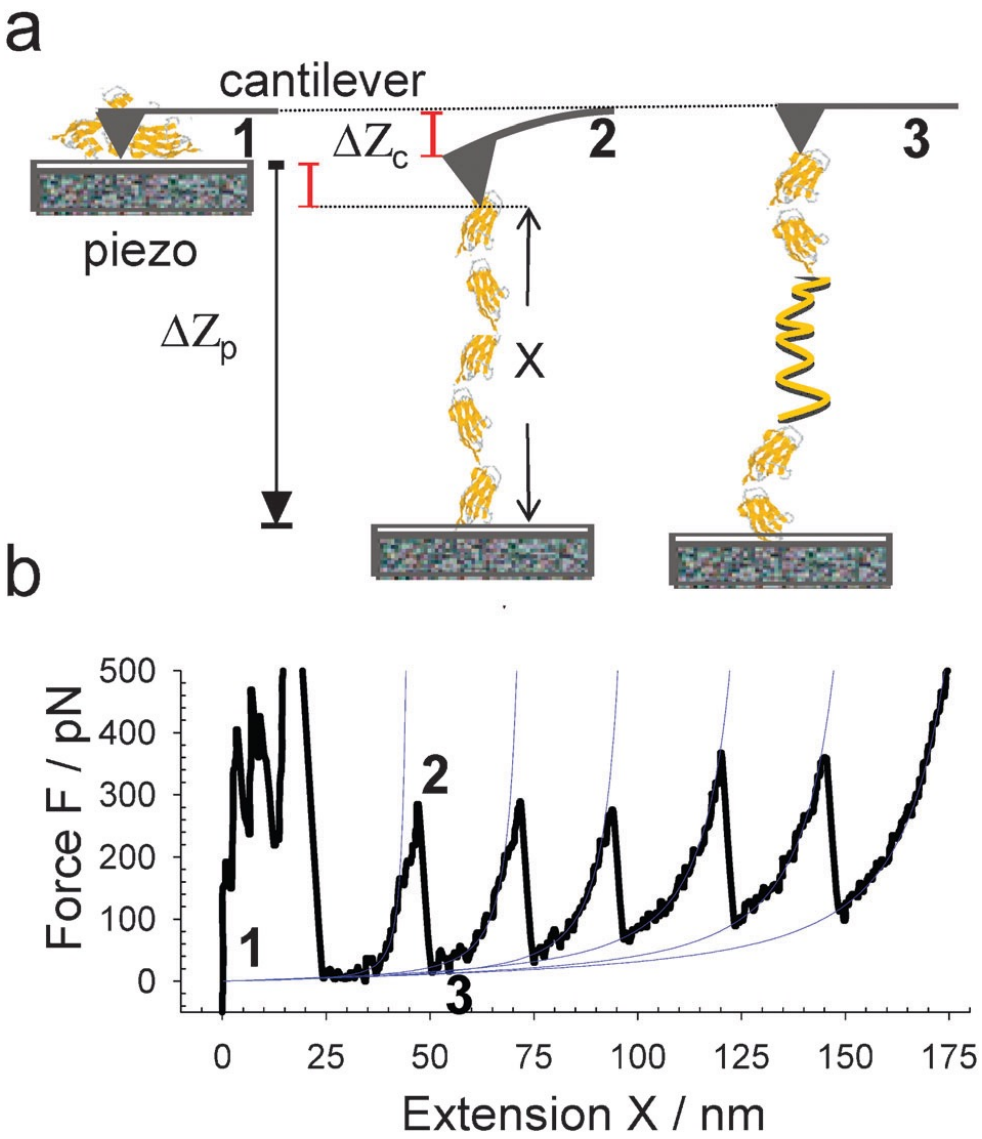

The resolution of force measurements depends on the dimensions of the AFM cantilever (the smaller the better) and on the range of measured frequencies

using small cantilevers in the measurement bandwidth of 1 kHz, the force noise that limits the resolution can be as small as 3–5 pN (resolution can be improved to below 1 pN)

$$X = \Delta Z_P - \Delta Z_c$$
$$F = k_c \Delta Z_c$$

Single molecule manipulation

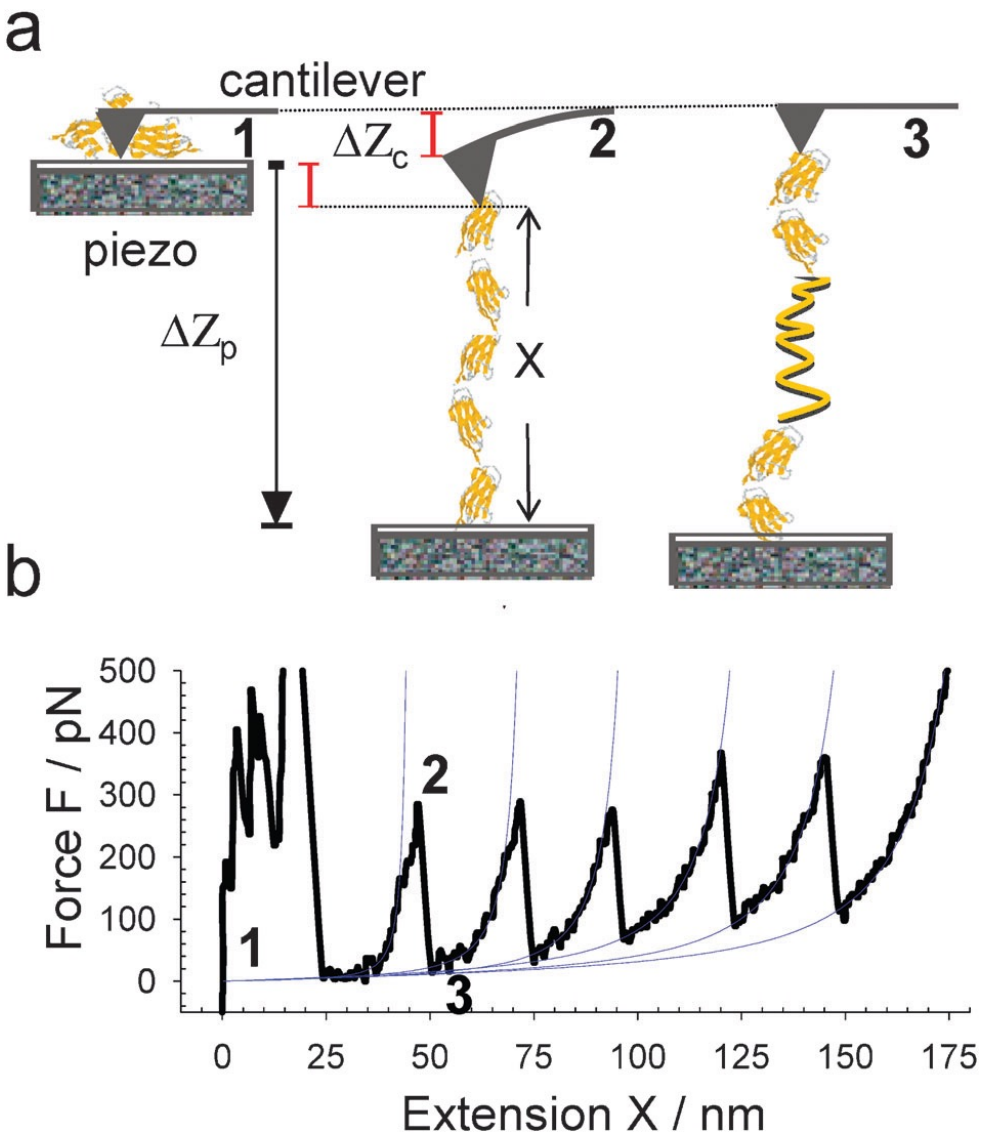

Mechanical proteins are frequently composed of either individually folded globular domains that are connected to each other by short flexible linkers (e.g. titin in muscle) or tightly stacked short helical segments that form elongated single-domain structures (e.g. ankyrin in the RBC skeleton),or longer helical domains that form coiled-coils structures (e.g. spectrin in the RBC skeleton, or myosin in muscle).

P.E. Marszalek, Y. F. Dufrene
Chem. Soc. Rev., 2012, 41, 3523–3534

Single molecule manipulation

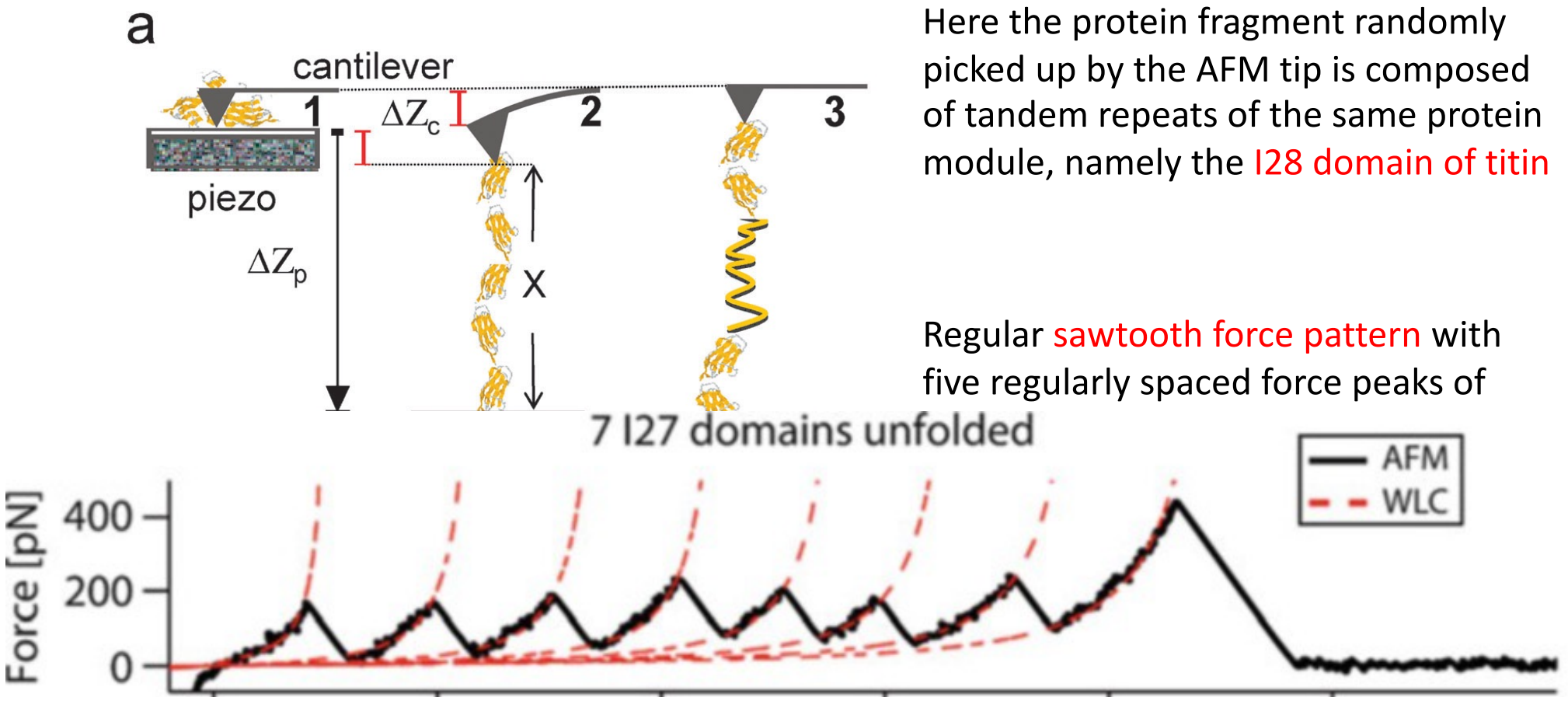

Here the protein fragment randomly picked up by the AFM tip is composed of tandem repeats of the same protein module, namely the I28 domain of titin

Regular sawtooth force pattern with five regularly spaced force peaks of

Fig. 33.5 Typical force–extension plot of the unfolding of a polyprotein consisting of seven I27 domains from the titin protein (also called I91 domains). Each peak corresponds to an unfolding event of a single domain. The unfolding force for each domain is ~200 pN. The dashed red line indicates a family of worm-like chain fits with a contour length spacing of 28.5 nm between unfolding events

Protein force spectroscopy

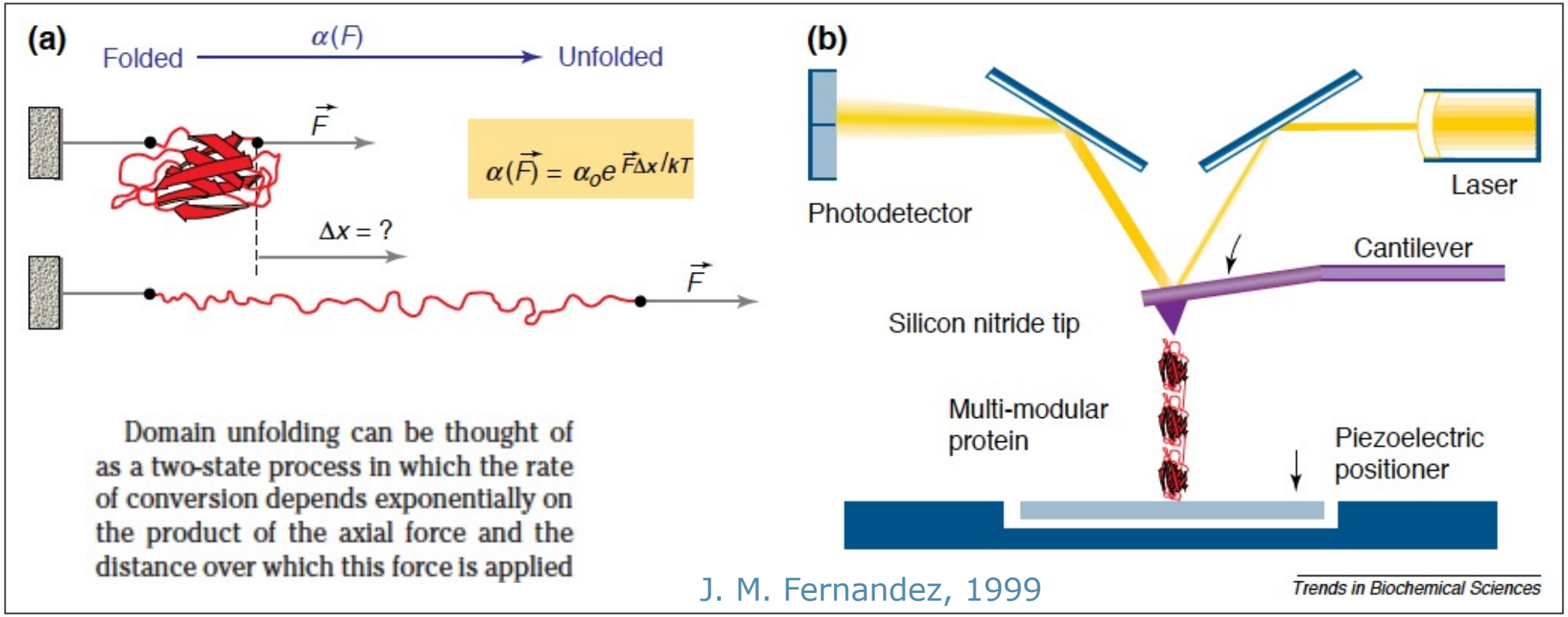

The unfolding of protein domains by an external force. **(a)** When axial stress is applied to a folded domain the protein will unravel. The inset shows an equation describing this transition, where F is the applied force, Δx is the distance over which the unfolding event occurs, α_0 is the rate constant in the absence of an applied force, k is Boltzmann's constant and T is the absolute temperature. Thus, the rate at which protein unfolding occurs increases exponentially with the applied force. This equation is similar to that describing the dissociation of non-covalent bonds placed under an external force[38,39]. **(b)** The force–extension mode of the atomic force microscope (AFM). When pressed against a layer of protein attached to a substrate, the silicon nitride tip can adsorb a single protein molecule. Extension of a molecule by retraction of the piezoelectric positioner results in deflection of the AFM cantilever. This deflection changes the angle of reflection of a laser beam striking the cantilever, which is measured as the change in output from a photodetector.

Polyprotein force spectroscopy

At small displacements, reduction in the number of conformations gives rise to entropic elasticity forces
At large extensions, tension in the molecular backbone may lead to enthalpic elasticity effects (bond deformation, rupture of intramolecular hydrogen bonds and even conformational changes of the entire molecule)

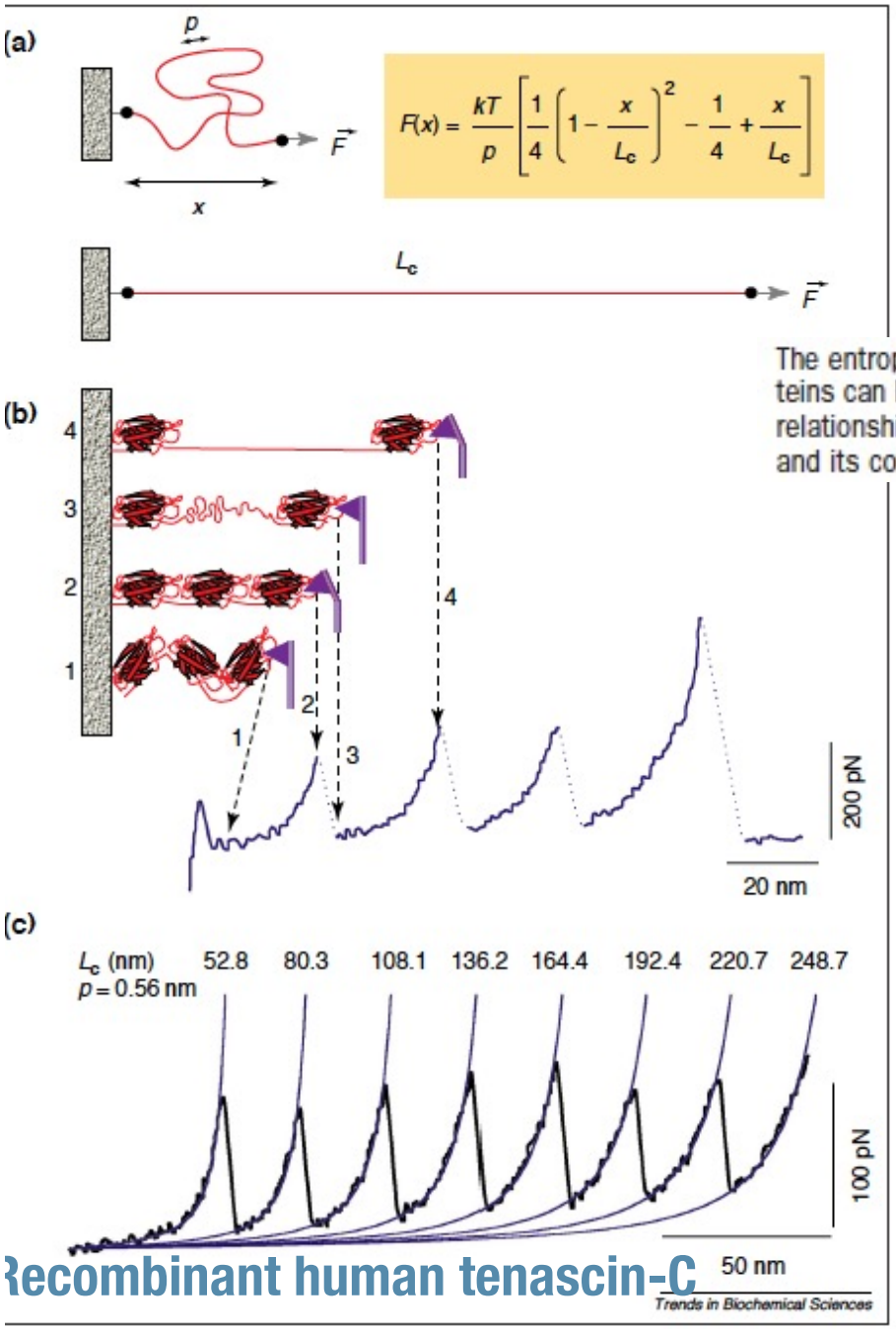

The entropic elasticity of proteins and domain unfolding. **(a)** The entropic elasticity of proteins can be described by the WLC (worm-like chain) equation (inset), which expresses the relationship between force (F) and extension (x) of a protein using its persistence length (p) and its contour length (L_c). k is Boltzmann's constant and T is the absolute temperature.

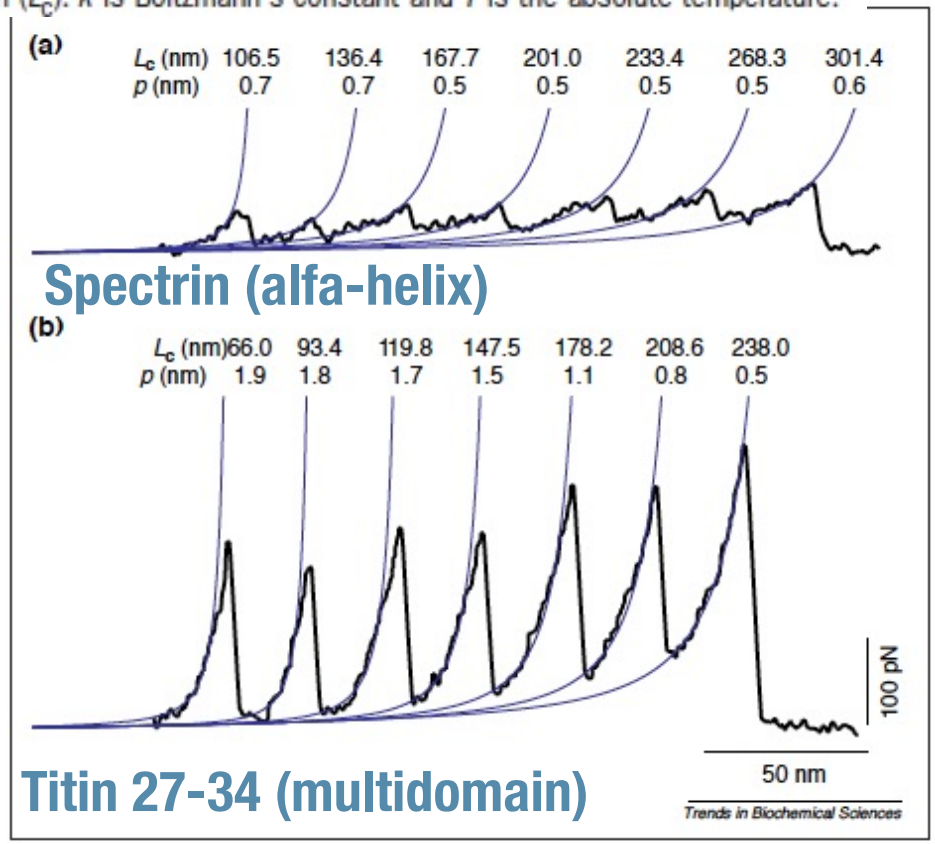

Polyprotein force spectroscopy

Interestingly, the measured unfolding forces generally increase with extension speed. Varying this parameter may provide an estimate of the unfolding off-rate and of the width of the unfolding energy barrier.

Reliable force data on a given molecule require recording several hundred force-curves using many independent tips and samples and proper model to fit data.

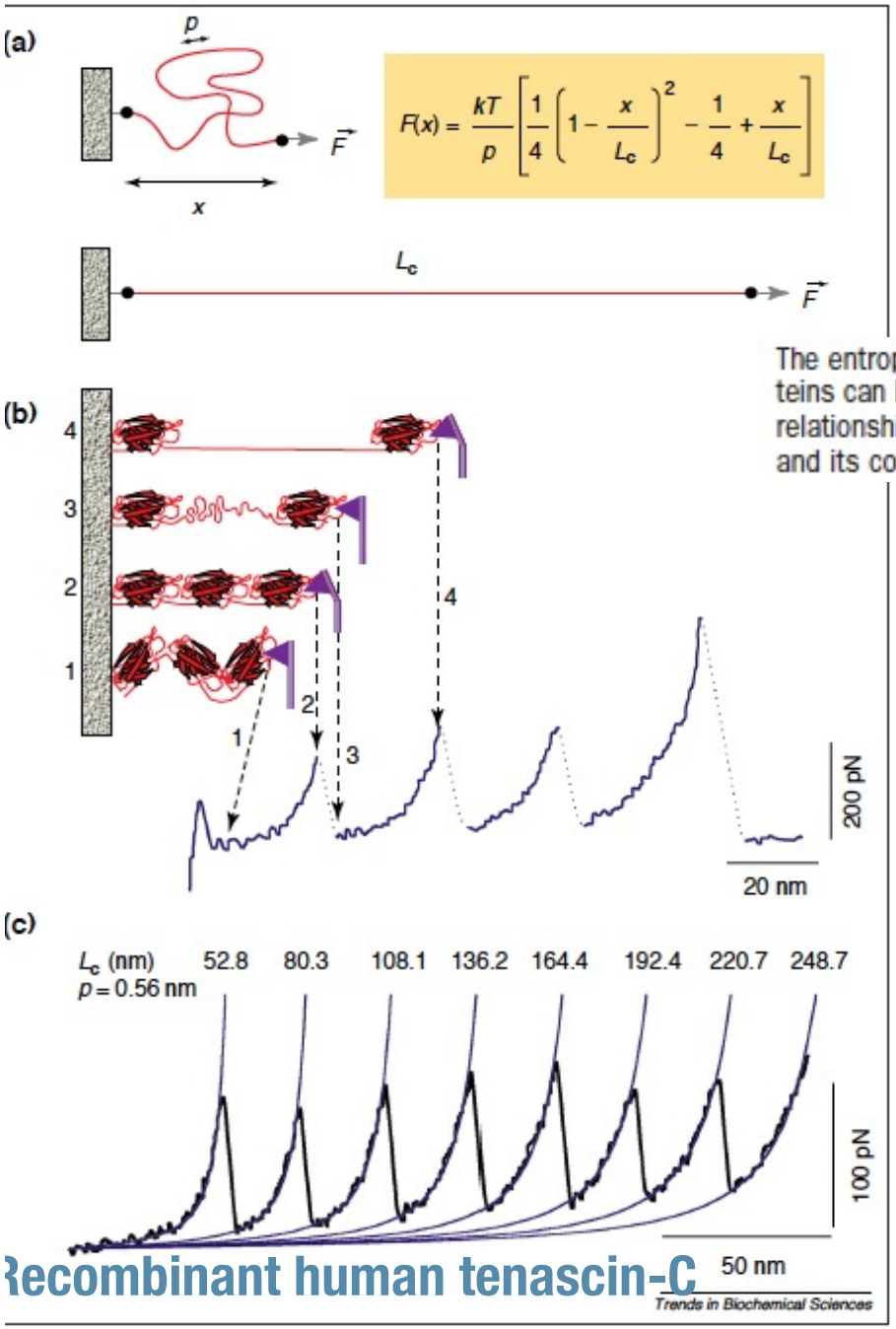

The entropic elasticity of proteins and domain unfolding. **(a)** The entropic elasticity of proteins can be described by the WLC (worm-like chain) equation (inset), which expresses the relationship between force (F) and extension (x) of a protein using its persistence length (p) and its contour length (L_c). k is Boltzmann's constant and T is the absolute temperature.

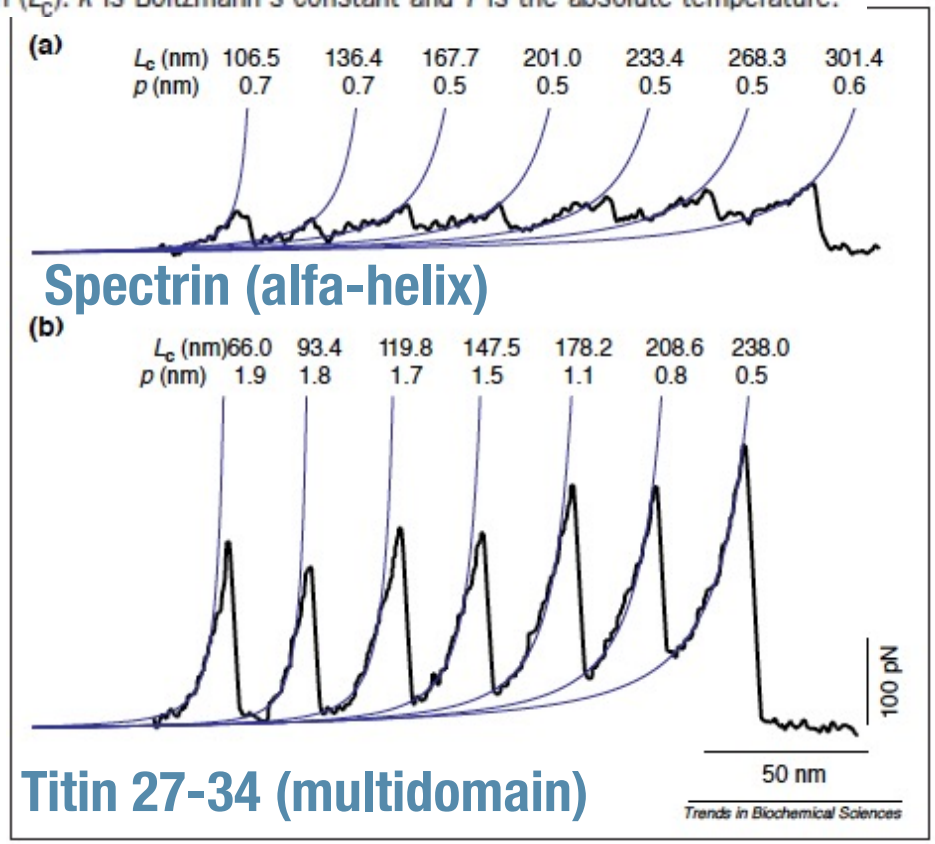

Polyprotein force spectroscopy

Engineered poly I27 Titin

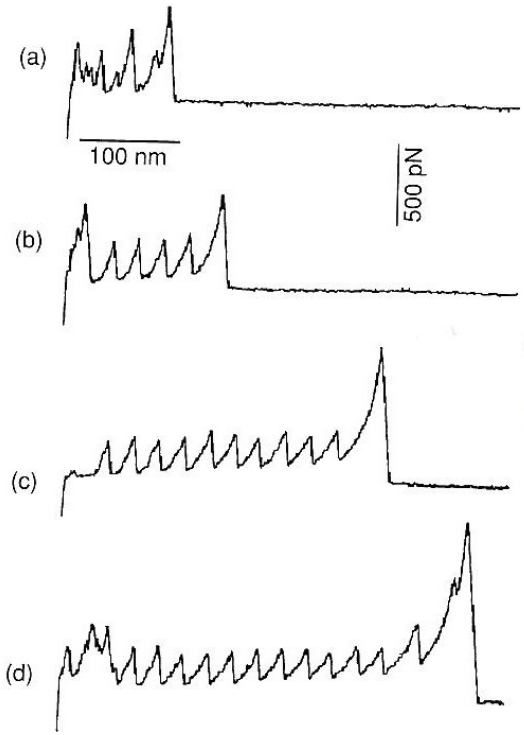

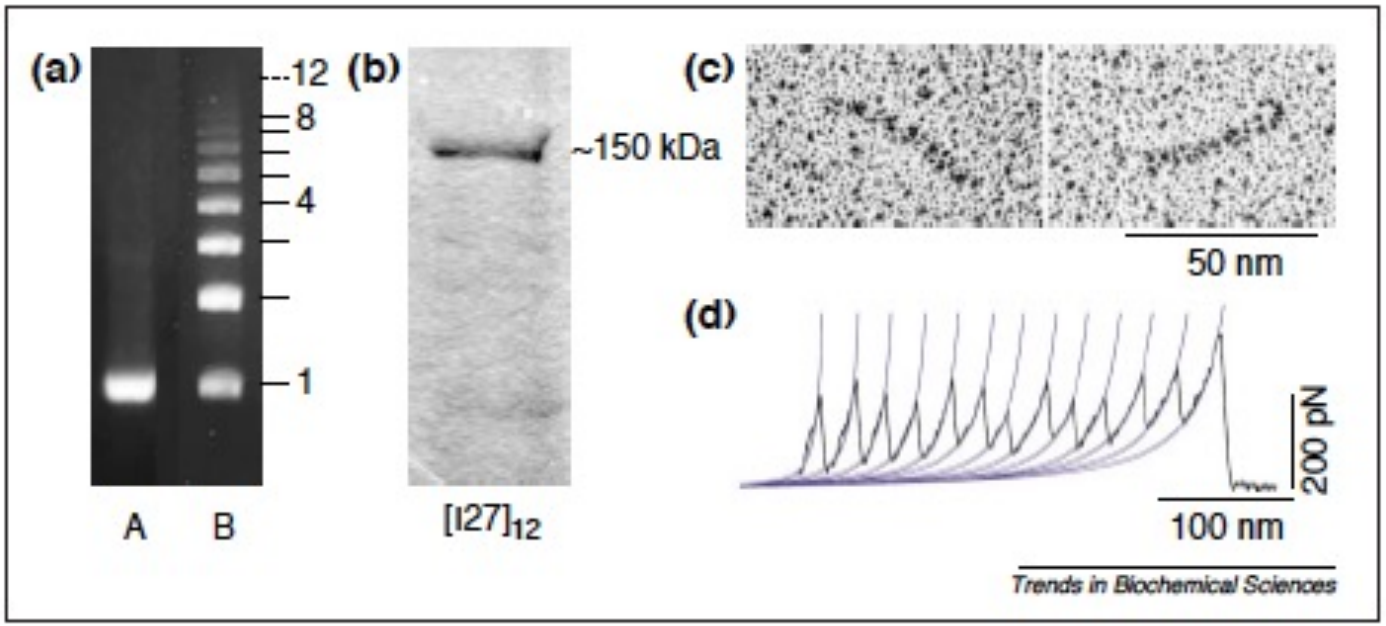

Unfolding-refolding

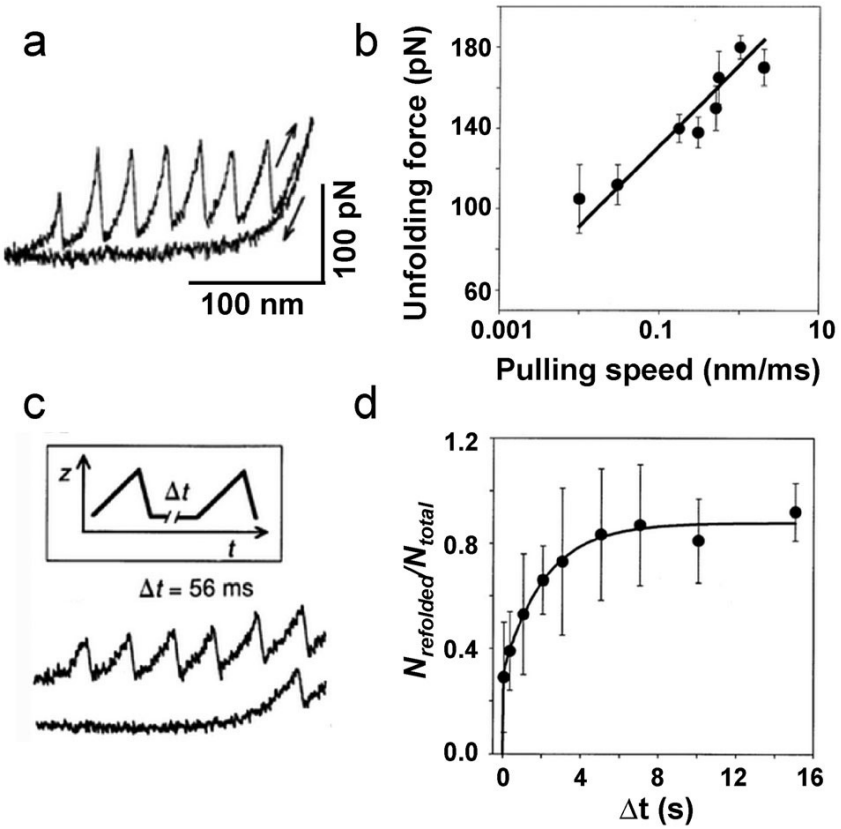

The data can be fitted using a Monte Carlo approach with a two-state model of the unfolding/refolding process, allowing the extraction of important parameters characterizing the unfolding reaction such as the distance to the unfolding transition state and the unfolding rate constant extrapolated to zero force

Fig. 3 Repeated unfolding and refolding cycles of tenascin. (a) The same TNfnAll fragment of tenascin was repeatedly stretched at various stretching speeds. (b) The average unfolding force *vs.* stretching speed. (c) A double-pulse experiment where the same molecule is stretched, relaxed for time Δt and stretched again. (d) The fraction of folded modules (counted from the second unfolding pulse) as a function of Δt.

Polyprotein force spectroscopy

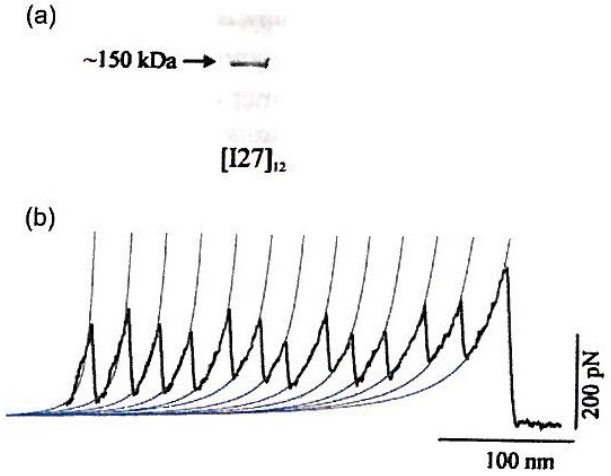

F= 204 pN

δLc=28 nm

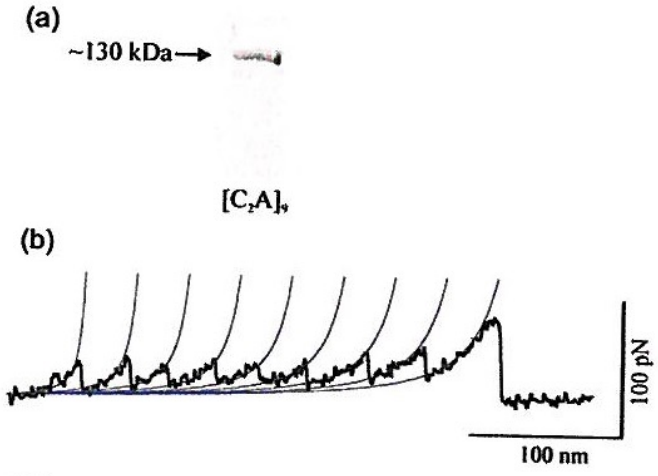

60 pN

38 nm

Two proteins with "all beta" structure and β-sandwich topology
-titin has seven β strands which fold face-to-face through backbone H-bonds and hydrophobic core interactions, perpendicular to stretching direction
-C2 β sandwich with 127 aminoacids arranged in 8 antiparallel strands.domains are in a zipper configuration

Polysaccarides

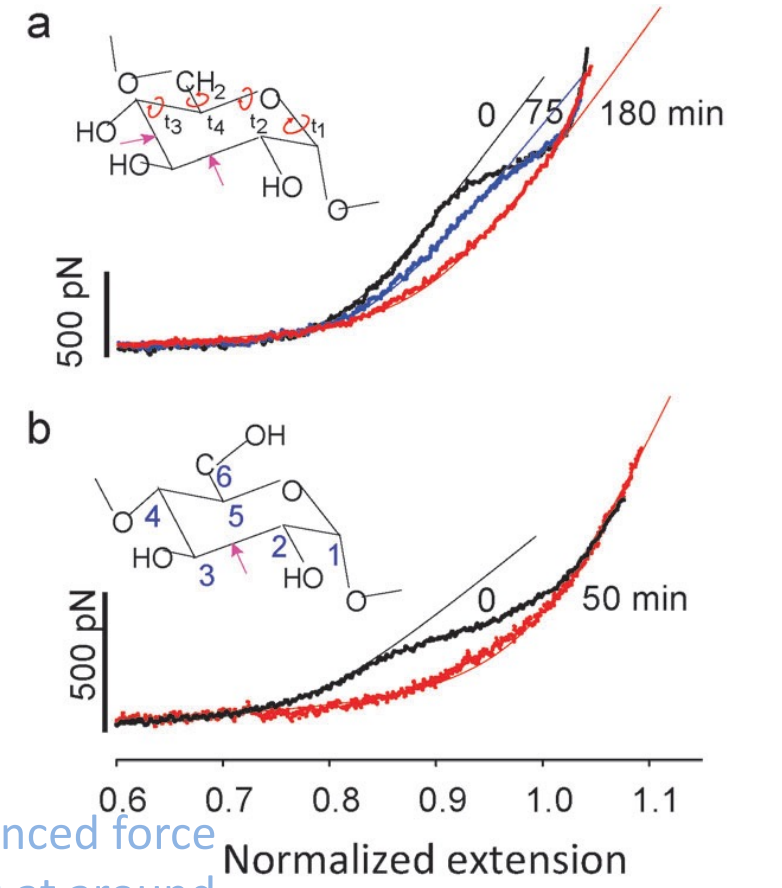

pronounced force plateau at around 300 pN

It is known that under some conditions, e.g. during enzymatic hydrolysis of glycosidic linkages, sugar rings are severely deformed into high-energy conformations.

Polysaccharides are ideal for SMFS studies because they are generally highly soluble in water and they are quite sticky, adsorbing easily to substrates such as glass or gold and to the AFM tip for stretching experiments

Fig. 2 SMFS captures force-induced conformational transitions in polysaccharides. (a) Force–extension curves of dextran subjected to periodate oxidation. The time indicated represents the duration of oxidation treatment. (b) Force–extension curves of amylose subjected to periodate oxidation. The time indicated represents the duration of oxidation treatment. (c) A schematic of a forced lengthening transition of the glucopyranose ring in amylose, from a chair to a boat-like structure. Adapted from ref. 20.

Herman E. Gaub (LMU Munich) : Unzipping DNA oligomers

Nano Letters **3**, 4, 493 (2003)

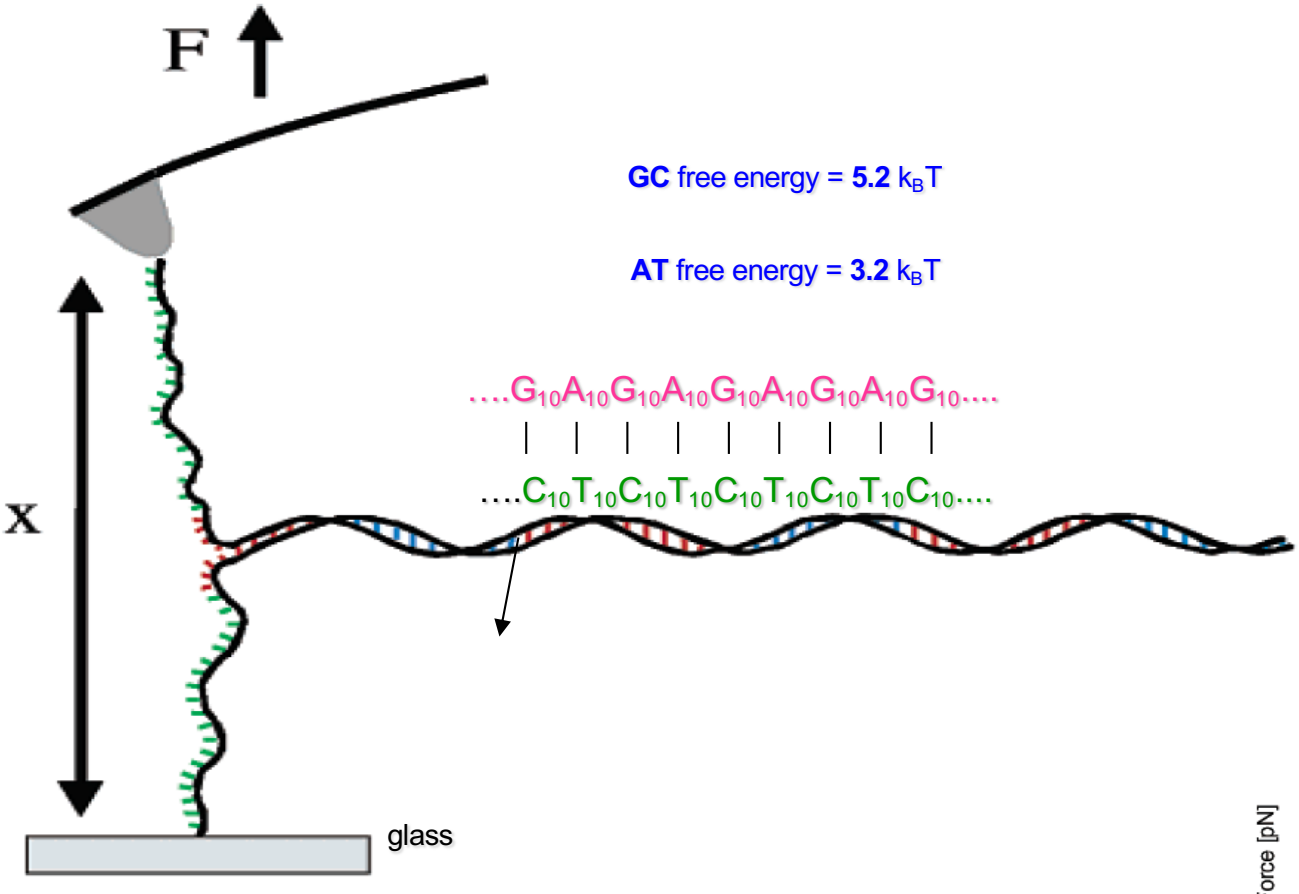

Complementary DNA oligonucleotides are chemically attached to an AFM tip and a glass slide. As the tip is brought in contact with the surface a ds-DNA forms, which can then be unzipped upon retractio the tip.

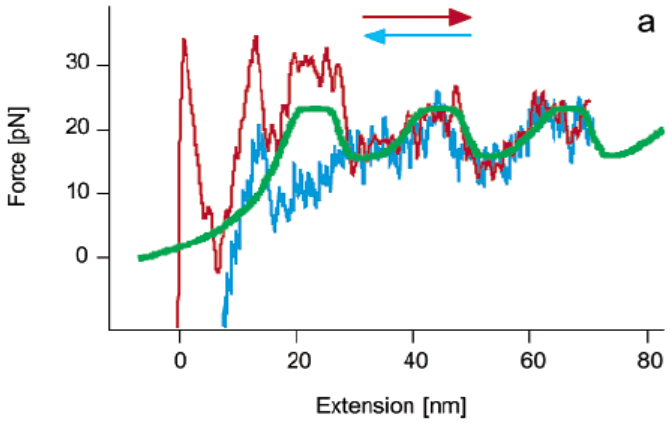

Experimental Results

Herman E. Gaub (LMU Munich) : Unzipping DNA oligomers

Nano Letters **3**, 4, 493 (2003)

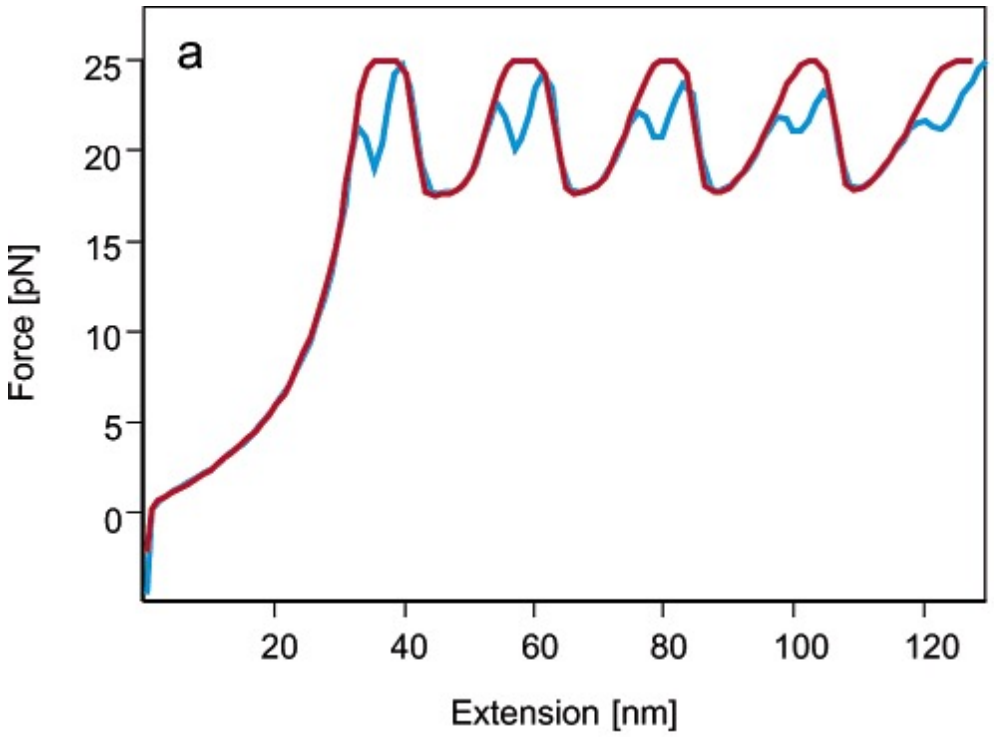

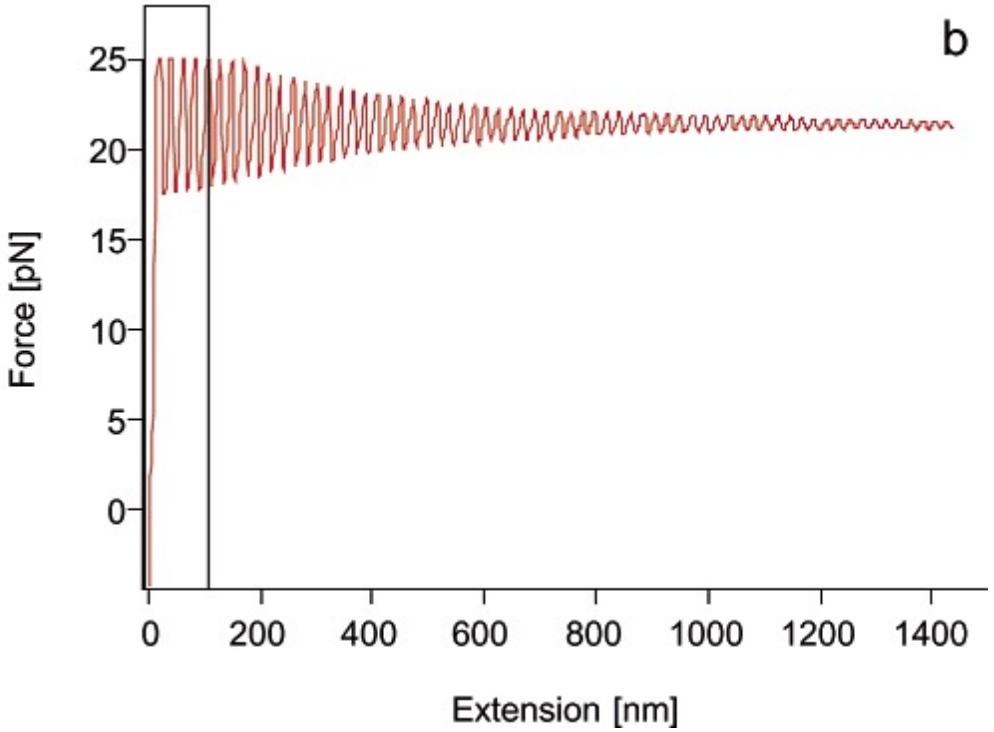

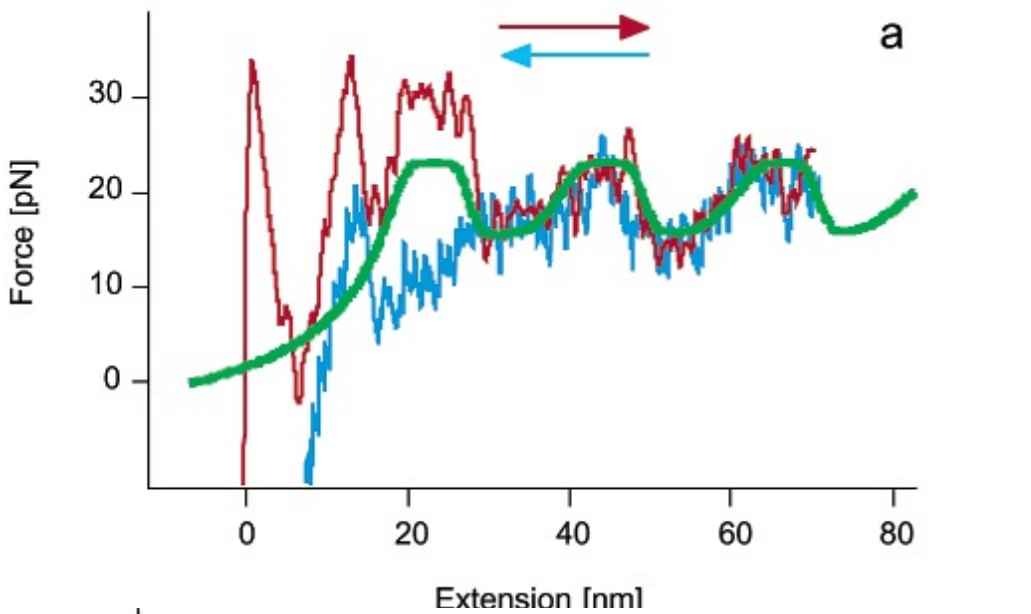

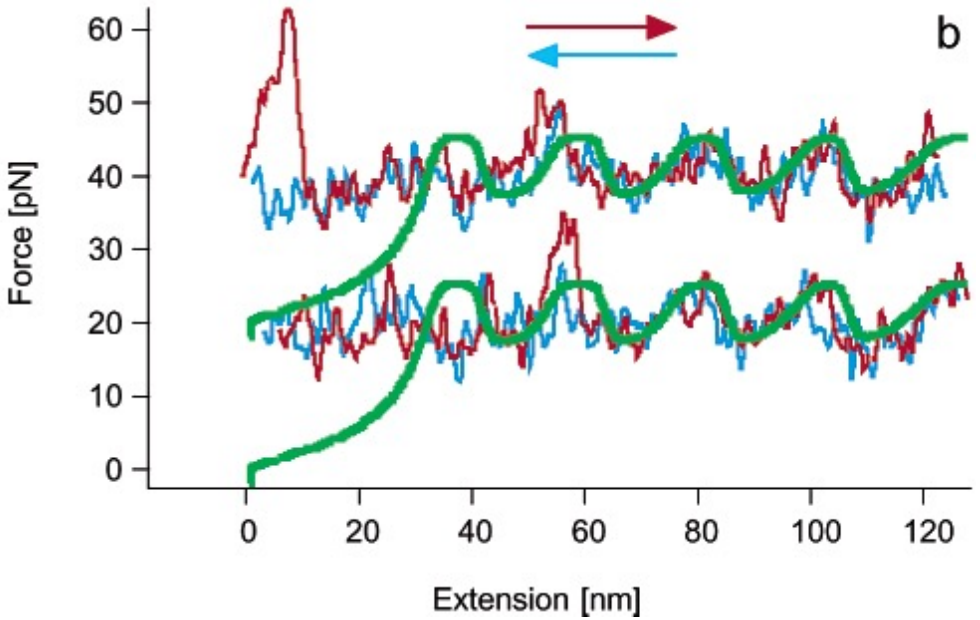

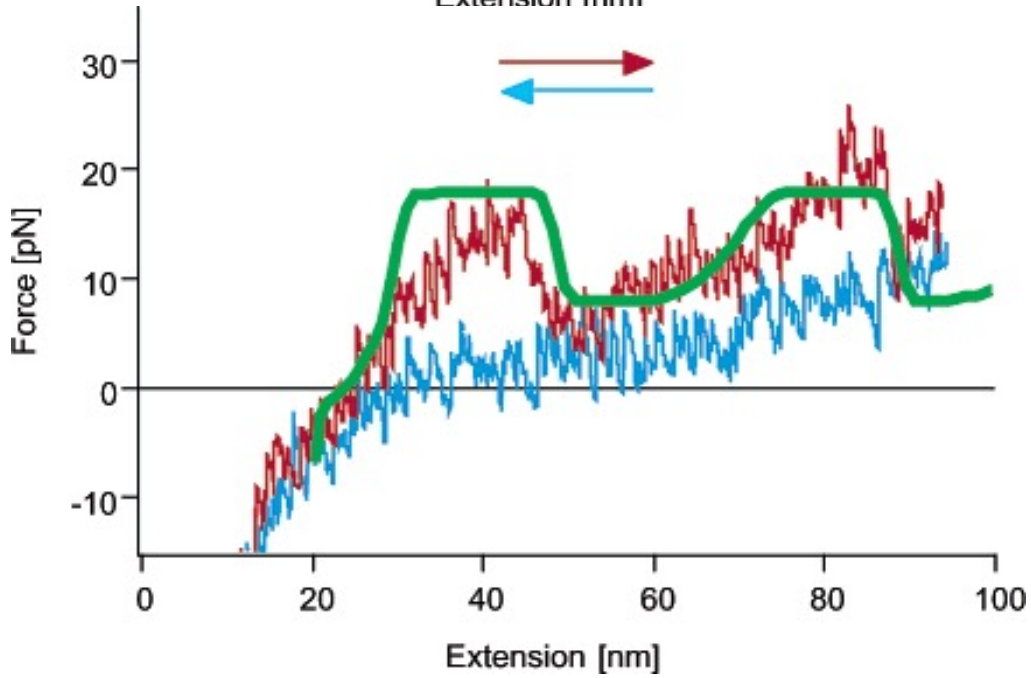

Figure 4. Force vs distance curve upon unzipping a dsDNA molecule with an alternating sequence of 20 pure AT and 20 pure GC base pairs ([dG20dA20dG20dA20dG20]([dC20dT20dC20dT20dC20]) and a simulated curve (green). The force upon unzipping the molecule varies because of the different stability of the AT and GC base pairs. The oscillation in force seen in the data corresponds well to the force vs distance profile calculated from the equilibrium thermodynamic model.

Cell mechanics

Extracellular Matrix

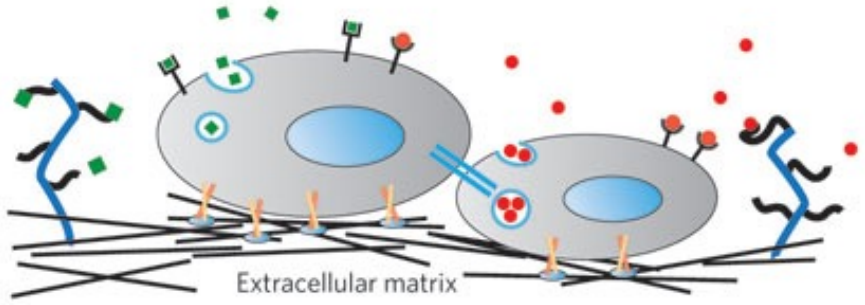

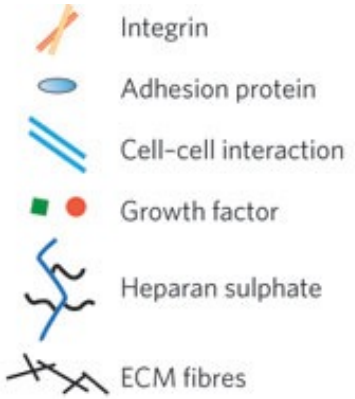

The ECM promotes a unique microenvironment that fosters tissue organization.

ECM key factors are:

- **ECM Molecules**
- **Growth Factor Concentration**
- **Topography**
- **Mechanical Properties**

- Protein fibres (collagen, elastin)
- Adhesive protein (laminin, fibronectin)
- Polysaccharides (hyaluronic acid, heparan sulphate)
- Cell adhesion (integrin, cadherin)

control the ECM → control the tissue

Dvir, Tal, *et al*. Nanotechnological strategies for engineering complex tissues. Nature Nanotechnology. 2011.

Substrate stiffness affects cellular fate

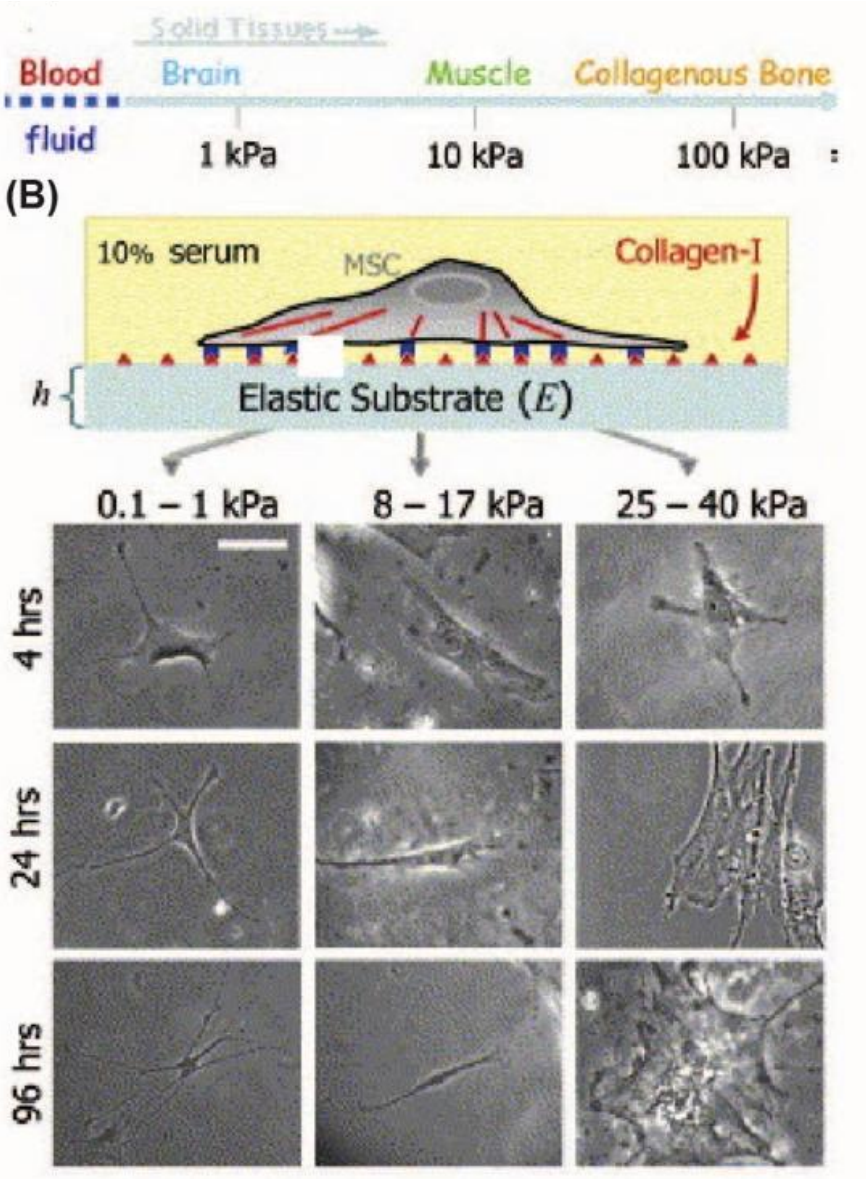

First evidences in the ’80s (Emerman, J.T.; Burwen, S.J.; Pitelka, D.R. Tissue Cell 1979)

hMSCs cultured on a polyacrylamide gel homogeneously coated with collagen I ligands.

The substrates had variable stiffness representing that of nerve (Young Modulus about 0.1–1 kPa), muscle (8–17 kPa) and bone tissue (25–40 kPa) and it was it was observed that the hMSCs differentiated along the neurogenic, myogenic and osteogenic lineage, respectively

Engler *et al.* Cell 2006

Playing with PDMS elastic properties:

The promotion of neuronal maturation on soft substrates

Embrional NeuralSCs cultured as monolayers on PDMS were able to maintain the stem cell state (when supported with FGF2) and differentiate in response to soluble factors, according to established protocols.

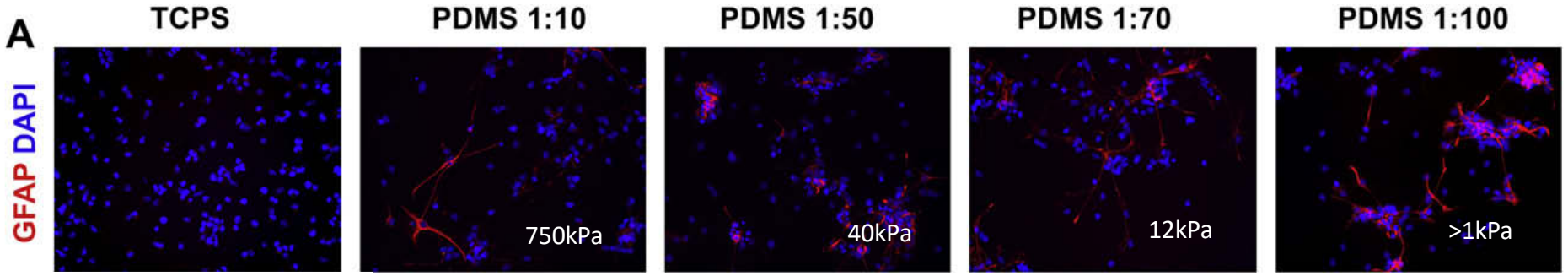

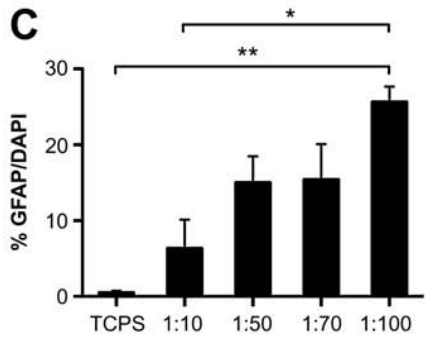

Less crosslinking agent (1:10>>1:100) impacts on rigidity of the PDMS (softer substrate)

Soft substrates promote astrocytic differentiation…

… and neurite length on neurons

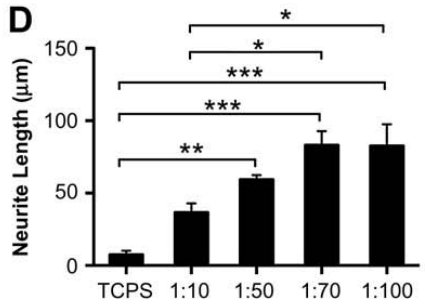

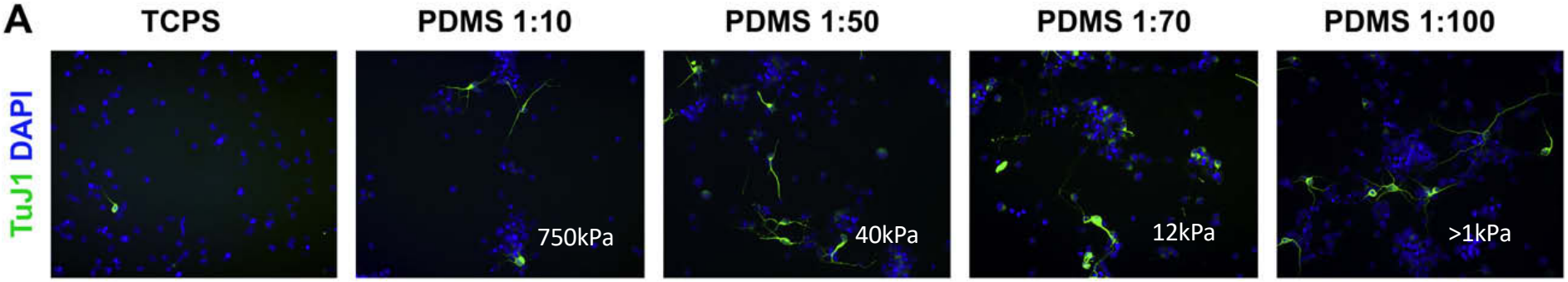

Teixeira AI et al. Biomaterials 2009.

Mechanical regulation of cell function with geometrically modulated elastomeric substrates

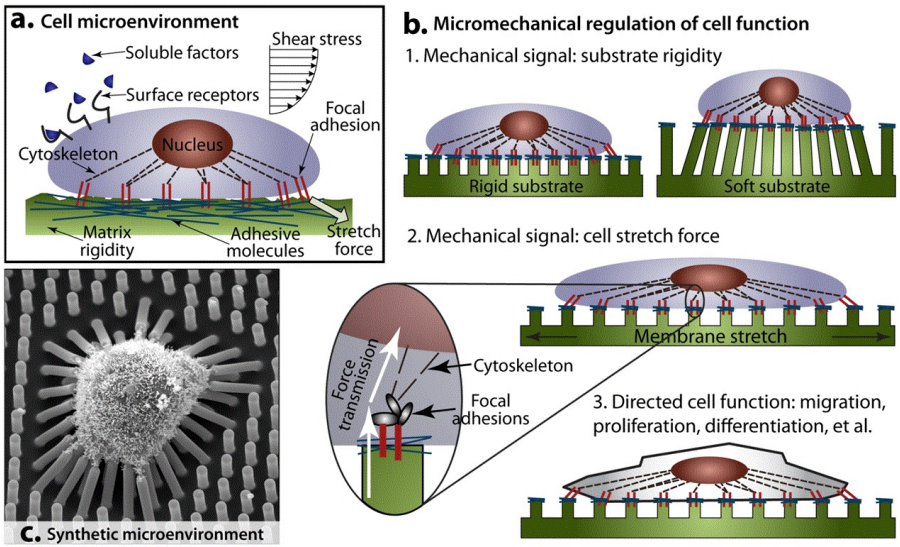

- Human Mesenchimal Stem cells
- growth medium or bipotential differentiation medium supportive of both osteogenic and adipogenic fates
- Micropost rigidity shifted the balance of hMSC fates: osteogenic lineage was favored on rigid micropost arrays whereas adipogenic differentiation was enhanced on soft ones.

Decouple substrate rigidity from adhesive and surface properties

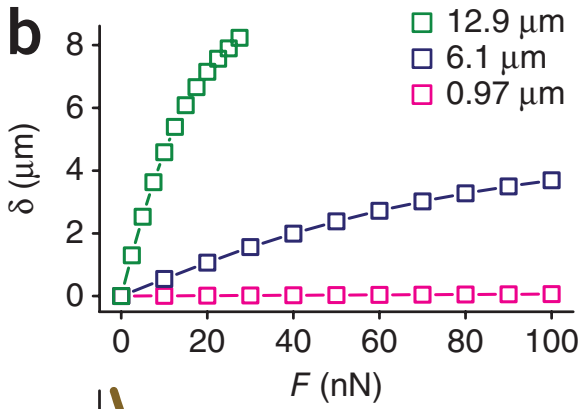

Higher Pillar → Softer substrate

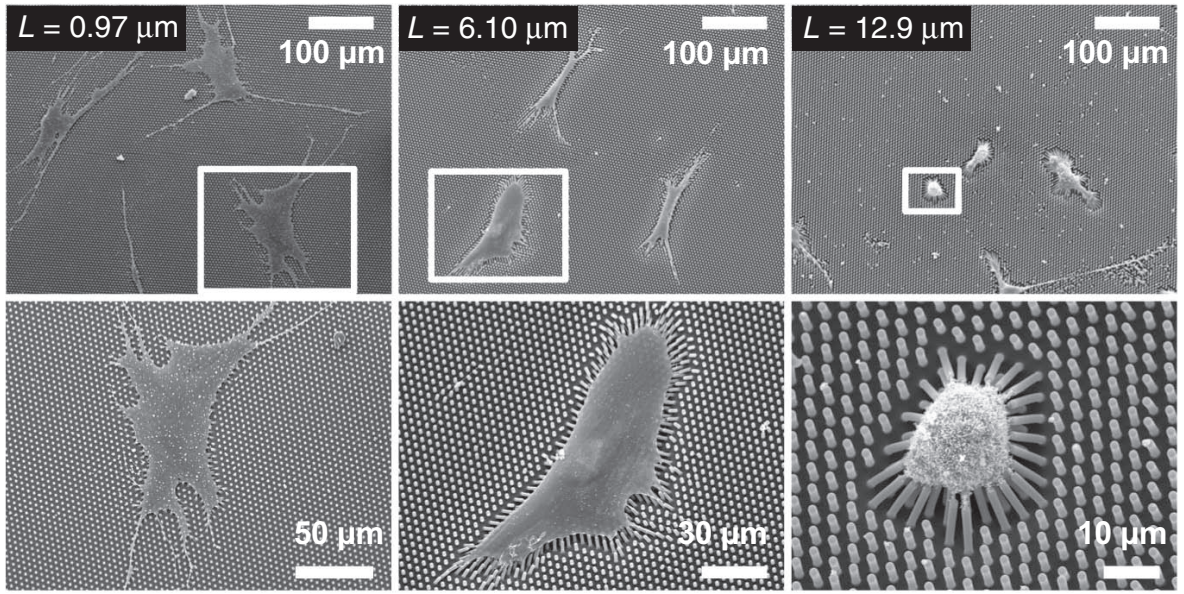

Fu J. *et al.* Nature Methods 2010.

Traction forces exerted by epithelial cell sheets

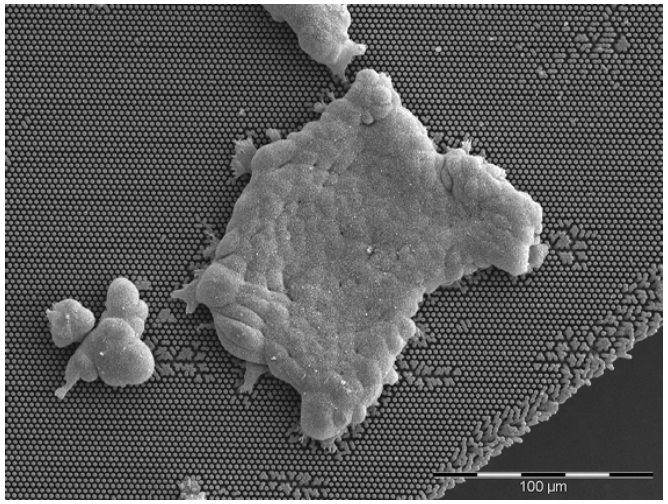

Forces exerted by Madin–Darby Canine Kidney (MDCK) epithelial cells using microfabricated substrates covered by an array of flexible micropillars

Epithelial cells act collectively in the transmission of forces within the group and exert large traction forces mostly localized at the periphery

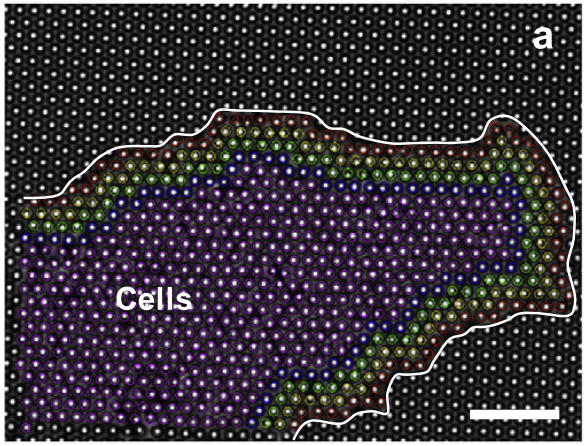

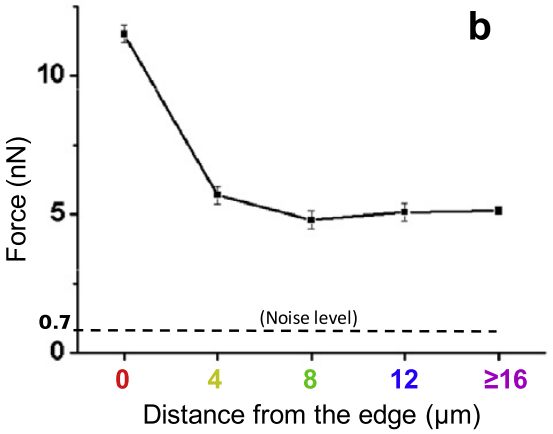

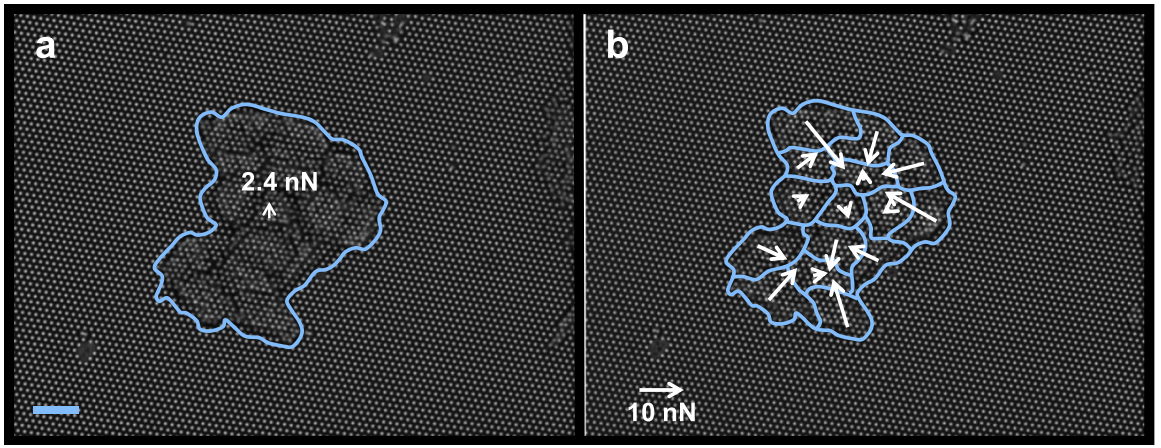

Mechanotransduction

Transmission of mechanical force is crucial for normal cell development and functioning. However, the process of mechano-transduction cannot be studied in isolation from cell mechanics. Thus, in order to understand how cells ‘feel’, we must first understand how they deform and recover from physical perturbations

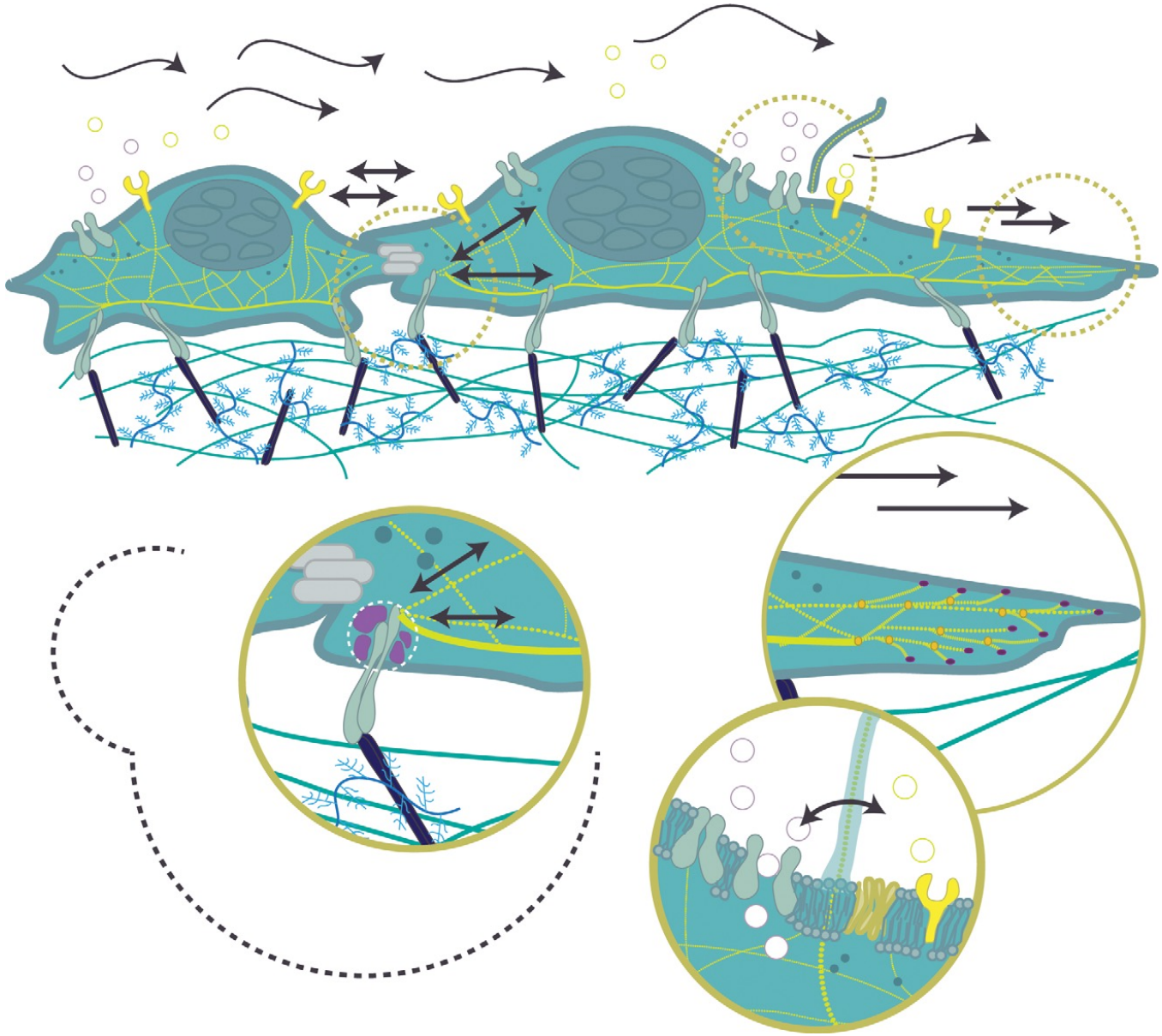

rsif.royalsocietypublishing.org J. R. Soc. Interface 12: 20140970

Mechanotransduction

The response to mechanical stimuli is complex and depends on both force magnitude and rate.

Strain rate, in particular, has been shown to affect stretch-induced remodelling of F-actin

External forces transmitted through the plasma membrane and focal adhesions (FAs) are conveyed to internal load-bearing structures of the cytoskeleton, influencing nuclear deformations, transcription processes and gene expression

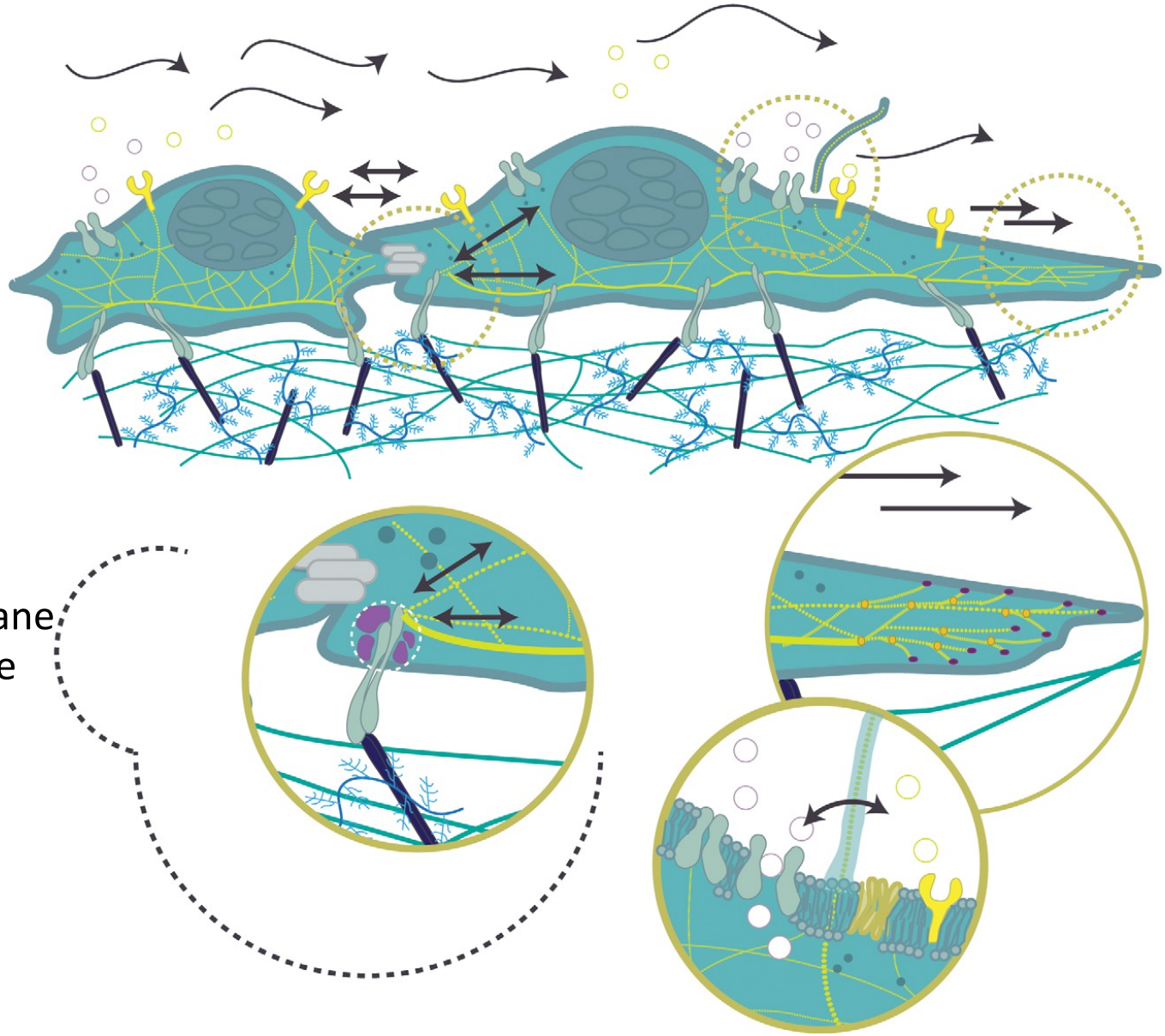

rsif.royalsocietypublishing.org J. R. Soc. Interface 12: 20140970

Mechanotransduction

The response to mechanical stimuli is complex and depends on both force magnitude and rate.

Strain rate, in particular, has been shown to affect stretch-induced remodelling of F-actin

External forces transmitted through the plasma membrane and focal adhesions (FAs) are conveyed to internal load-bearing structures of the cytoskeleton, influencing nuclear deformations, transcription processes and gene expression

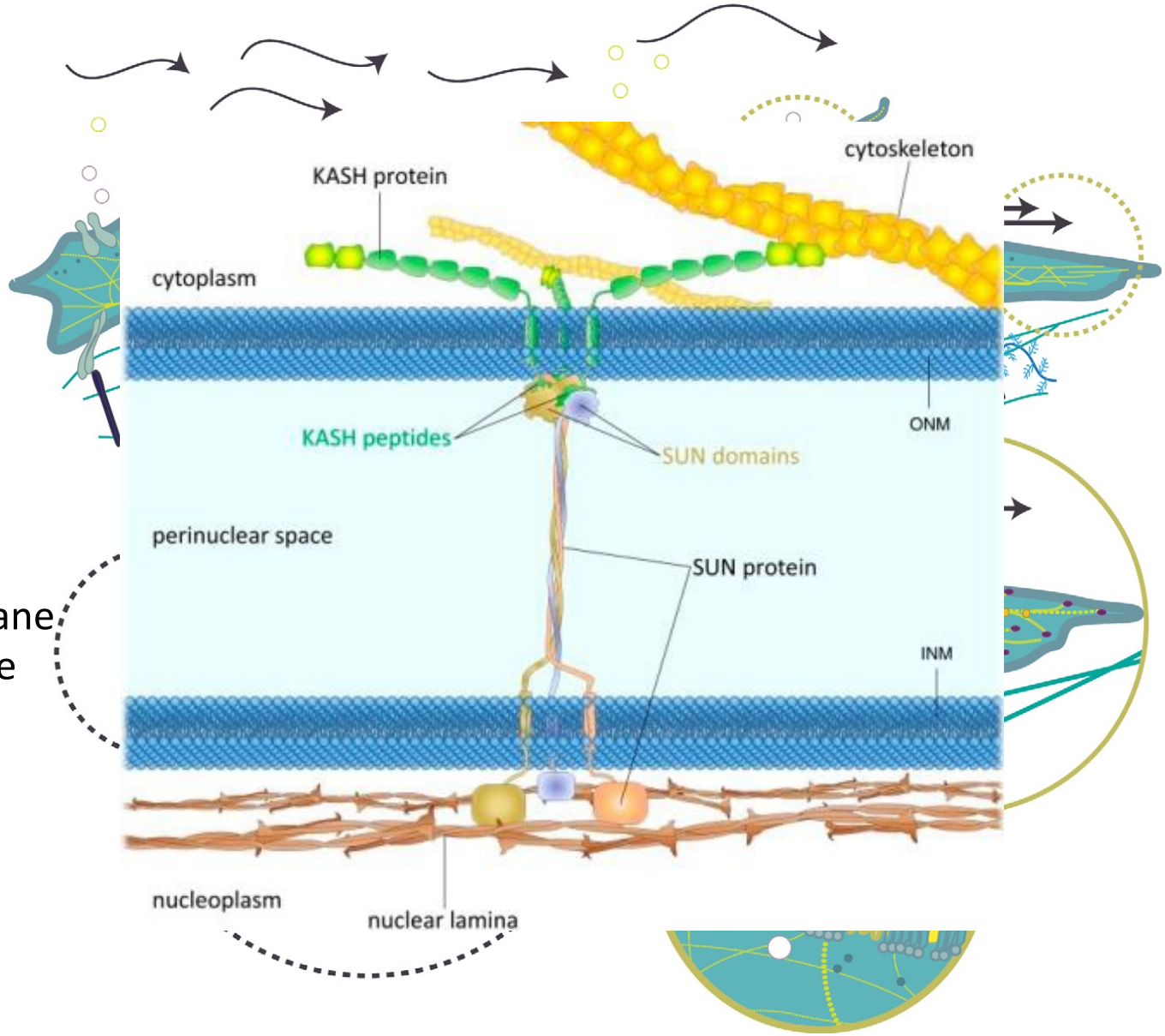

rsif.royalsocietypublishing.org J. R. Soc. Interface 12: 20140970

Mechanotransduction

Internal forces generated via molecular motors and actin polymerization are transmitted to the substrate in order to facilitate migration, undergo mitosis and communicate with neighbouring cells.

This continual process of sensing (stretch-activated ion channels, Integrins and primary cilia), transmission and response is known as **mechanotransduction** and is essential for maintenance of normal cell functioning and development

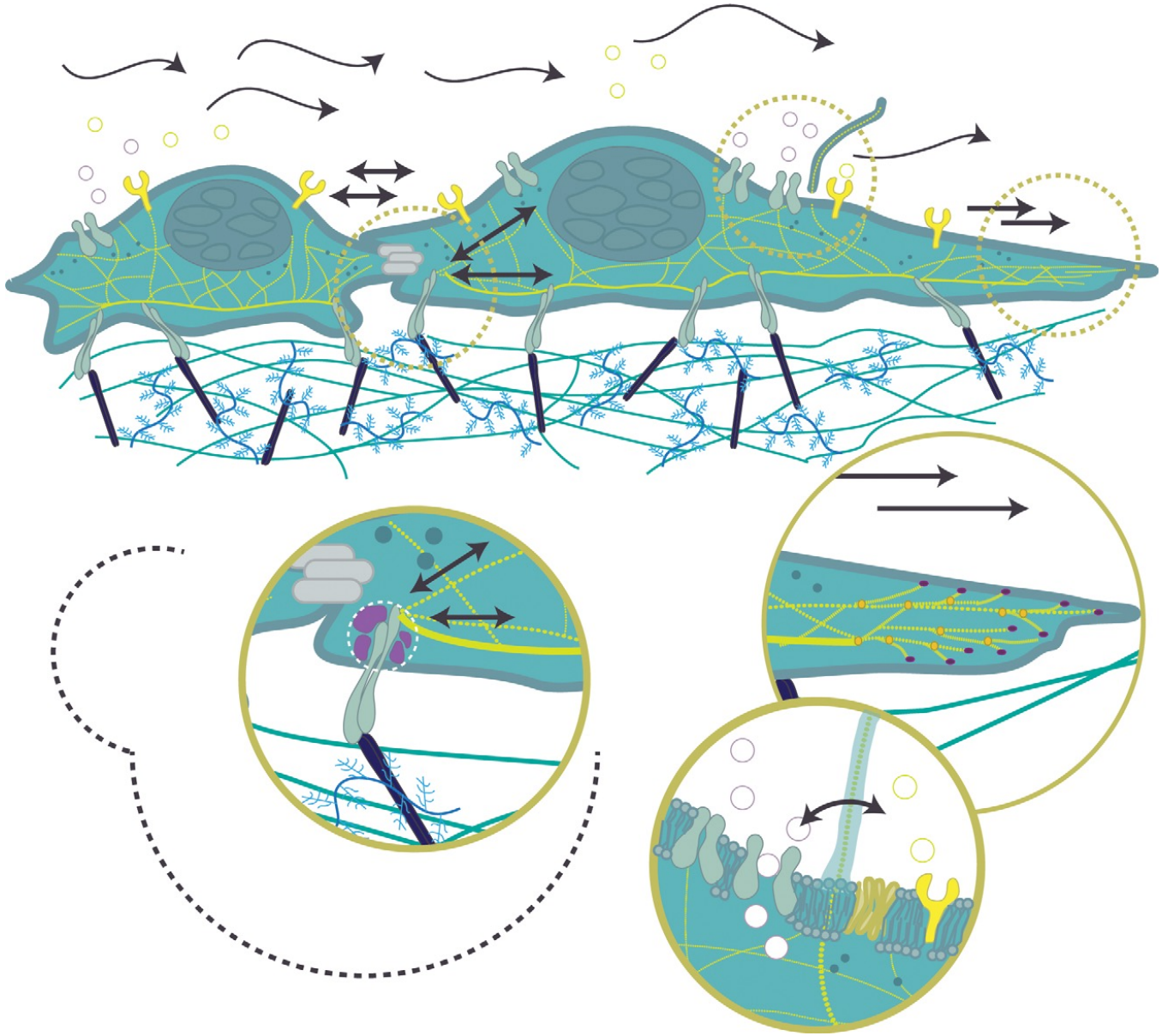

rsif.royalsocietypublishing.org J. R. Soc. Interface 12: 20140970

How to study cell mechanics

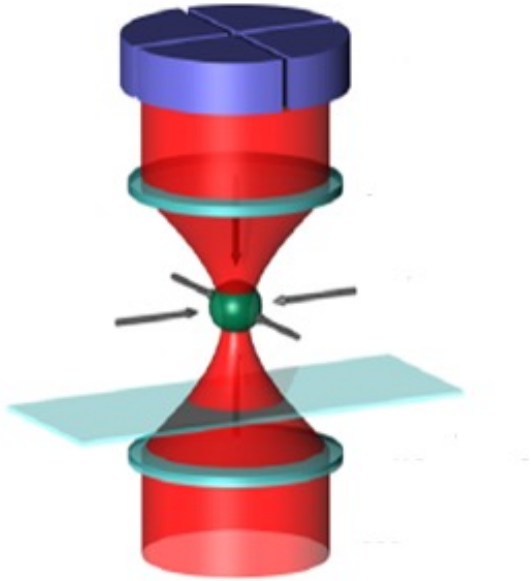

OPTICAL TWEEZER

- Two lasers in order to trap a bead
- The bead displacement converted to force by the software
- Force applied from 0.1 to 100 pN

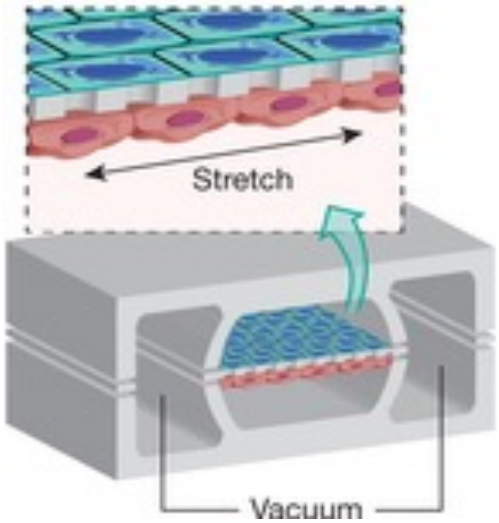

STRETCHING IN MICROFLUIDIC CHANNELS

PDMS soft lithography

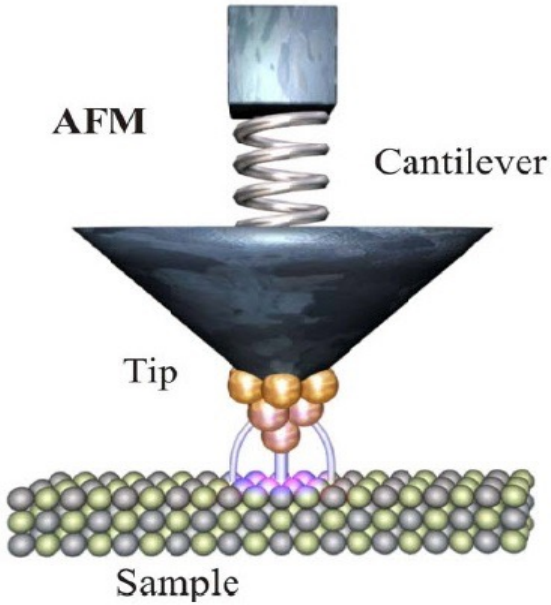

ATOMIC FORCE MICROSCOPY

- Tip mounted on a flexible cantilever
- Tip/sample interaction monitored by a laser
- Force applied from 10 pN to 100 nN

AFM and cell mechanics

AFM has been used to measure both **elastic** and **viscous** cellular responses

AFM can be used to **directly apply and simultaneously measure cellular forces**. Its advantage is its **versatility**, as AFM can be used for imaging as well as force transmission and measurement.
By altering tip geometry or chemistry, a multitude of both local and whole-cell studies can be performed on living cells in their native environments.

These studies induce a rapid response of cells through shape change, remodelling of the cytoskeleton and calcium signalling, which all depend on frequency, duration, magnitude and location of applied force

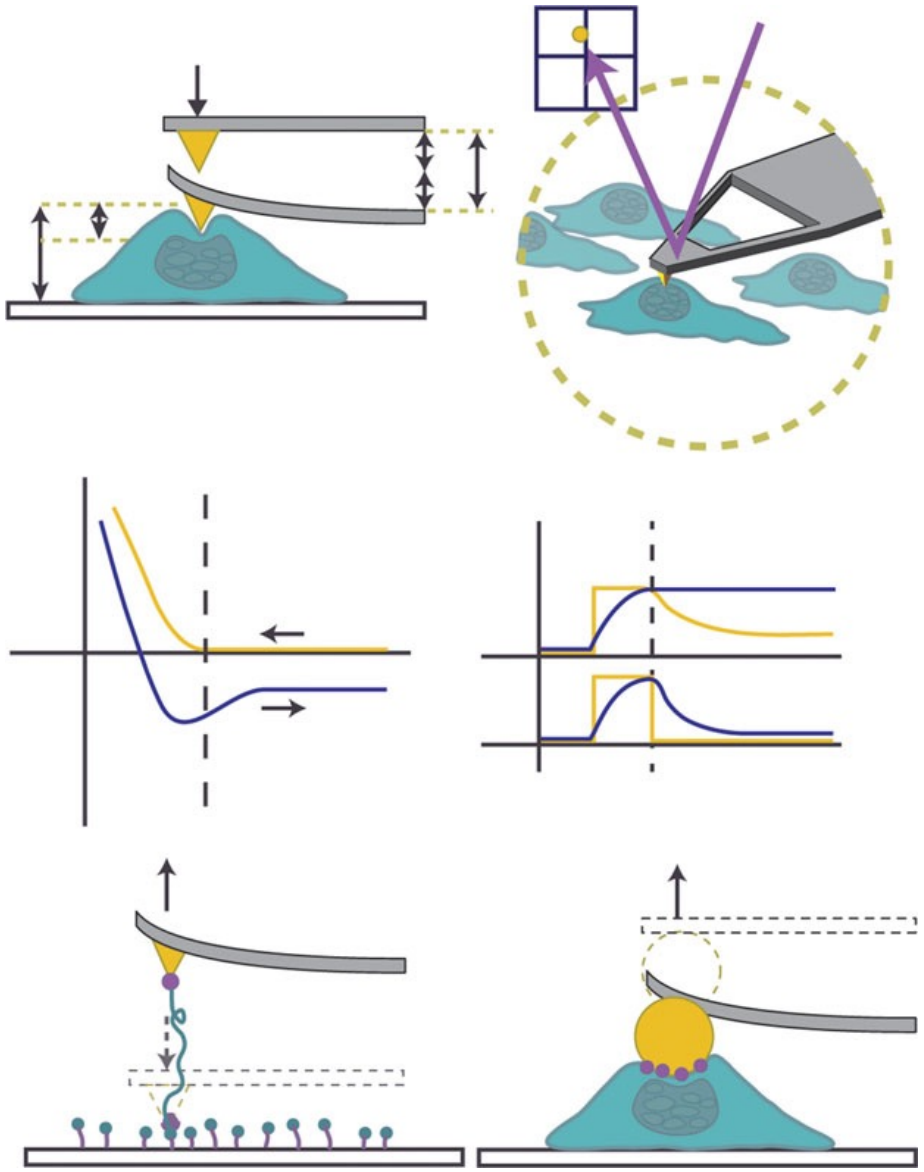

rsif.royalsocietypublishing.org J. R. Soc. Interface 12: 20140970

AFM and cell mechanics

AFM indentation data demonstrated that in many pathologies such as the anemia, diabetes, cardiomyopathies, Parkinson's and Alzheimer's diseases, cancer and many others, the mechanical properties of affected cells are perturbed resulting in a characteristic fingerprint for these diseases

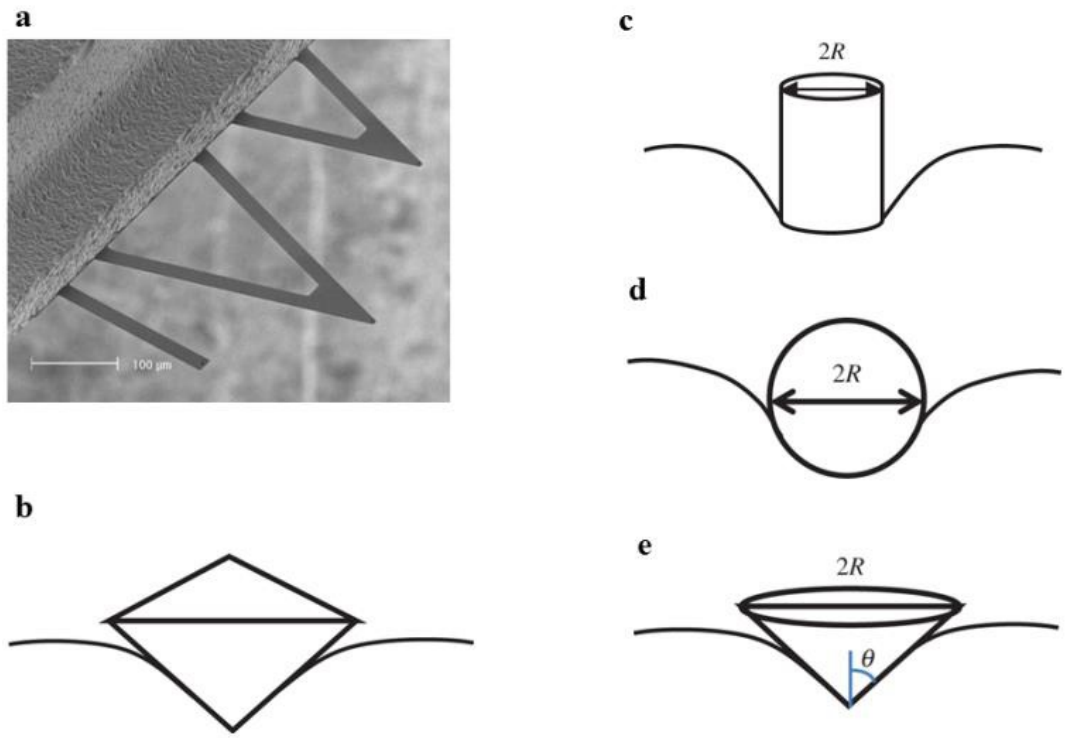

AFM and cell mechanics

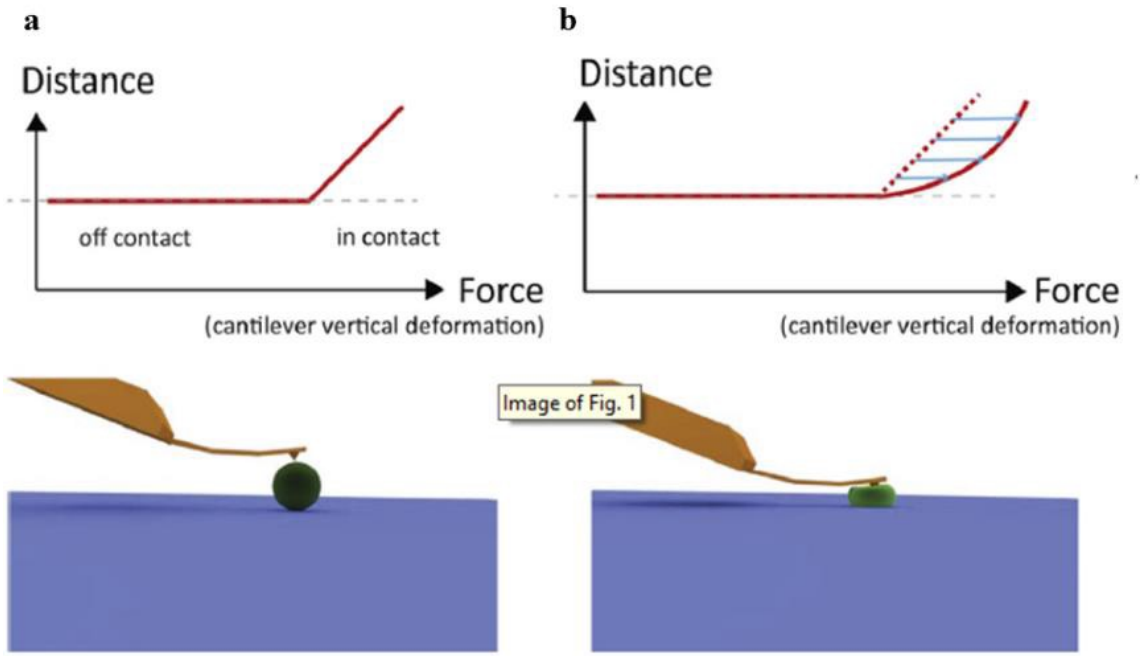

Before contact, the base of AFM cantilever - surface distance is the same as tip apex – surface distance.
From contact point on:
-if the material has **infinite rigidity**, tip-surface distance will be zero while base of the AFM - surface distance further reduces -- **cantilever deformation**
-if the material is **soft**, tip penetrates the surface. The entity of this penetration is inverse function of the stiffness of the sample.

Cantilever deflection due to the further reduction of the distance between the cantilever base and the surface has to be corrected by the distance the apex tip penetrate into the material

AFM Force-Spectroscopy

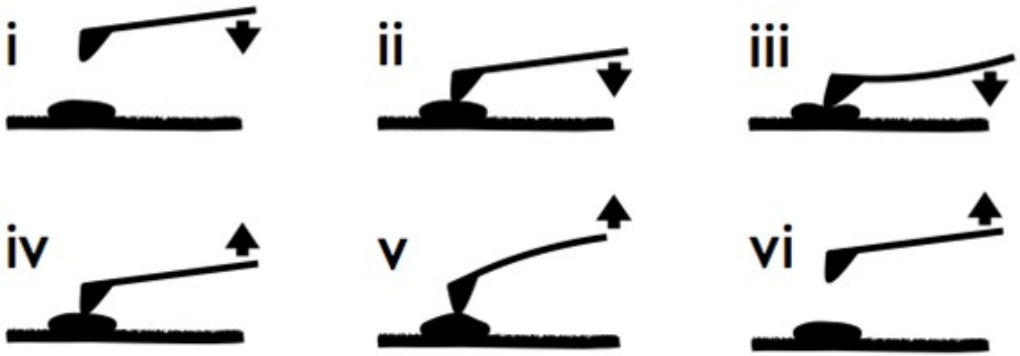

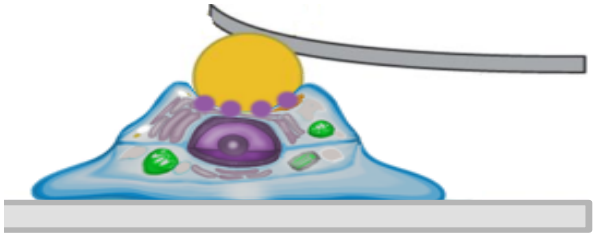

$$F = \frac{4}{3}\frac{E}{1-\mu^2}\sqrt{R\delta_0^3}$$

F … applied force
R … radius of the probe
δ_0 … indentation of the sample
E … elastic modulus
μ … POISSON's ratio

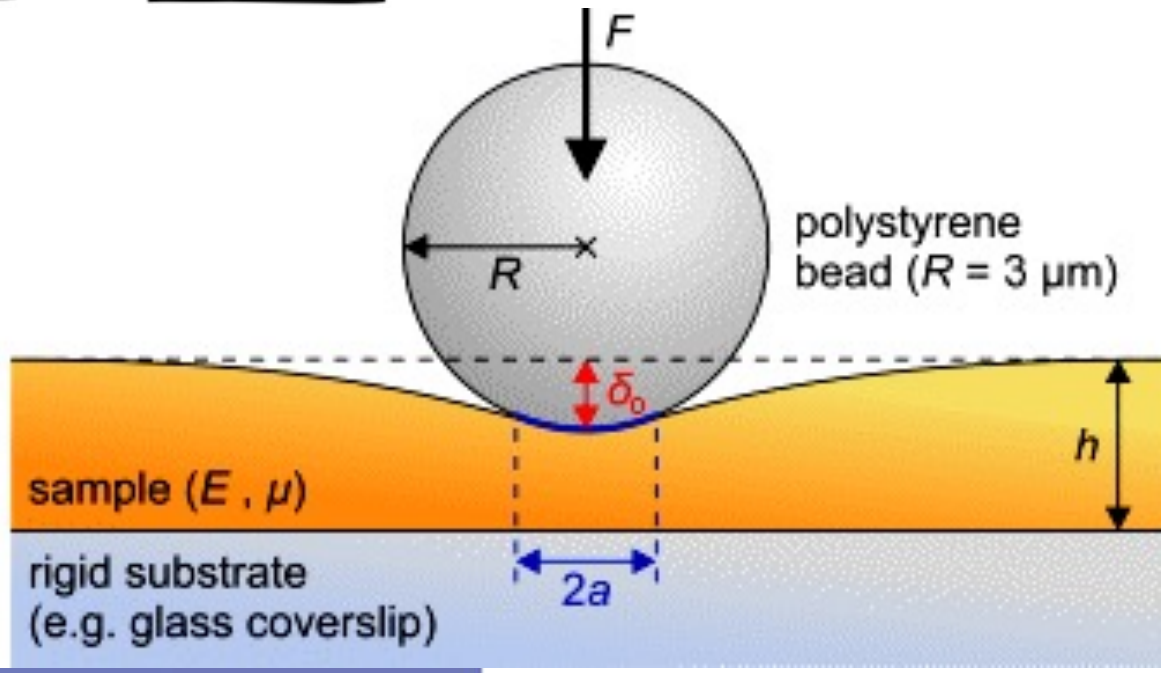

An elastic sphere of radius R indents an elastic half-space to depth d, and thus creates a contact area of radius

$$a = \sqrt{Rd}$$

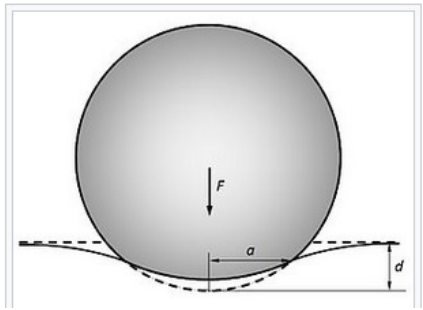

The applied force F is related to the displacement d by [4]

$$F = \frac{4}{3} E^* R^{\frac{1}{2}} d^{\frac{3}{2}}$$

where

$$\frac{1}{E^*} = \frac{1-\nu_1^2}{E_1} + \frac{1-\nu_2^2}{E_2}$$

and E_1,E_2 are the elastic moduli and ν_1,ν_2 the Poisson's ratios associated with each body.

The distribution of normal pressure in the contact area as a function of distance from the center of the circle is

$$p(r) = p_0 \left(1 - \frac{r^2}{a^2}\right)^{\frac{1}{2}}$$

where p_0 is the maximum contact pressure given by

$$p_0 = \frac{3F}{2\pi a^2} = \frac{1}{\pi}\left(\frac{6FE^{*2}}{R^2}\right)^{\frac{1}{3}}$$

The radius of the circle is related to the applied load F by the equation

$$a^3 = \frac{3FR}{4E^*}$$

The depth of indentation d is related to the maximum contact pressure by

$$d = \frac{a^2}{R} = \left(\frac{9F^2}{16E^{*2}R}\right)^{\frac{1}{3}}$$

The maximum shear stress occurs in the interior at $z \approx 0.49a$ for $\nu = 0.33$.

AFM and cell mechanics

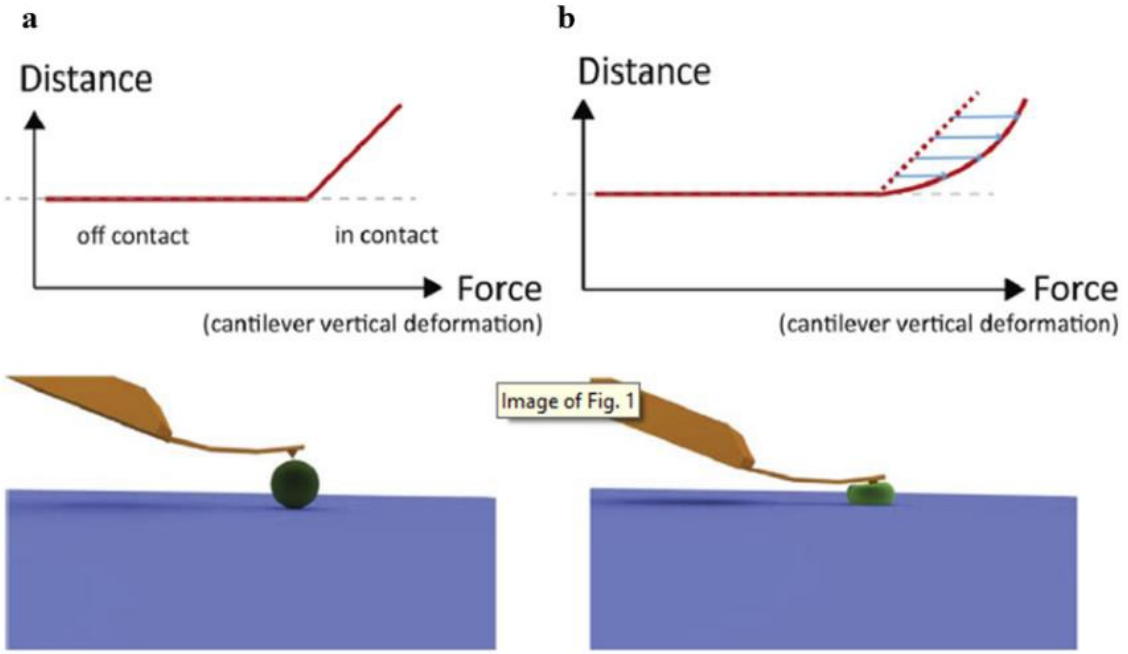

different fitting models are available to analyze force spectroscopy data extrapolating information about cell stiffness.

The most used is the Hertz model. The Hertz formalism is founded on the theory of linear elasticity and must satisfy a Hookean relationship which describes the elastic deformation of two sphere, where the relation between the applied force (F) and the resulting indentation is:

$$F = \frac{4ER^{\frac{1}{2}}}{3} \frac{\delta^{\frac{3}{2}}}{(1-\mu^2)}$$

E = Young's modulus

μ = Poisson's ratio of the indented material (ranging from 0 to 0.5)

R is the radius of the rigid indenter.

δ determines the contact radius (α)

$$\alpha = R^{\frac{1}{2}}\delta^{\frac{1}{2}}$$

Application: Calcific Aortic Valve Disease (CAVD)

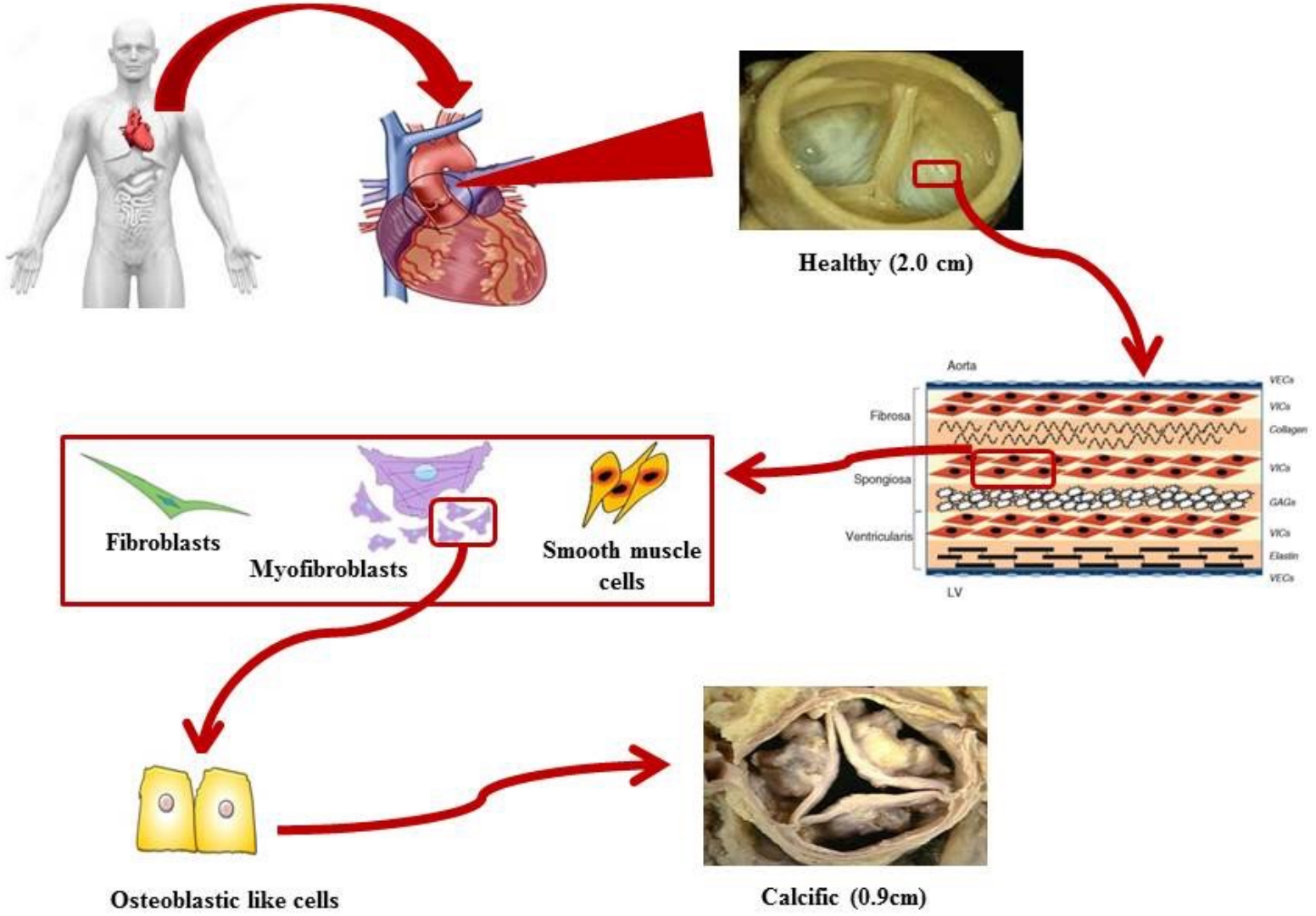

Aortic Valve Interstitial Cells (VICs)

on Polyacrylamide gels

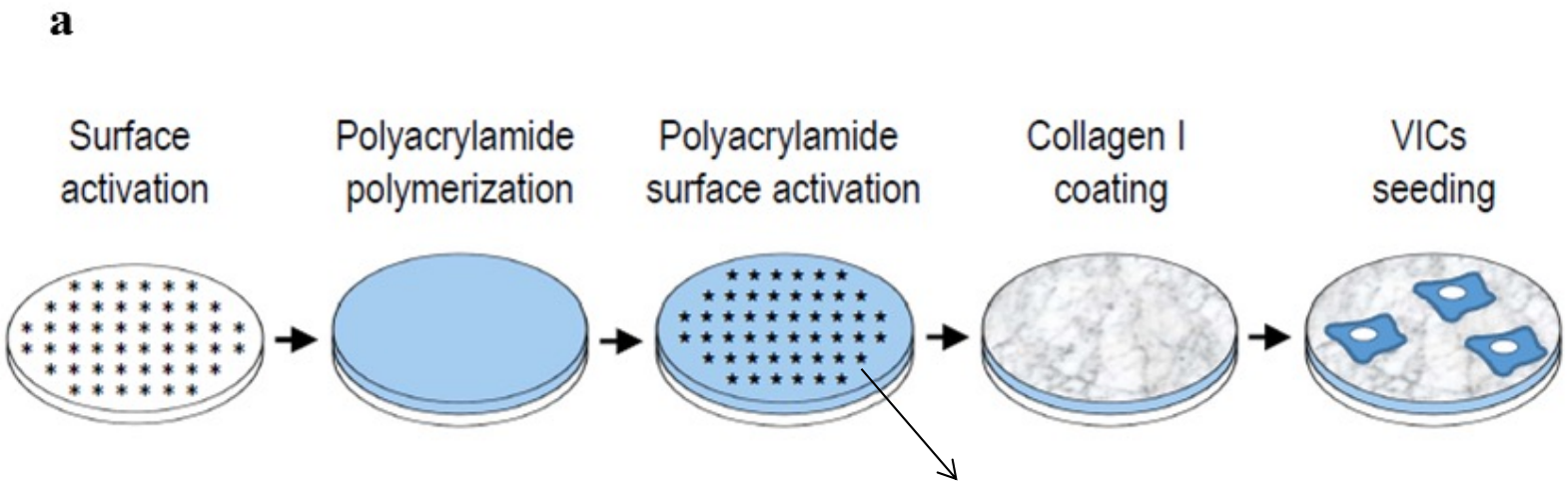

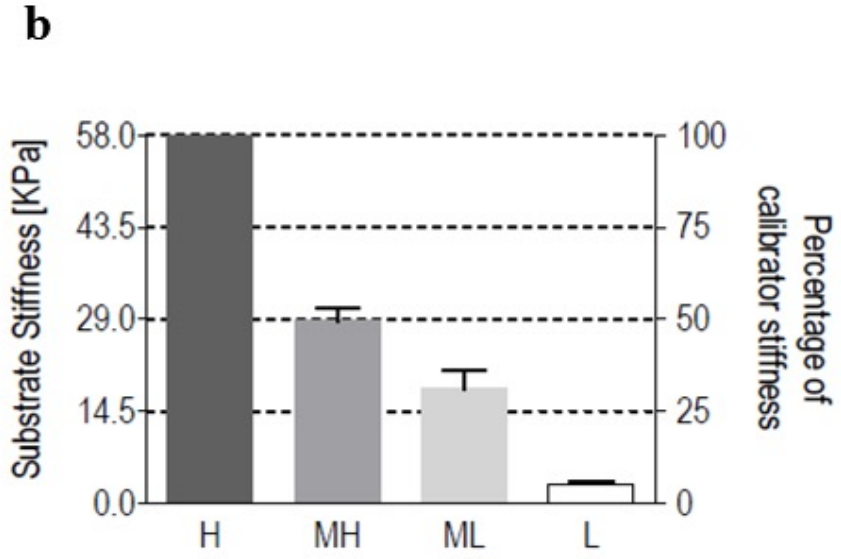

Cellular rigidity is determined by the rearrangement of the cytoskeleton

red: phalloidin; blue: DAPI; green: α-SMA;
white arrow: high levels of α-SMA and co-localization; yellow arrow: intermediate levels of α-SMA and co-localization; blue: low levels of α-SMA and co-localization;
purple arrow: no α-SMA

a

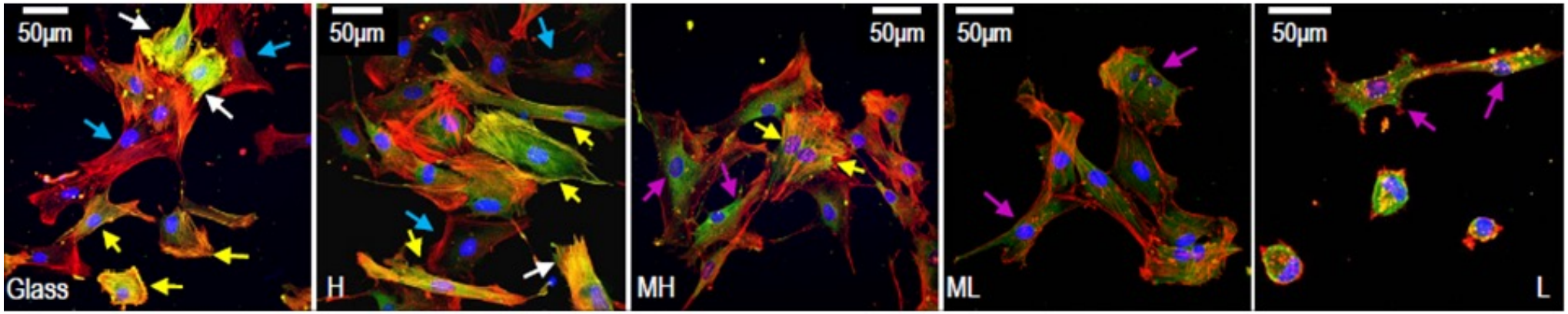

b

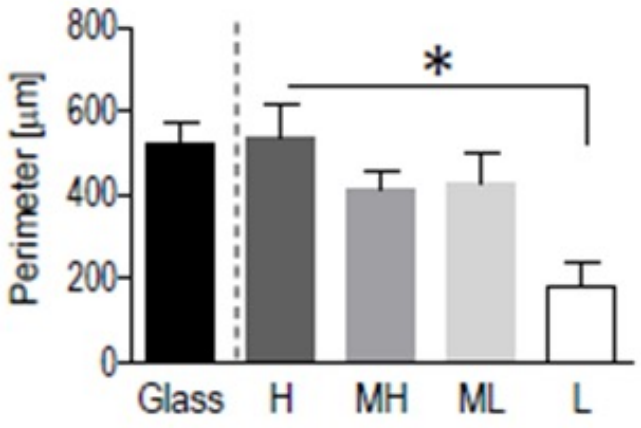

c

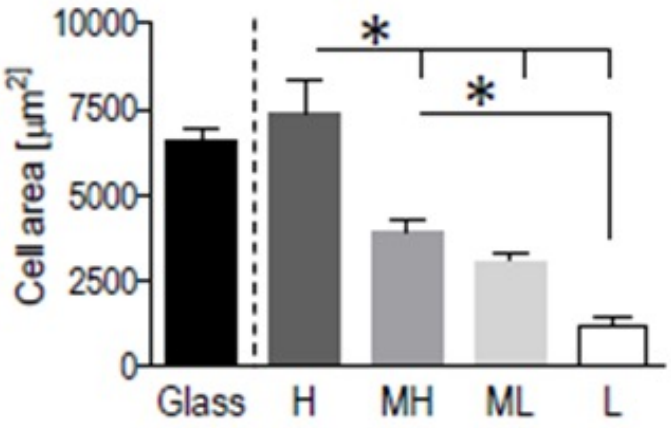

d

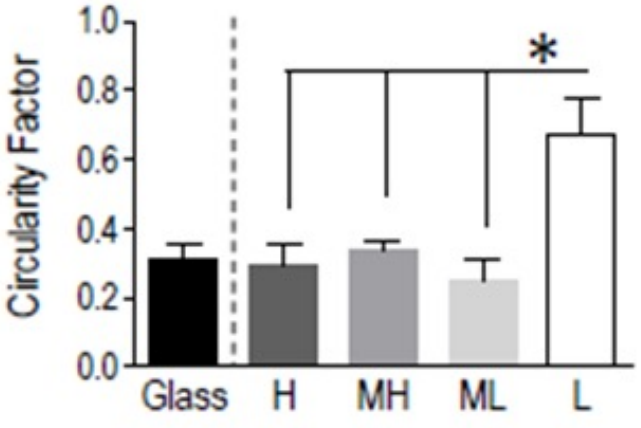

Rearrangement of the Cytoskeleton and cell stiffness

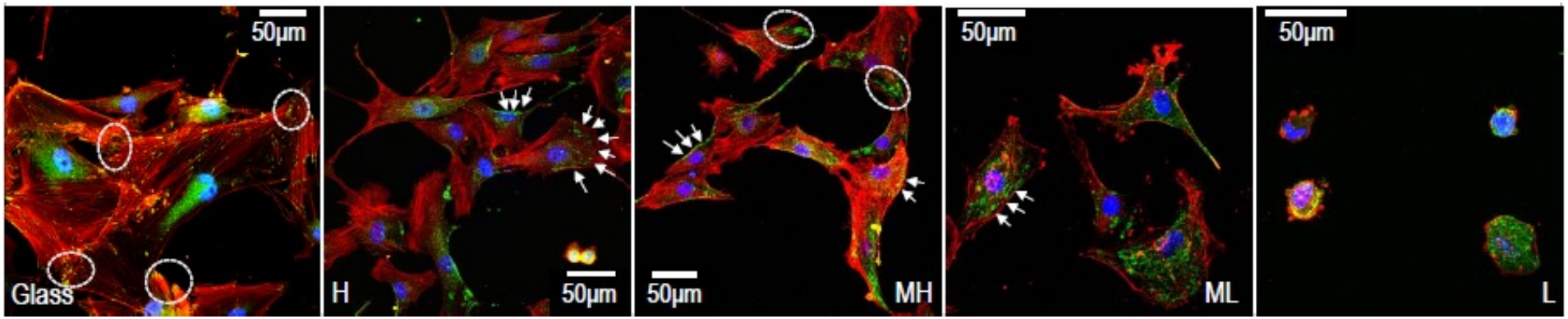

red: phalloidin; blue: DAPI; green: vinculin;

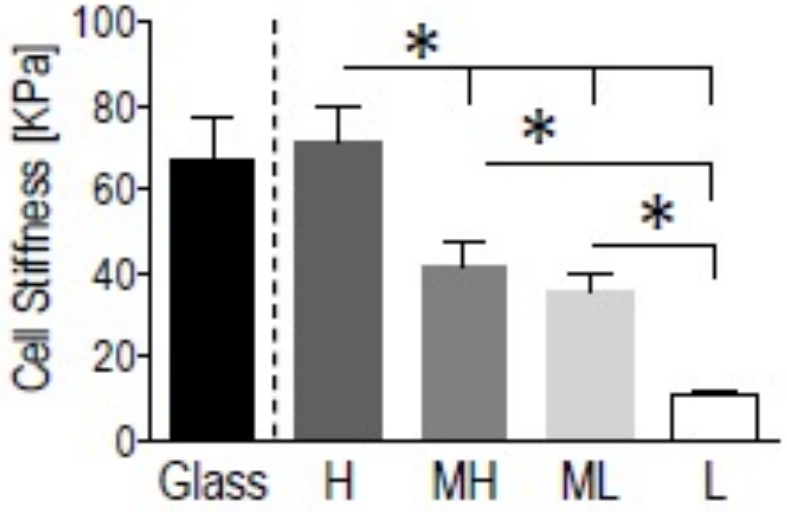

High cytoskeleton tensioning determines high levels of YAP nuclear localization

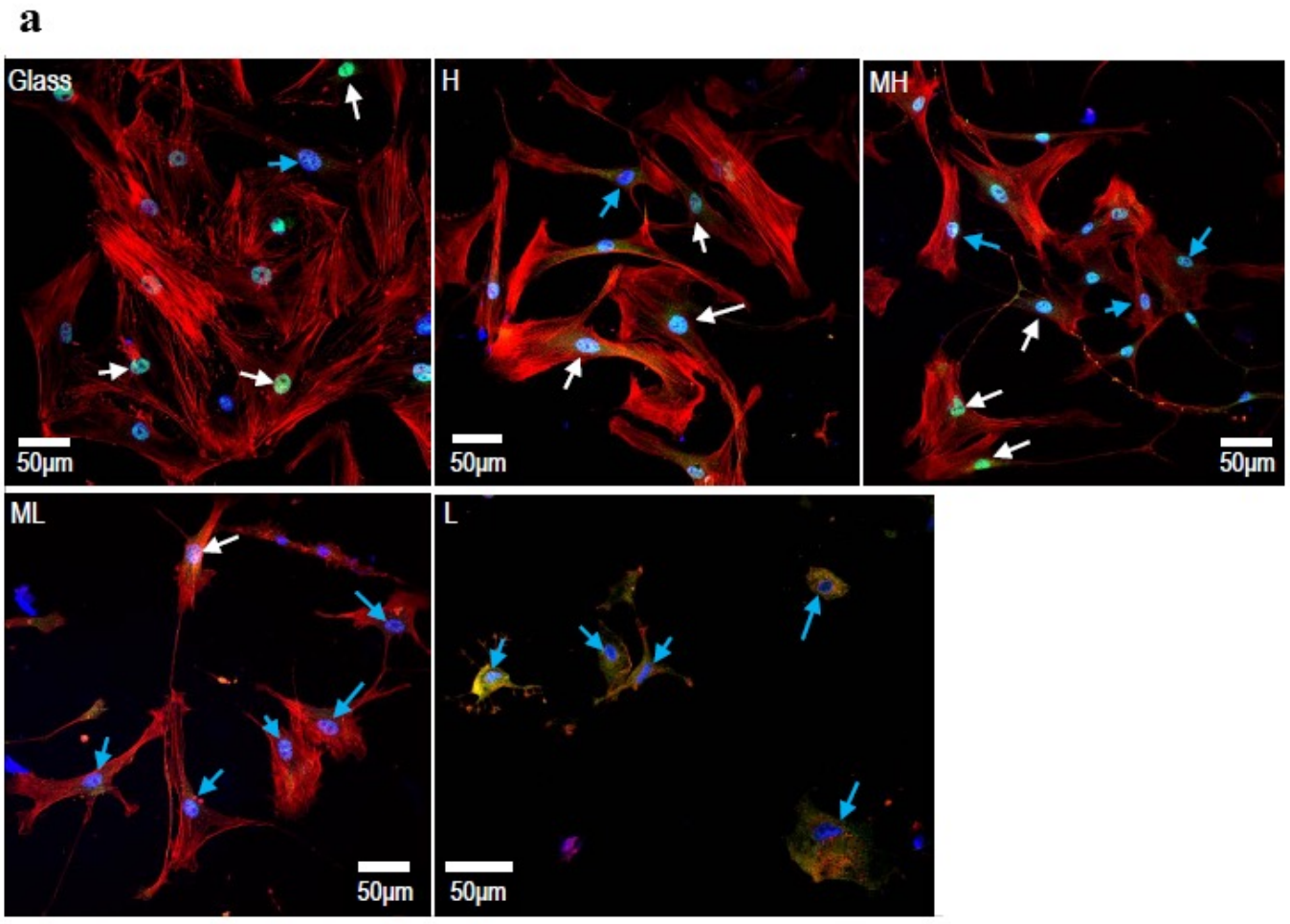

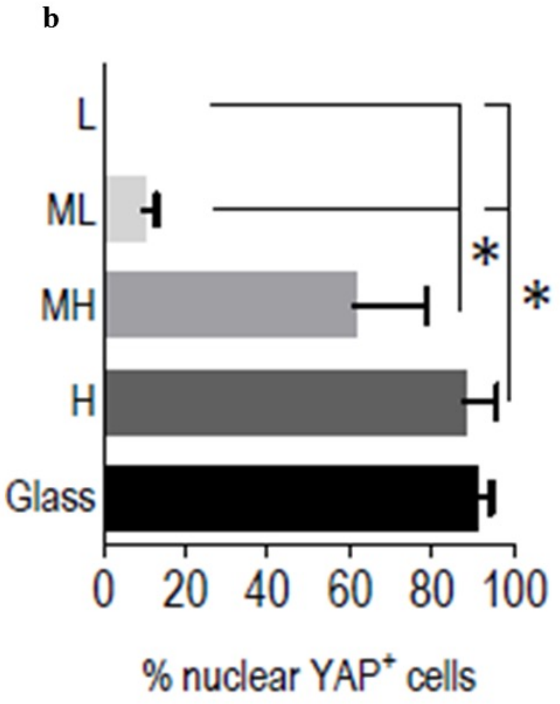

red: phalloidin; blue: DAPI; green: YAP

Atomic force microscopy of single virus shells

A. Ortega-Esteban,…J. Gomez-Herrero, Ultramicroscopy 114 (2012) 56-61

F. Moreno-Madrid, …Pedro J. de Pablo, Biochemical Society Transactions **(2017)** 45 **499–511**

Imaging of single soft objects in liquid: jumping mode AFM

Imaging of soft biological specimens method of choice extremely depend on the kind of sample.
Contact mode is adequate for scanning two dimensional protein crystals, such as purple membrane which can stand the high lateral forces exerted by the tip.
Conversely, individual weakly adsorbed biomolecules, such as small viruses, are prone to undesired modifications by lateral forces since they are not held and surrounded by a neighborhood

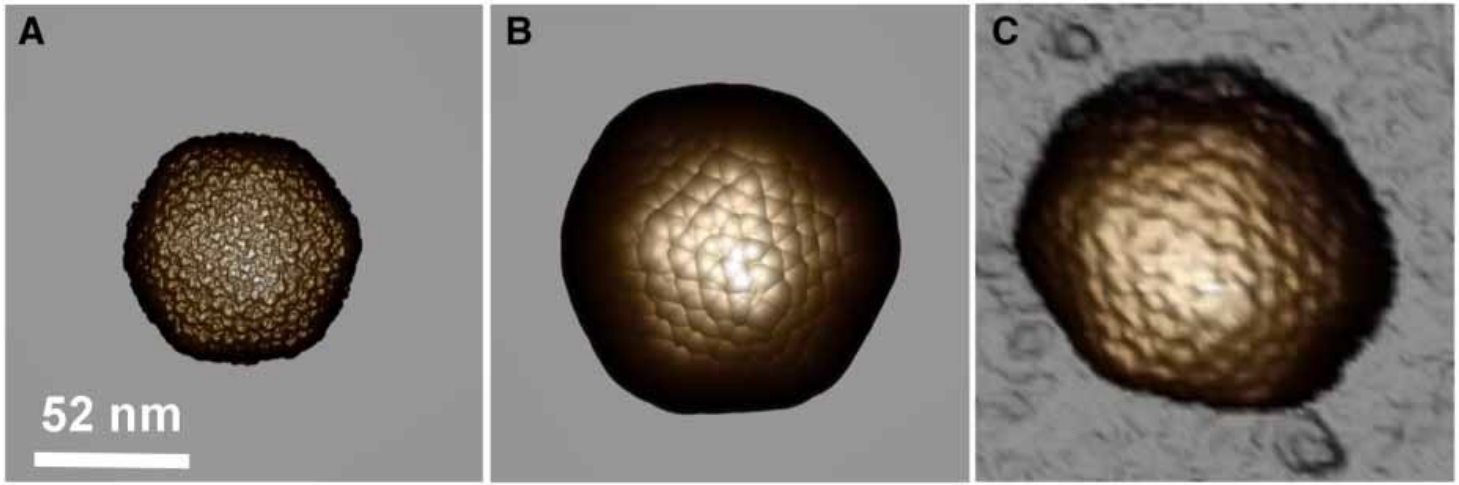

Imaging of single soft objects in liquid: jumping mode AFM

High resolution in dynamic mode requires a good control of the cantilever free oscillation, which is difficult on liquid, where the cantilever oscillation is the convolution of cantilever resonance and the mechanical resonance of the fluid cell ("forest of peaks"). As the liquid in the fluid cell changes shape, volume and composition throughout an experiment, these resonances shift, changing the tip-sample applied force.

New imaging modes needed!

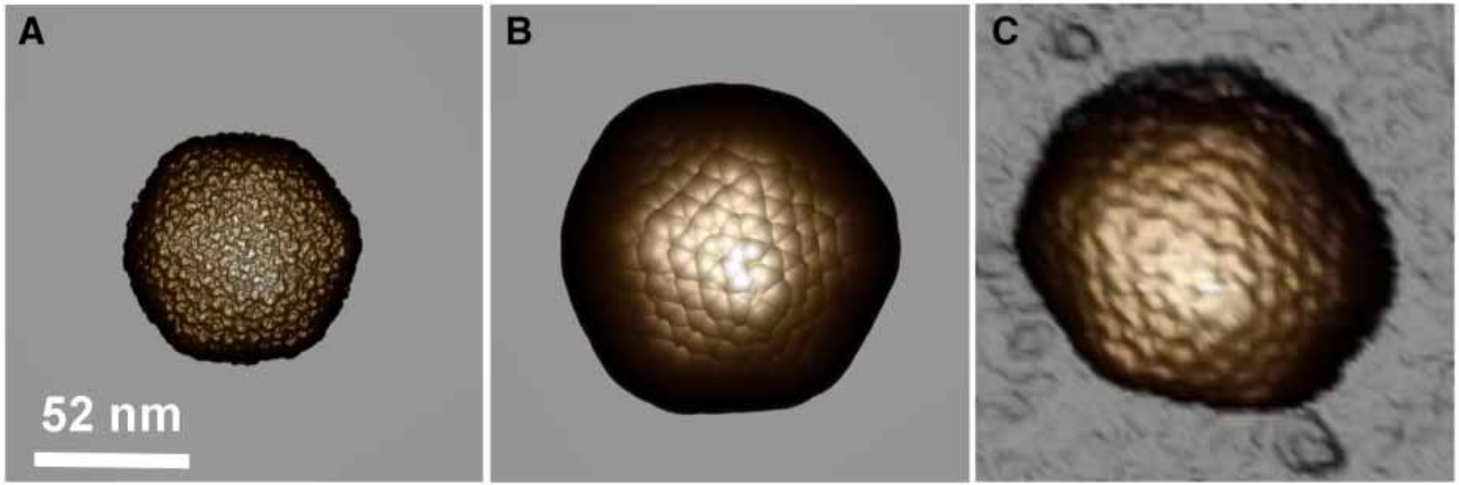

cantilever oscillation in liquid

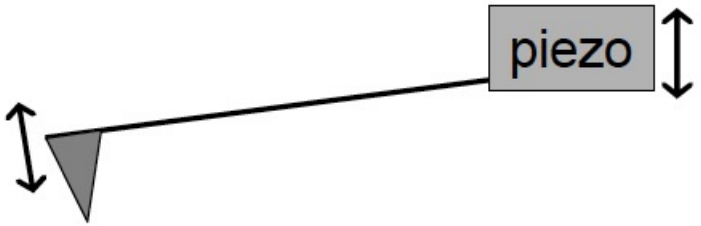

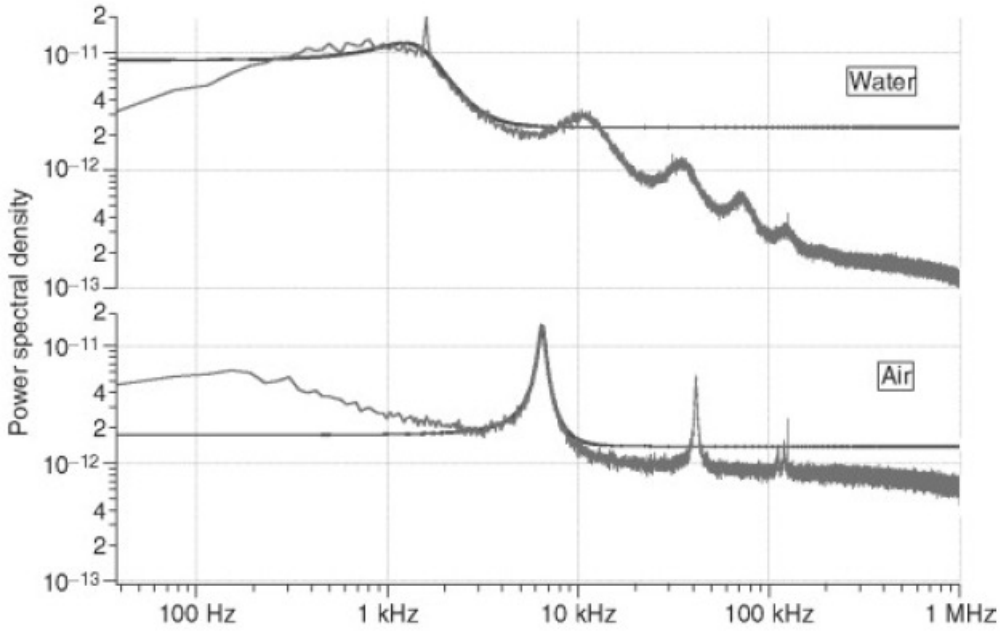

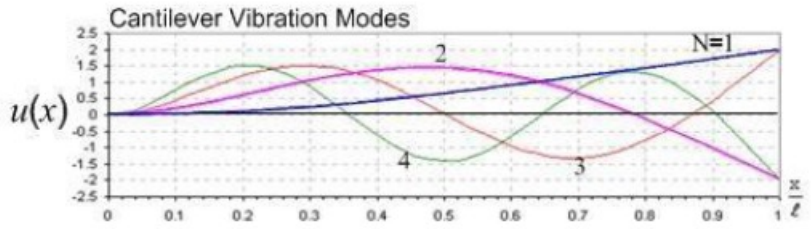

$$f_{0vacuum} = \sqrt{\frac{k}{m}} \Big/ 2\pi = \frac{t}{4\pi\, l^2} \sqrt{\frac{E}{\rho_{cantilever}}}$$

k = spring constant
m = mass
ρ = density
t = thickness cantilever
l = length cantilever

in water the viscous damping reduces both the resonance frequency and the Q-factor

resonance frequency (here 2 kHz) can limit imaging speed

Jumping mode or “peak force” AFM

Jumping-mode AFM: quick F-Z scan at each point of the scanned area, moving laterally the tip at the farthest tip-sample distance to minimize lateral forces.

In order to reduce piezoelectric resonance the FZ is performed using a sinusoidal voltage wave al low frequency (few kHz, i.e thousands F-Z curves per second) that is applied to the scanning piezoelectric.

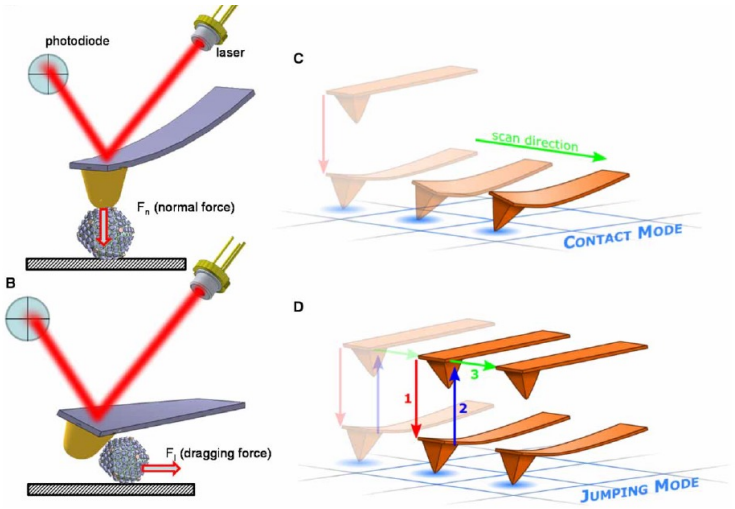

Figure 3. AFM working modes.
(**A** and **B**) The normal and lateral force concepts, respectively. (**C** and **D**) Contact and jumping modes, respectively.

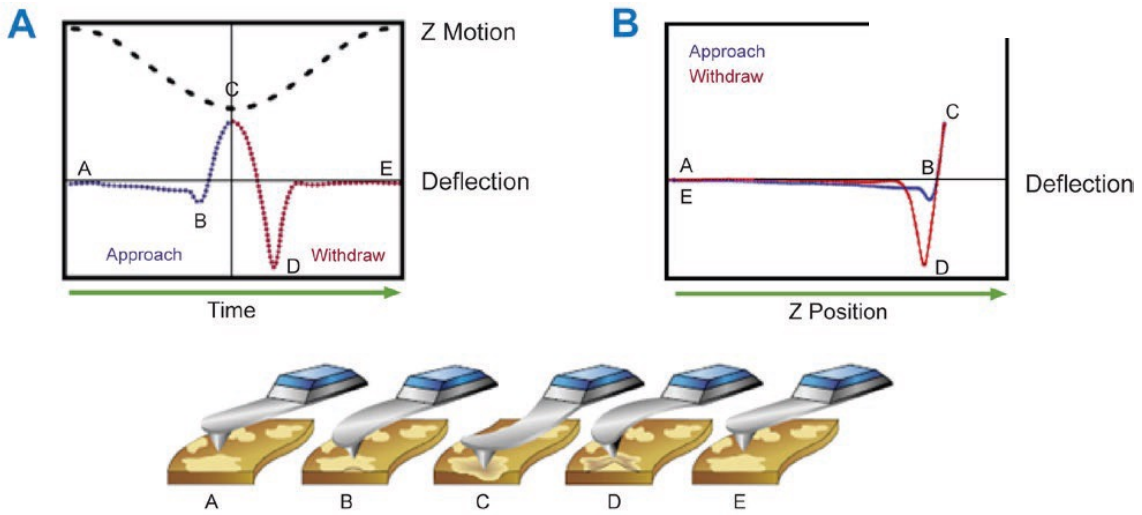

When the AFM probe is brought into contact with the sample surface, the tip-sample interaction is controlled by maintaining the maximum force, or “peak force,” between the tip and the sample constant

Jumping mode or “peak force” AFM

Undesirable characteristic of this procedure is that when the tip moves uphill its vertical excursion is overestimated and the sample is over-indented, resulting in an additional force that can damage delicate samples.

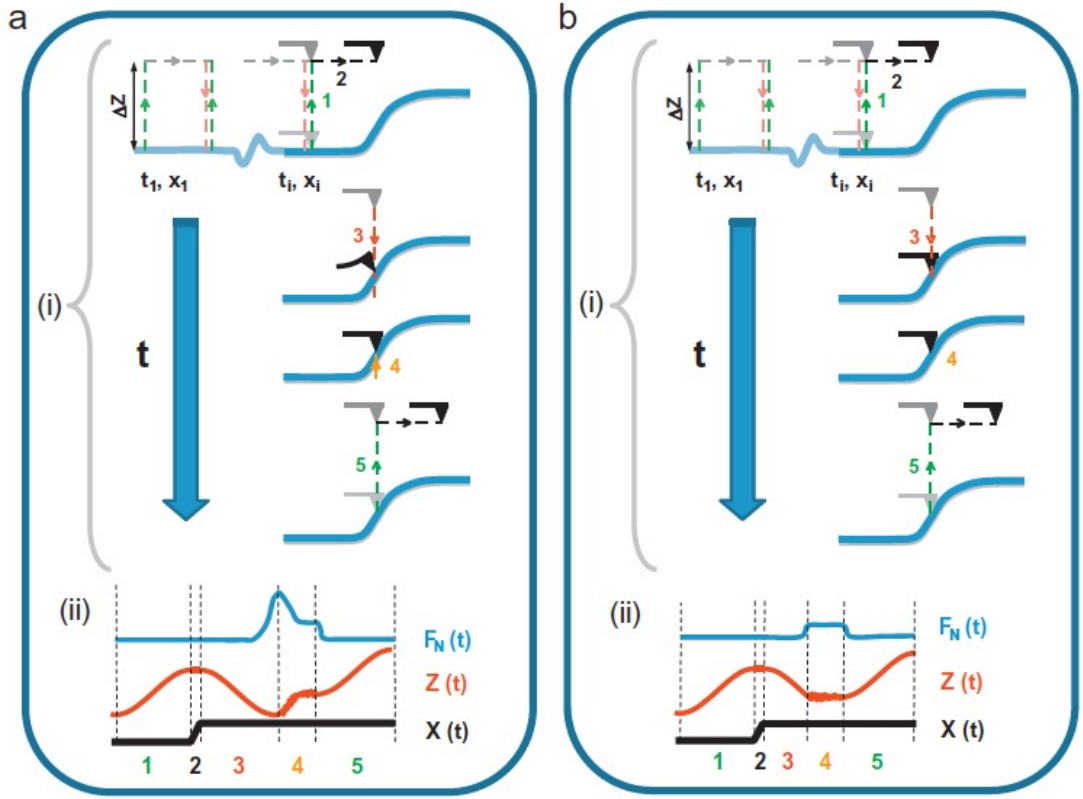

Remedy for that: instead of moving the tip a previously set distance z for the forward and backward cycles, check for the cantilever deflection as it is approached to the and stop it if the deflection is greater than the setpoint.
Spurious deflections coming from liquid viscous dragging forces can be limit this process, and can be reduced by slow JM acquisition or by acquiring and fitting the dragging force induced deflection and subtracting it from the total deflection curve.

Jumping mode or “peak force” AFM

JM is particularly suitable for scanning in liquids, where the low adhesion forces allow using small Z displacement at each point. Because of the oscillation damping in liquid in amplitude modulation modes (NC, Tapping), JM although slow can give better performance.
N.B.: Dynamic modes use as feedback the oscillation amplitude. JM the cantilever deflection! Like in contact mode…easier. Is like a CM with the fine tuning of the zero interaction force

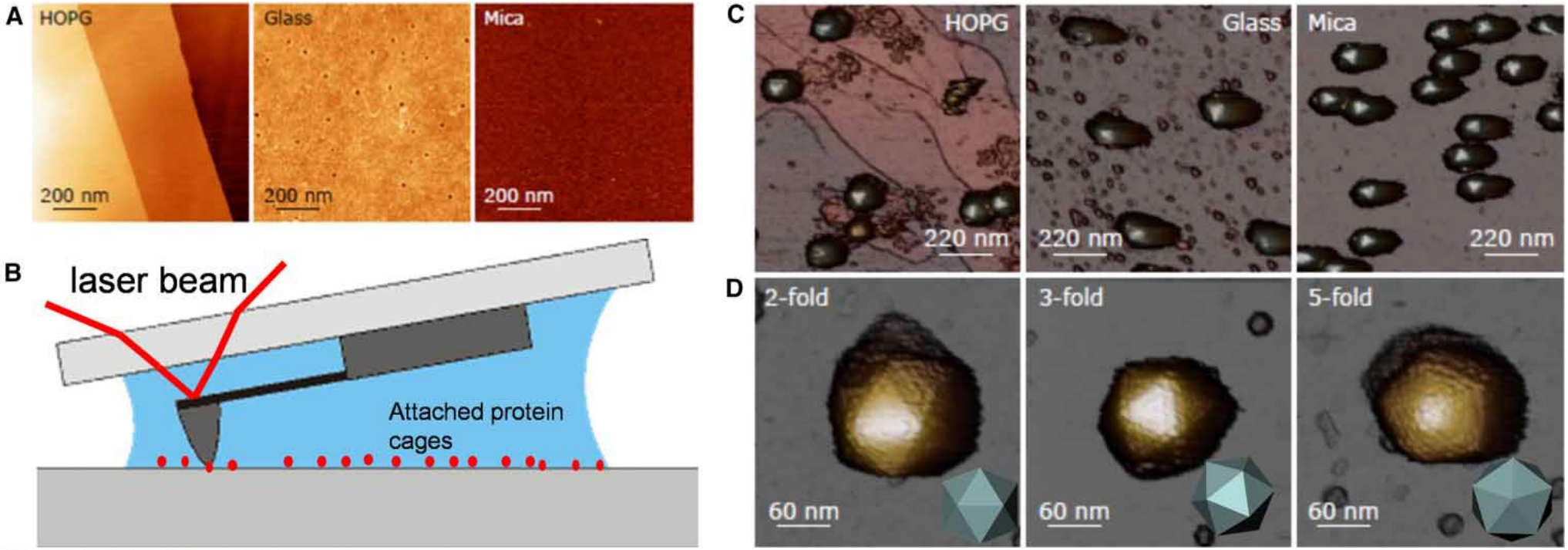

Figure 1. Attaching protein shells on surfaces.
(**A**) HOPG, glass, and mica bare substrates before attaching the samples. (**B**) Cartoon of the experimental system. Protein cages and cantilever are not in scale. (**C**) HAdv on HOPG, glass, and mica. (**D**) Individual HAdv particles showing 2-fold, 3-fold, and 5-fold symmetry axis orientations after adsorption on the surface.

HAdV has a 95 nm diameter icosahedral, non enveloped capsid enclosing a ds DNA genome

Jumping mode or “peak force” AFM

JM is particularly suitable for scanning in liquids, where the low adhesion forces allow using small Z displacement at each point. Because of the oscillation damping in liquid in amplitude modulation modes (NC, Tapping), JM although slow can give better performance.
N.B.: Dynamic modes use as feedback the oscillation amplitude. JM the cantilever deflection! Like in contact mode…easier. Is like a CM with the fine tuning of the zero interaction force

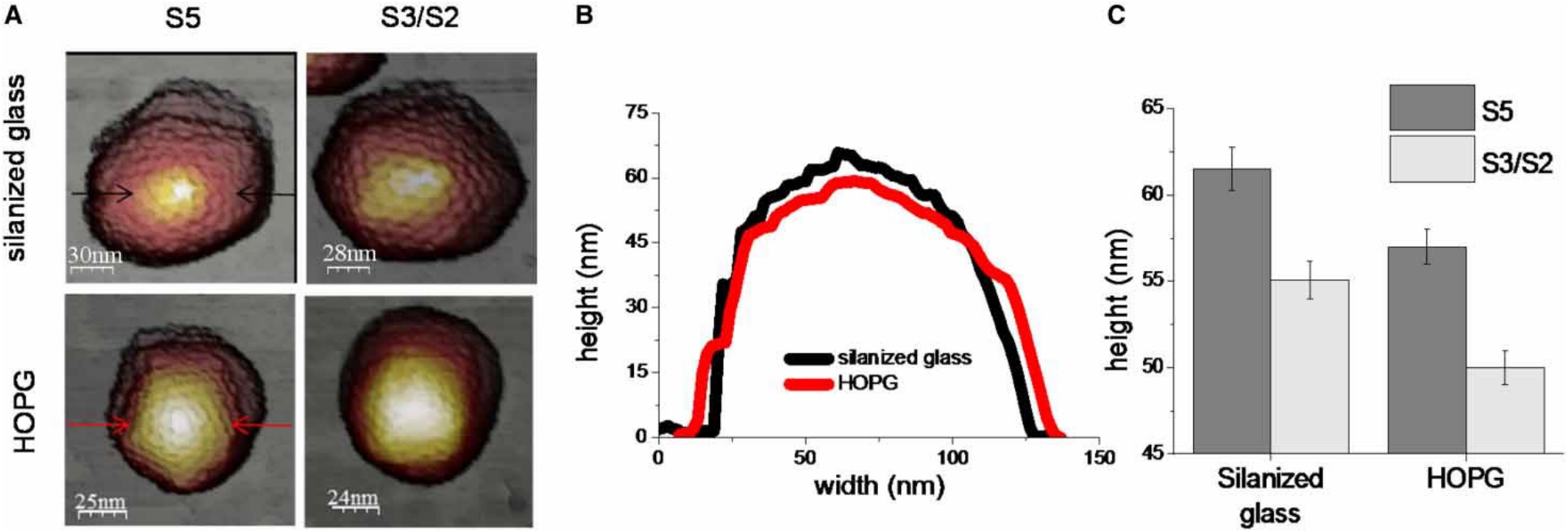

Figure 2. Protein shells collapse on the surface.
(**A**) P22 bacteriophage particles on glass and HOPG oriented to 5-fold and 3-/2- fold symmetry axes. (**B**) Comparison of topographical profiles obtained on two particles adsorbed on glass (black) and HOPG (red) obtained from **A**. (**C**) Comparison of average height of particles adsorbed at different orientations and substrates.

Jumping mode AFM

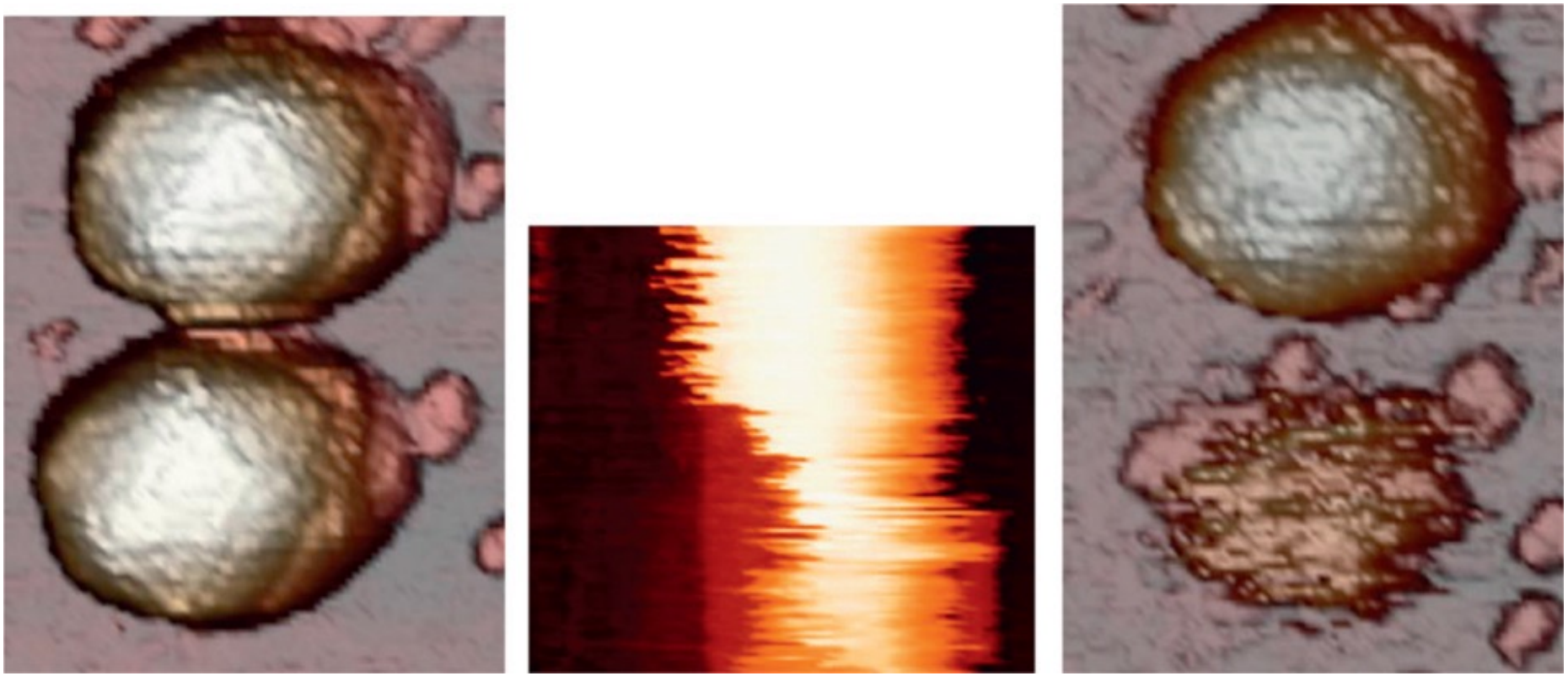

Fig. 4. (a) 250 nm × 330 nm AFM topography image of two HAdV particles acquired with JM+. (b) Time evolution (downwards) of the topography at the dashed line of figure (a). At the horizontal solid line the new algorithm is switched off, reverting to conventional JM. Notice the sudden change in the scanning profile. (c) Subsequent imaging of the same area with JM+ procedure demonstrates total destruction of the scanned virus while the other particle remains unmodified. Set point 150 pN.

under the new JM procedure, HAdV particles can be scanned for a long time without significant damage.

Jumping mode AFM

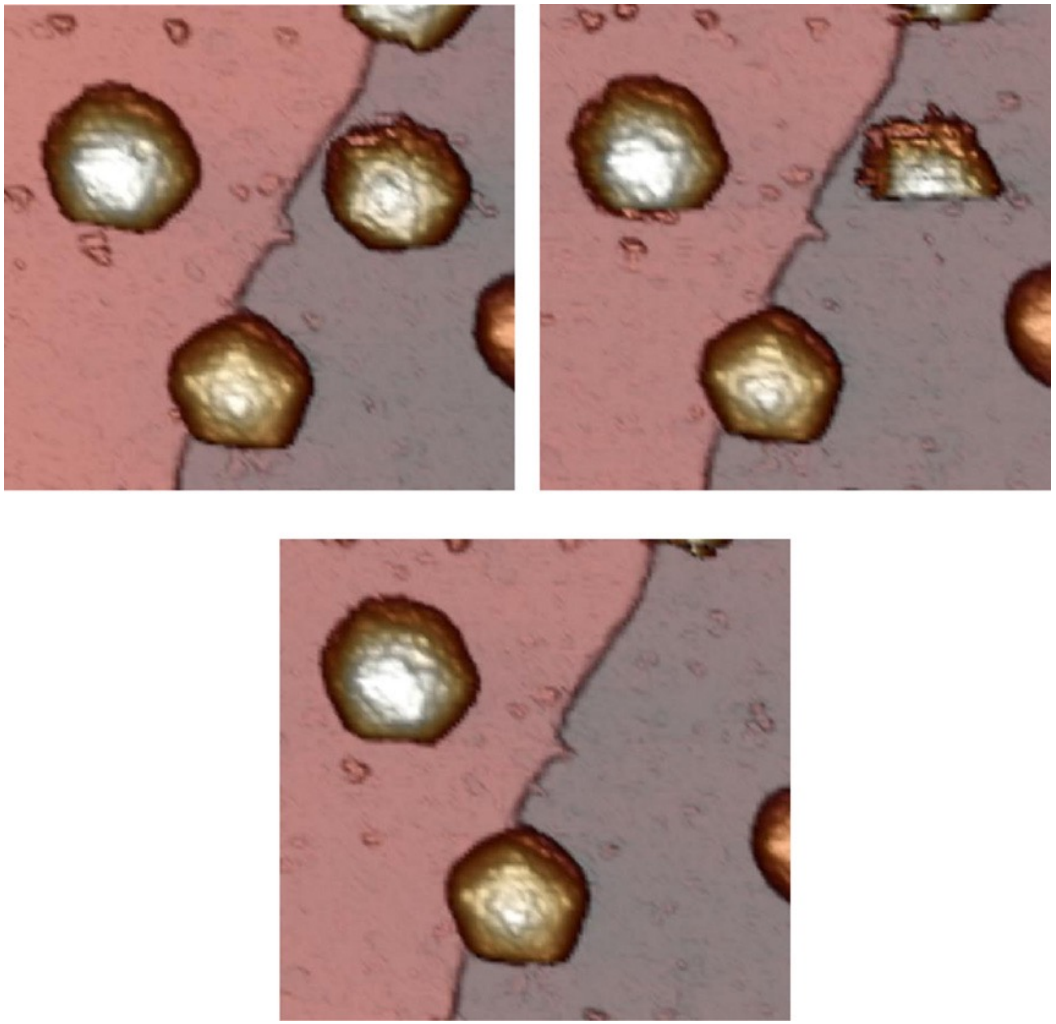

Bacteriophage T7 has an icosahedral capsid around 51nm diameter, with a triangu lation number T=7, and a non-contractile tail. The shell is made of 415 copies of the gp10protein that encloses a dsDNA 40 kb in size.

Fig. 5. (a) 500 nm × 500 nm AFM topography image acquired applying the new algorithms of bacteriophage T7. (b) When JM+ is switched off a particle is detached (circled particle in Fig. 5a). (c) Switching back to JM+ confirms that the particle has been completely removed. Set point 115 pN.

Imaging of single virus particles on different surfaces

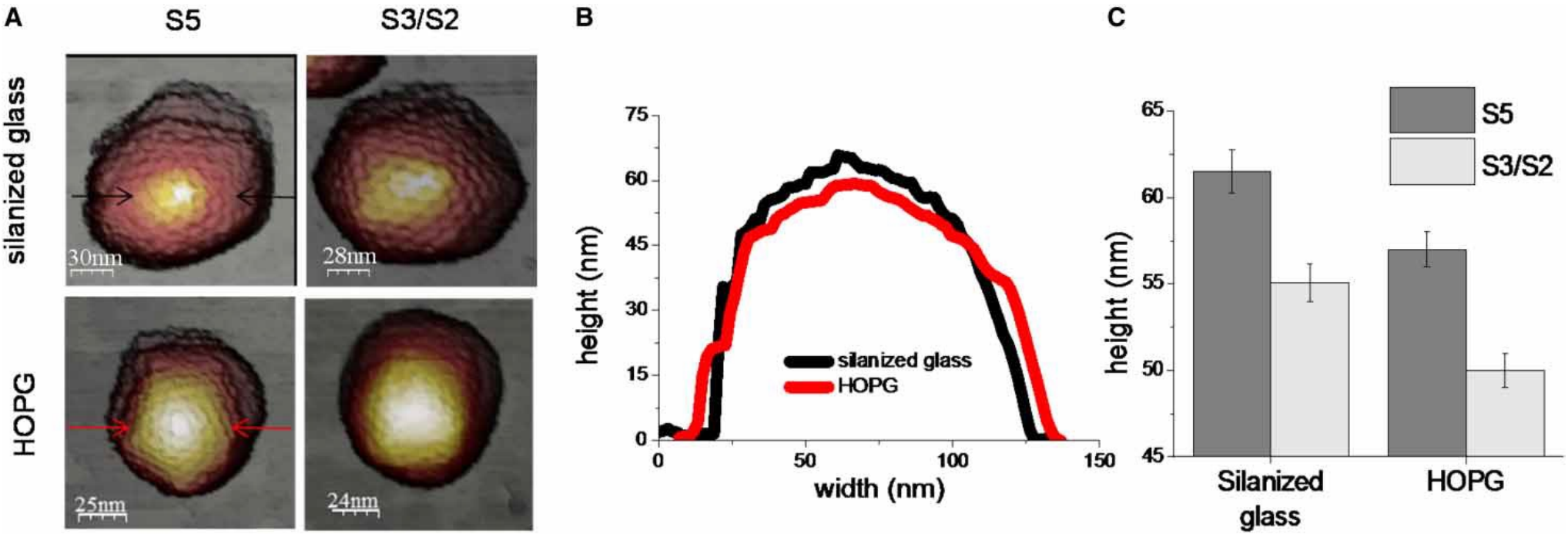

Figure 2. Protein shells collapse on the surface.

(**A**) P22 bacteriophage particles on glass and HOPG oriented to 5-fold and 3-/2- fold symmetry axes. (**B**) Comparison of topographical profiles obtained on two particles adsorbed on glass (black) and HOPG (red) obtained from **A**. (**C**) Comparison of average height of particles adsorbed at different orientations and substrates.

Figure 5. Dilation effects in the protein shell of bacteriophage P22.

(**A**) The EM-1826 model of P22 bacteriophage oriented to the 2-fold symmetry axis. (**B**) Dilated data of (**A**) obtained with a tip of 10 nm in diameter by using the dilation algorithm of the WSxM software. (**C**) AFM image of a single P22 bacteriophage oriented to the 2-fold symmetry axis. The cartoon of (**D**) indicates the dilation as a function of the tip size: black, red, and blue curves are the topographical profiles obtained with tips of 0.5, 10, and 15 nm in diameter, respectively.

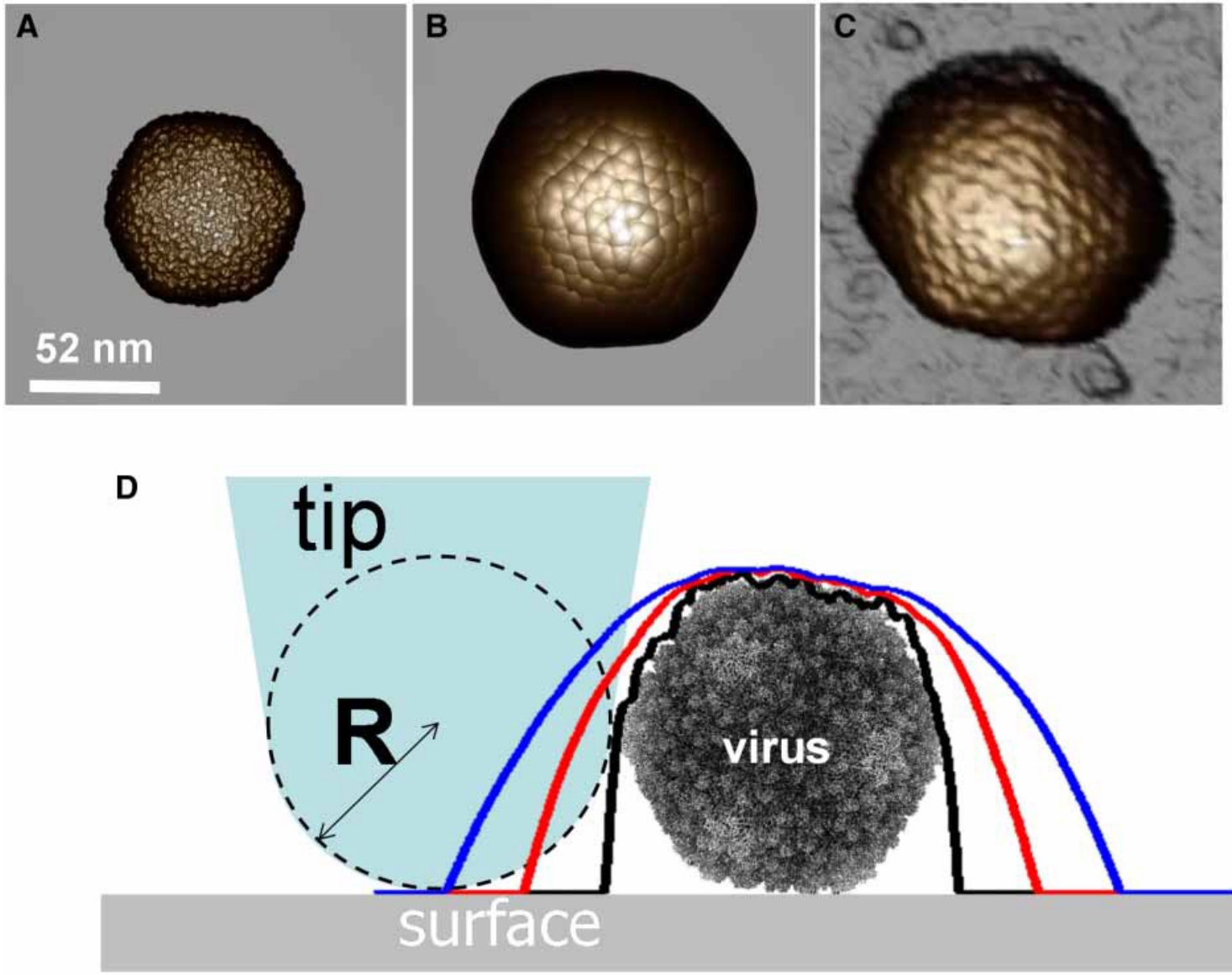

Nanoindentation

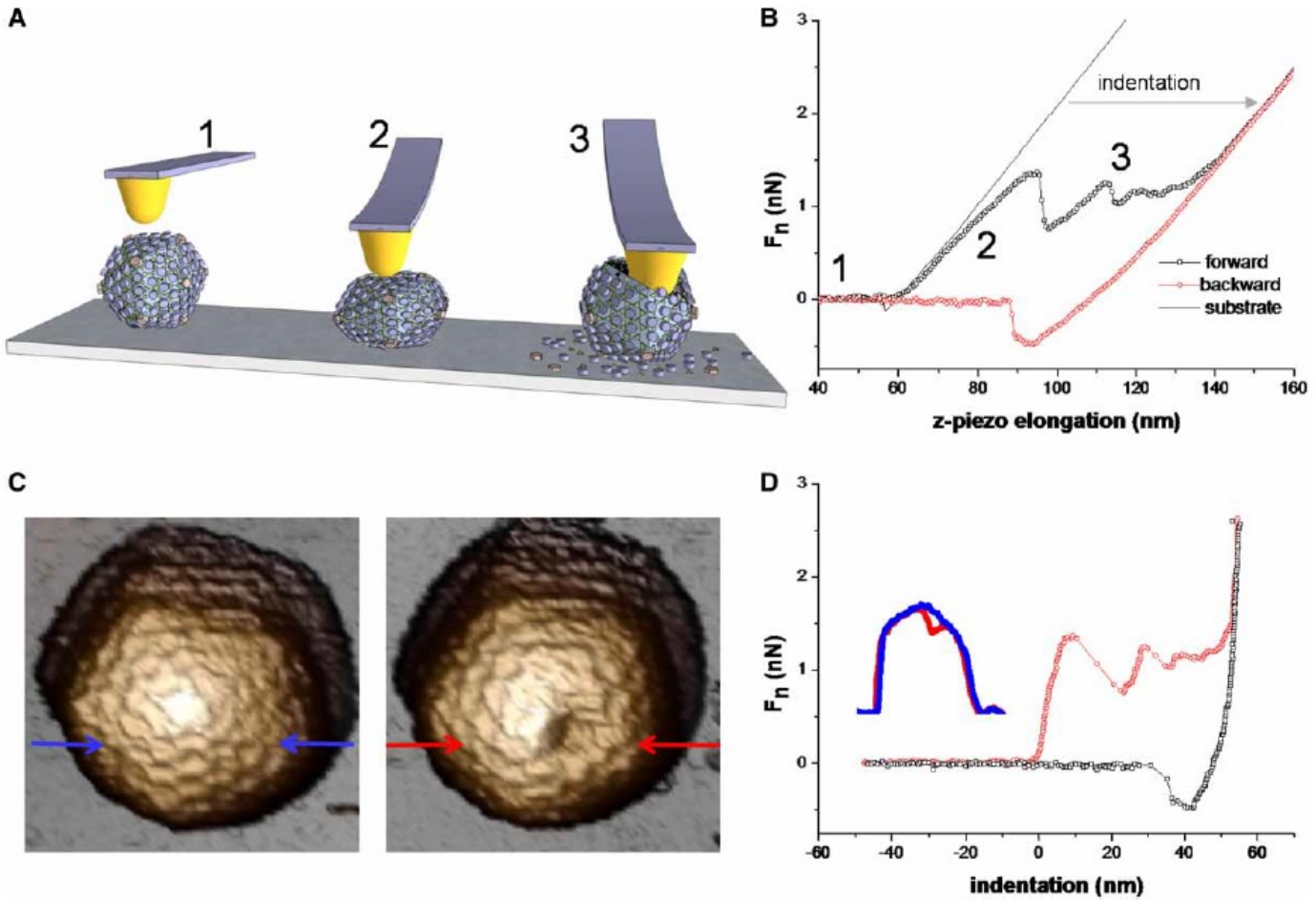

Figure 6. Single indentation assay.

The subtraction of sample from substrate curves allows isolating the deformation of the cage (Figure 6D)

Stiffness or spring constant: obtained by fitting the elastic part from 0 to 8 nm (k = 0.18 N/m);
breaking or yield force: force value when the elastic regime f nishes at 8 nm (Fb = 1.4 nN),
critical indentation δc :deformation of the virus when it breaks (8 nm).
Thin shell theory relates the protein shell stiffness with the Young' s modulus as k Et2=R , where t is the thickness of the shell and R is its radius

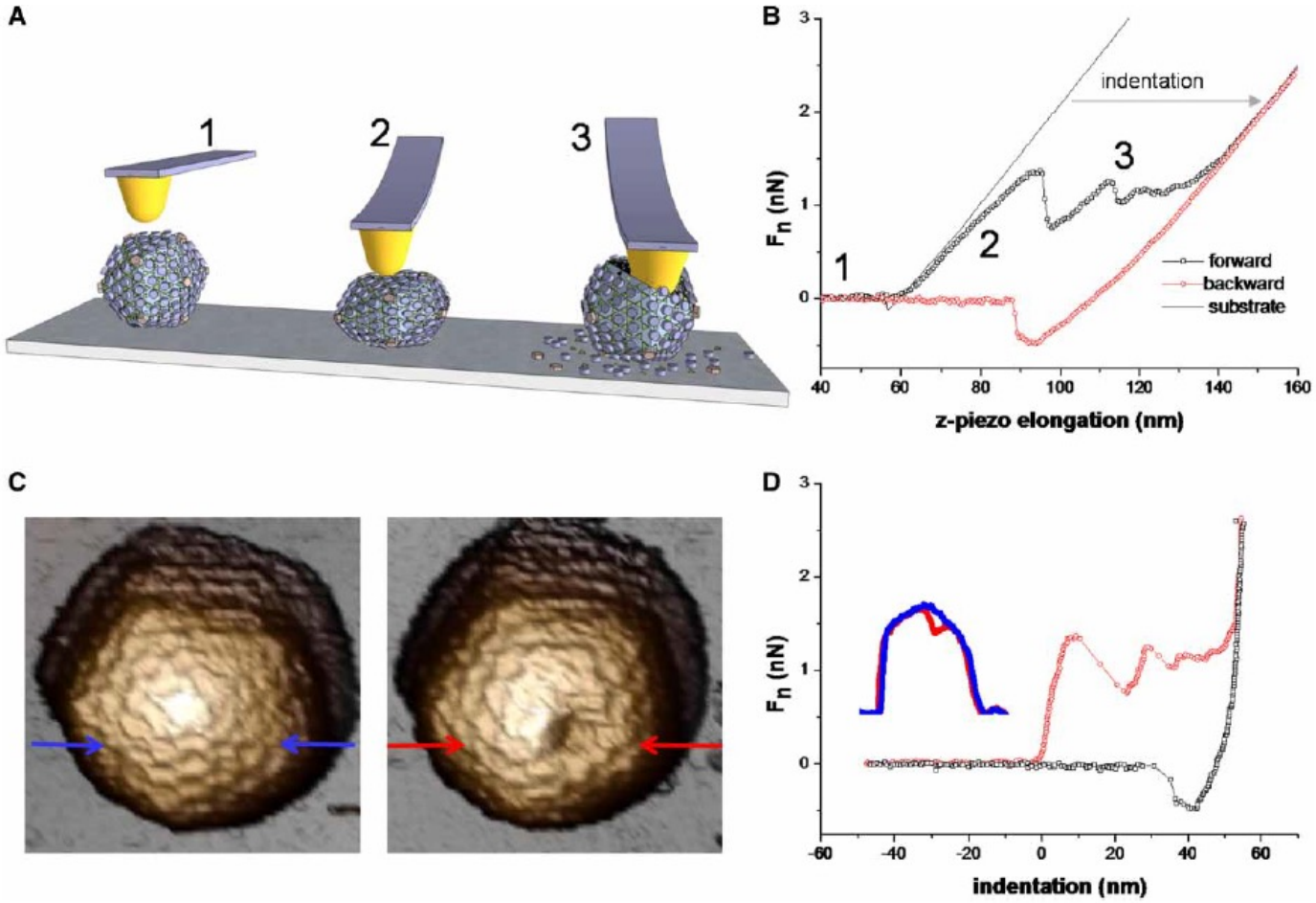

Figure 6. Single indentation assay.

The area enclosed between forward and backward curves from indentation 0 up to 8 nm is the energy used to break the cage. In this case, it is about 8.8 nm x nN, i.e. 8.8 x 10^{-18} J or 2141$\mathbf{k_BT}$, which approaches the order of magnitude of the total energy for assembling all the proteins

The precise control of nanoindentation permits access to the inner cargo of protein cages. For instance, the consecutive application of nanoindentaion cycles in human adenovirus cracks open the shell in a controlled fashion to probe the mechanical properties of the core. These mechanical properties are related with the condensation state of dsDNA.

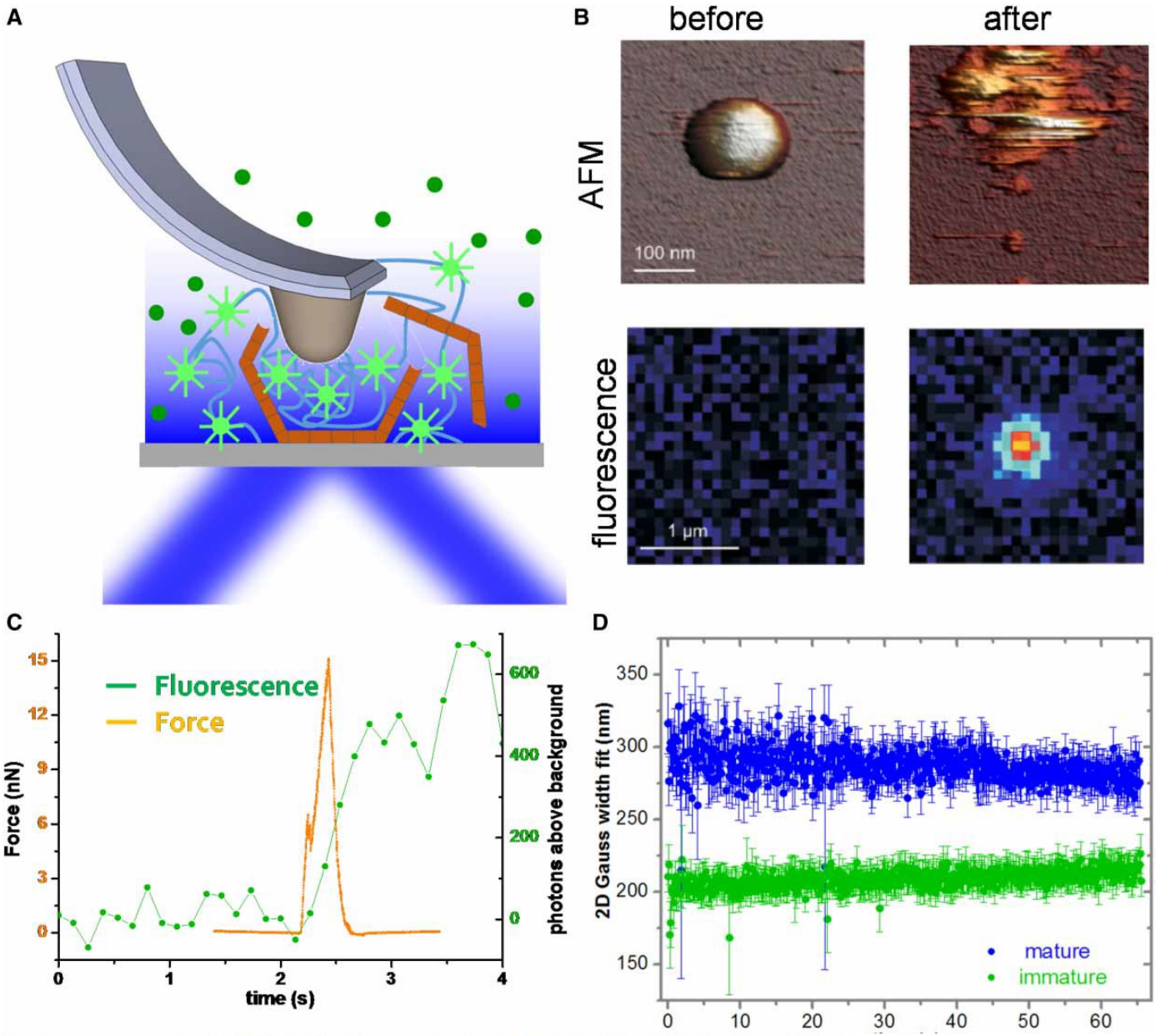

Figure 8. AFM/fluorescence combination for monitoring mechanical unpacking.

(**A**) Sketch of AFM/fluorescence combination for monitoring the access of YOYO-1 to released DNA. (**B**) AFM and fluorescence data of an HAdv particle before and after releasing DNA. (**C**) Simultaneous force (orange) and fluorescence (green) data during a nanoindentation experiment that disrupted the particle and released DNA. (**D**) Evolution of the fluorescence signal along time after particle disruption for mature (blue) and immature (green) particles (adapted from ref. [60]).

Other scanning probe microscopies

Scanning Ionic Current Microscopy (SICM)

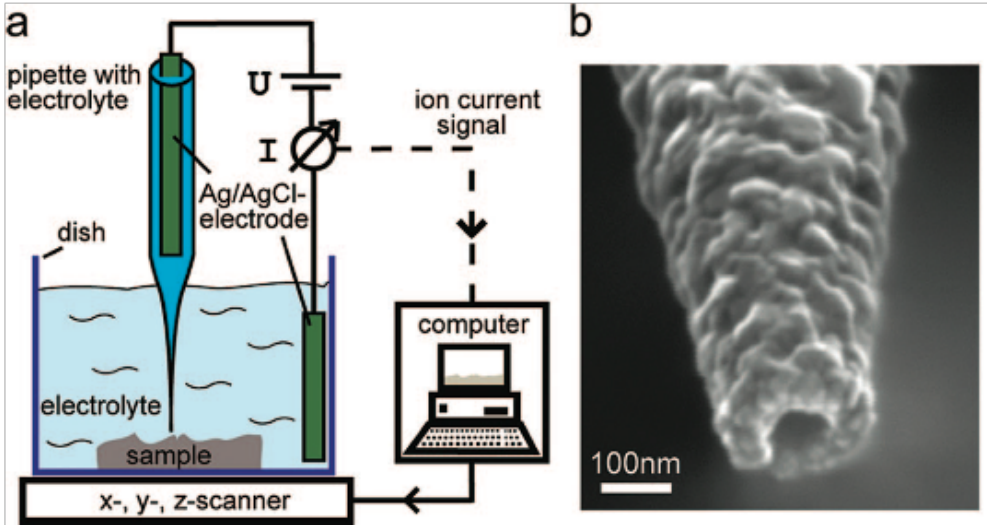

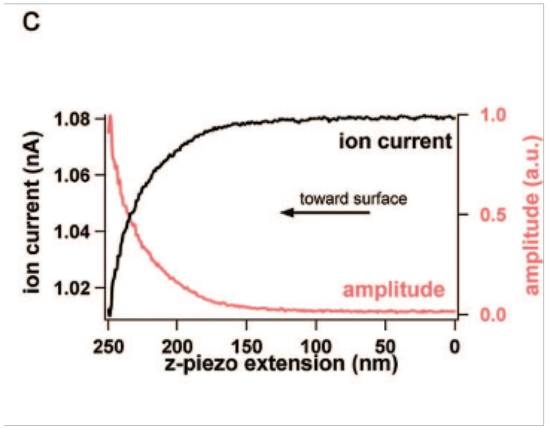

hart Patch Clamp 32

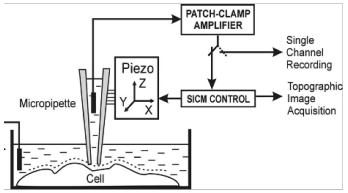

GURE 1 Schematic diagram of the scanning patch-clamp setup. The cropipette is mounted on a three-axis piezo actuator controlled by a nputer. The ion current that flows through the pipette is measured by a ch-clamp amplifier, and it is used for the feedback control to keep a nstant distance between the micropipette and the sample during scan- g. Upon completion of the scanning procedure, computer control is used position the micropipette at a place of interest based on the topographic age acquired, and finally the same patch-clamp amplifier is used for ctrophysiological recording.

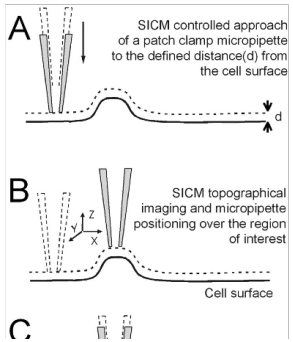

hopping probe Scanning ion conductance microscopy (HP-SICM)

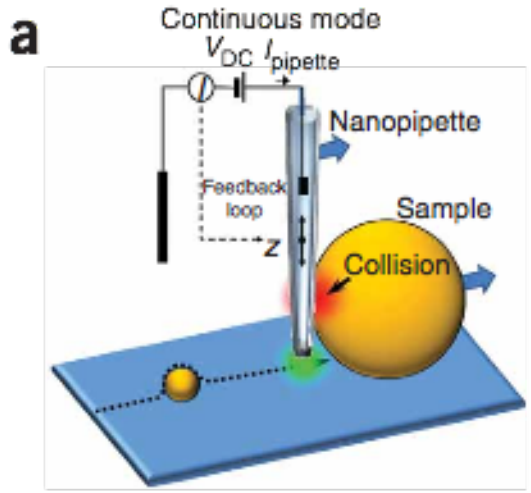

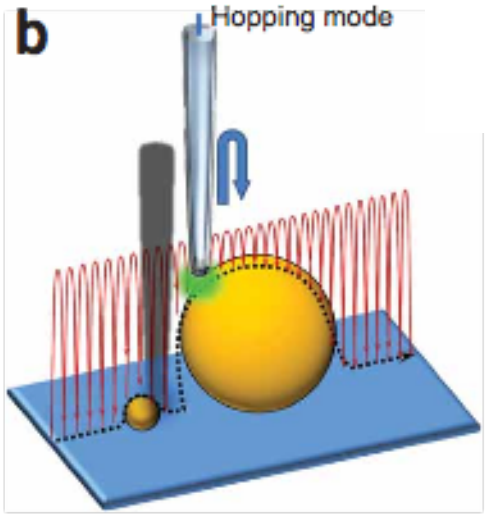

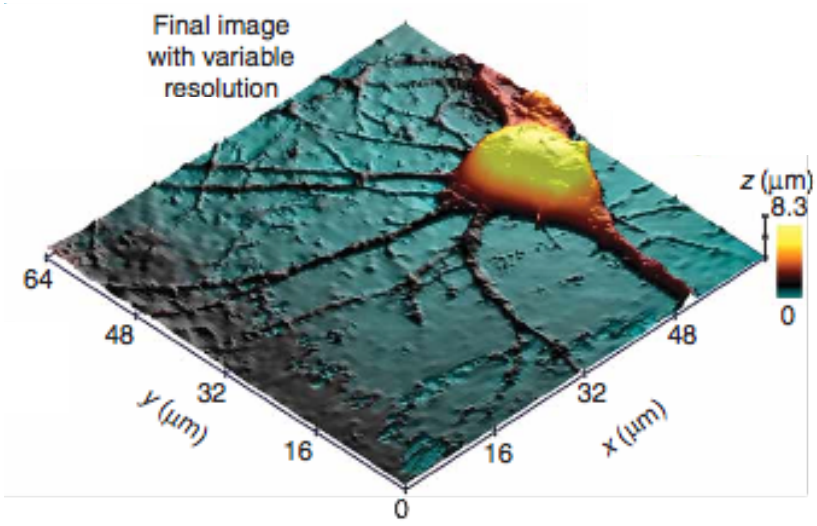

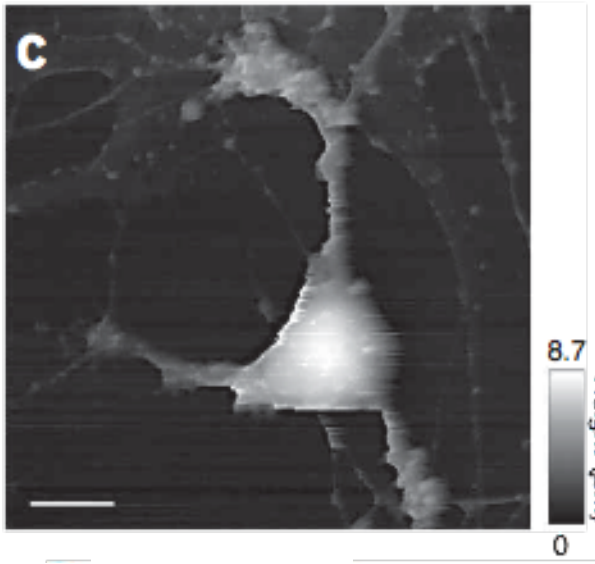

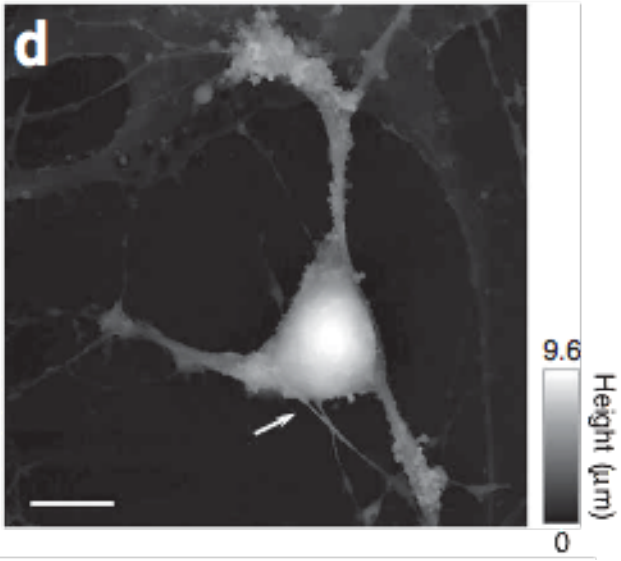

1. Novak, P. *et al.* Nanoscale live-cell imaging using hopping probe ion conductance microscopy. *Nat Meth* **6**, 279–281 (2009).

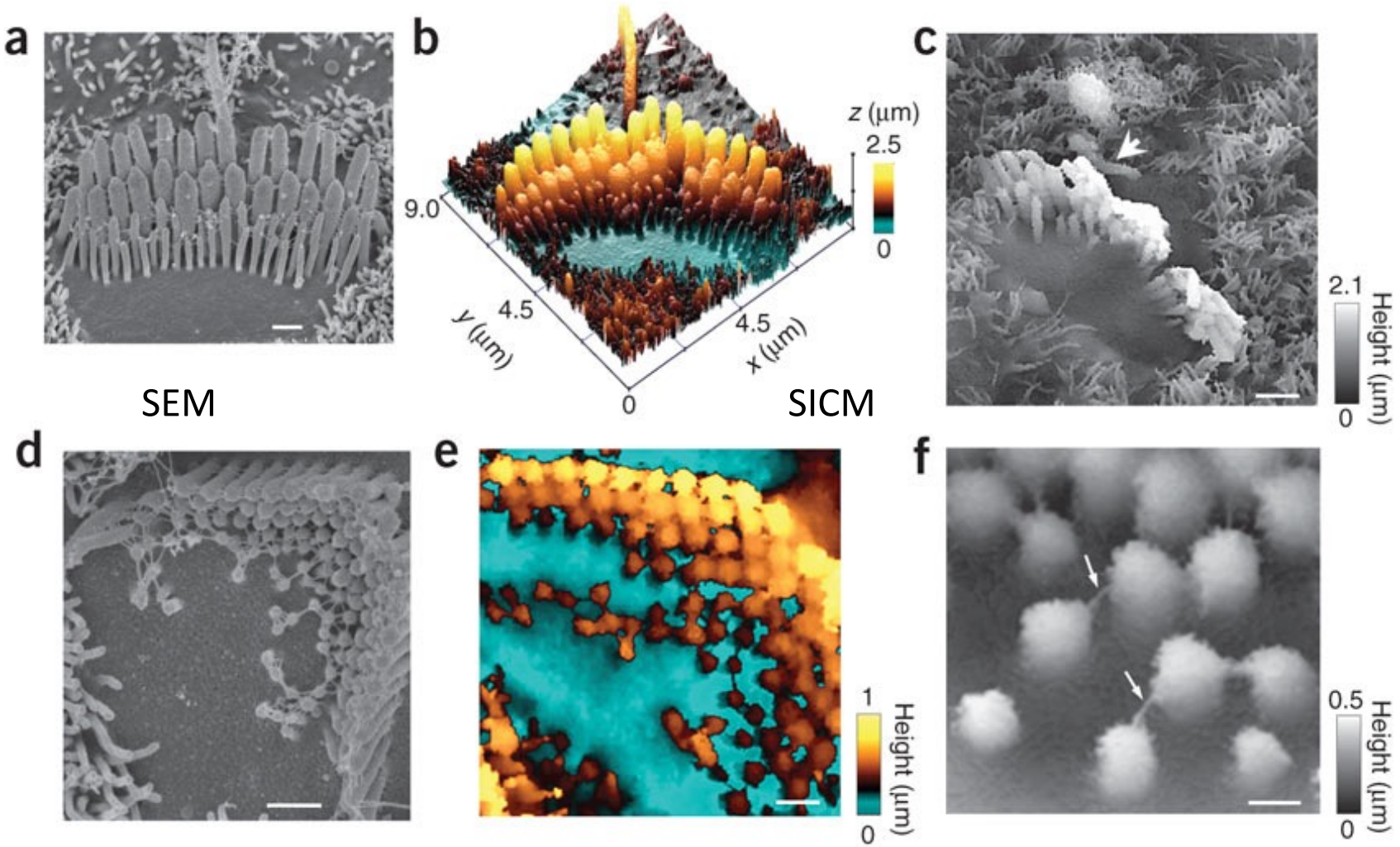

Visualization of vertically protruding **mechanosensitive stereocilia of auditory hair cells**. (a–c) Stereocilia of wild-type inner hair cells. Arrow indicates a kinocilium (a true cilium).
(d–f) Stereocilia of outer hair cells in young postnatal Shaker 2 **mice** with the extracellular filaments interconnecting stereocilia (arrows). All hair cells were approximately at the middle of the cochlea. Images of the cultured organs of Corti from the same mouse were obtained with SEM (a,d) and HPICM (b,c,e,f). Three-dimensional topographical rendered images are presented in colorscale (b,e) or grayscale (c,f). Scale bars, 500 nm (a,d,e), 1 μm (c) and 200 nm (f).

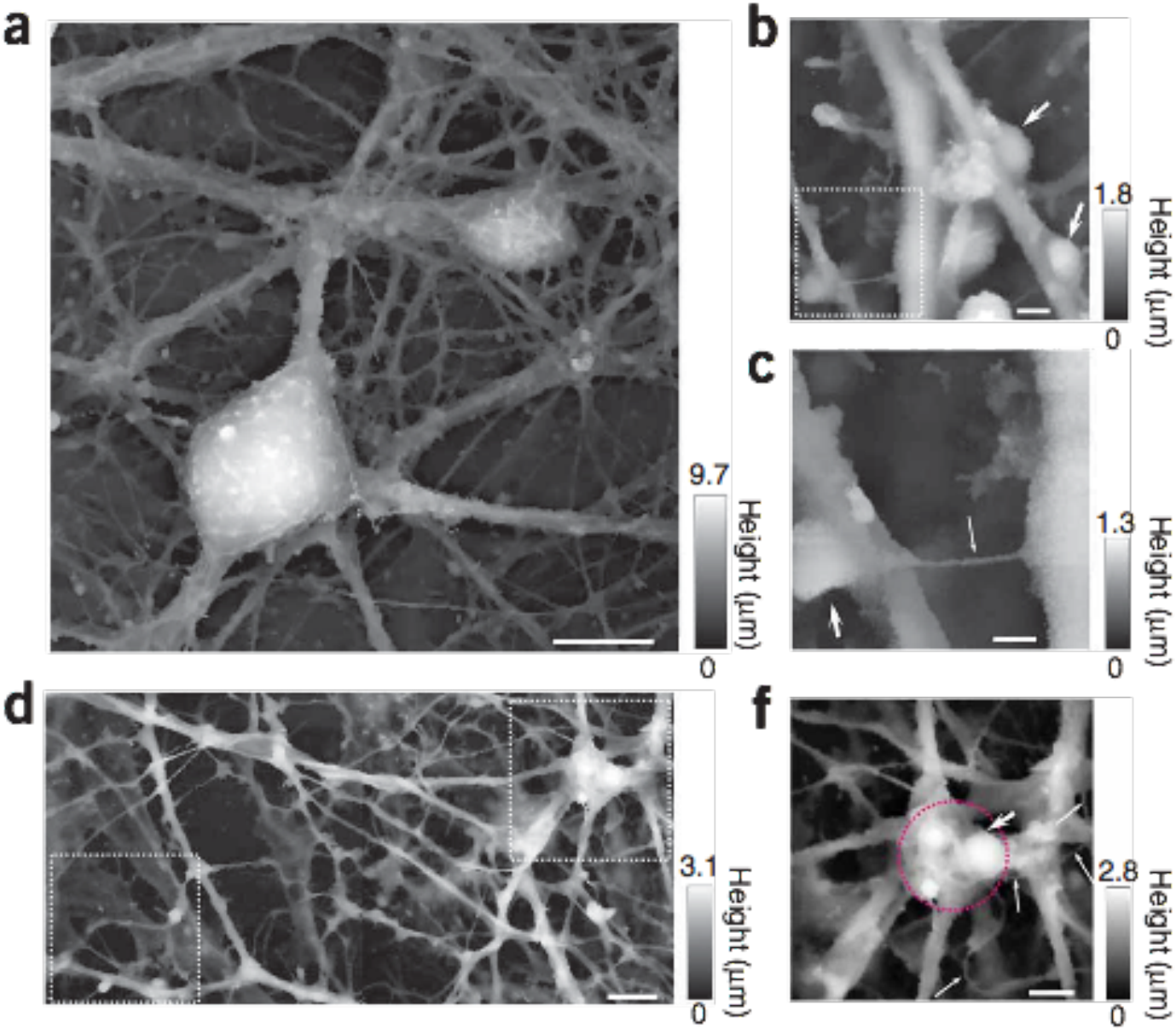

HPICM images of live hippocampal neurons. (a) An image of a large area of a neural network. (b) An image of different area showing potential synaptic boutons (arrows). (c) A higher resolution image of the dotted region in b with another possible bouton (arrow). The process with a diameter of50 nm (thin arrow) is likely to be an axon. (d,e) HPICM (d) and fluorescence (e) images of the same neuronal network area that has been stained with a live marker of synaptic activity, FM1-43. (f,g) High-resolution images of the dotted areas in d (top right, f and bottom left, g). Potential synaptic boutons are circled in red or marked with a large arrow. Fine processes, probably axons, are marked by thin arrows. Scale bars, 10 μm (a), 1 μm (b), 500 nm (c), 5 μm (d,e) and 2 μm (f,g).

1. Novak, P. *et al.* Nanoscale live-cell imaging using hopping probe ion conductance microscopy. *Nat Meth* **6**, 279–281 (2009).

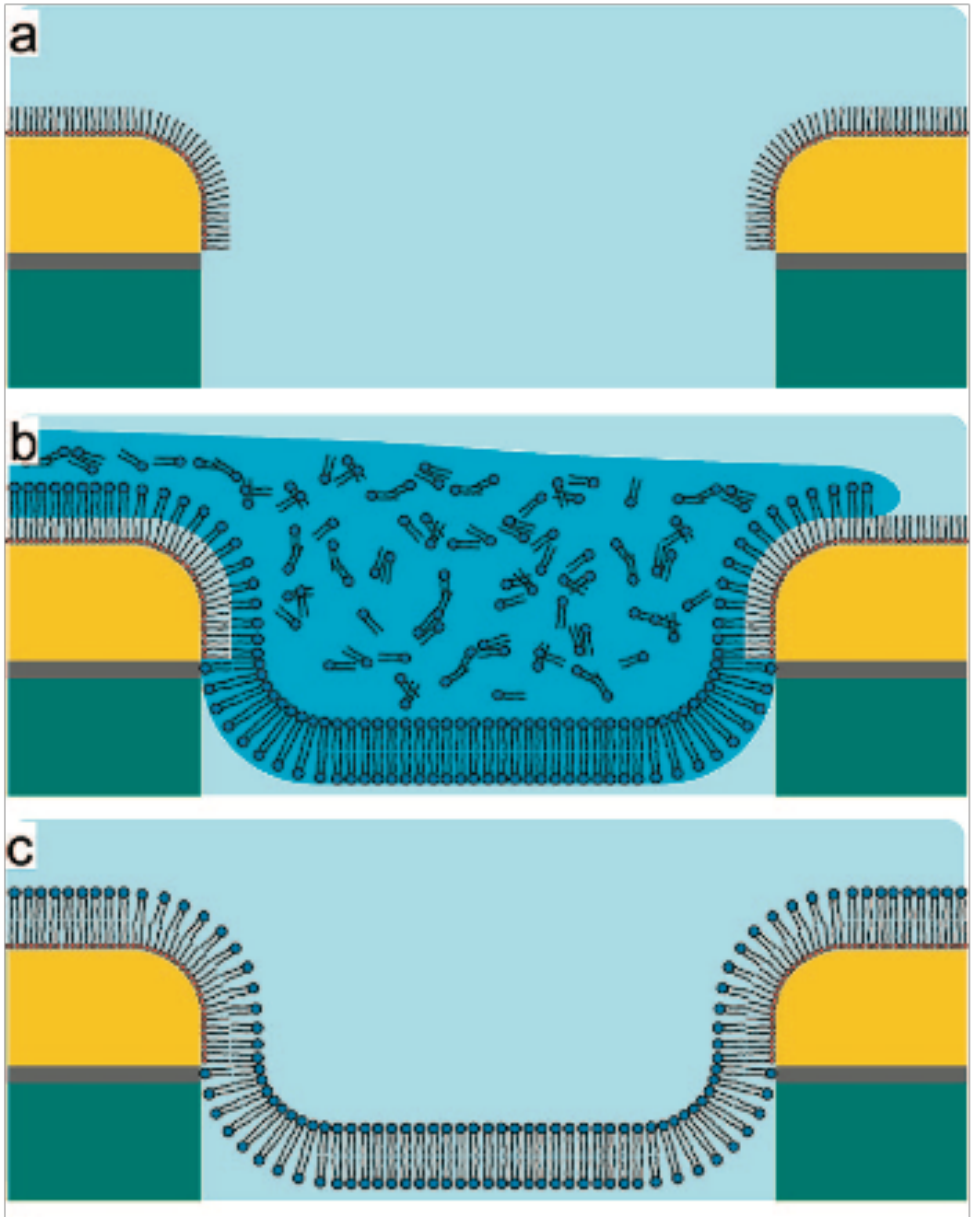

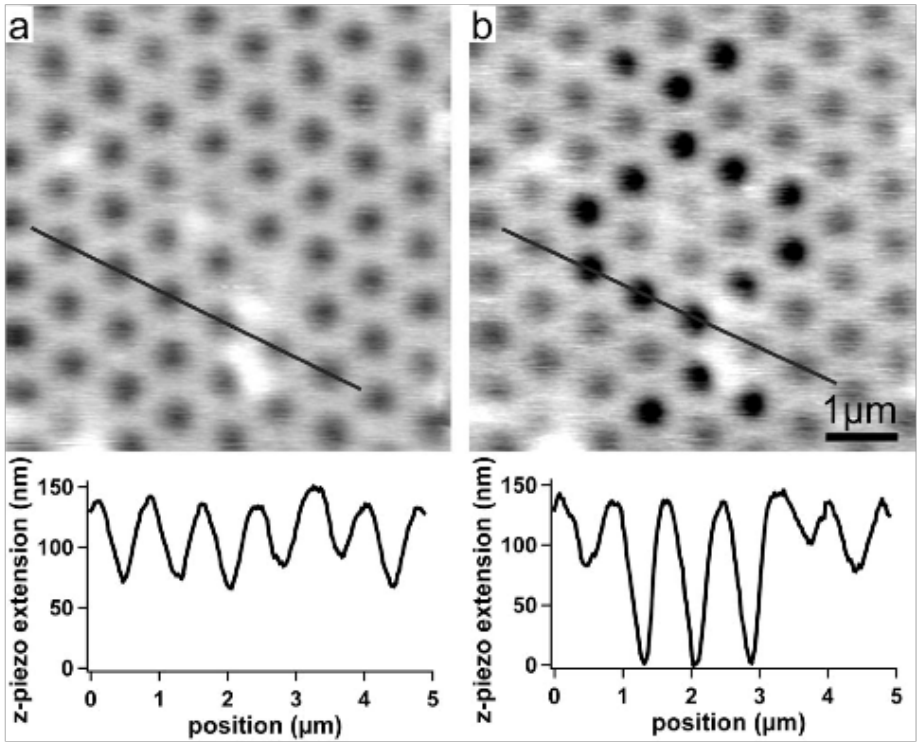

Figure 7. SICM topography images of a membrane-covered silicon substrate with pores (a) before and (b) after writing a Φ-shaped pattern into the membrane surface. Cross sections are shown along the black lines in the images. The pore diameter was 450 nm. The acquisition time for each image was 14 min. The image sizes are 6 × 6 μm^2 with a resolution of 256 × 256 data points. The grayscale ranges from black to white over 150 nm. The frequency of vertical pipette oscillation was 600 Hz.

1. Böcker, M., Muschter, S., Schmitt, E. K., Steinem, C. & Schäffer, T. E. Imaging and Patterning of Pore-Suspending Membranes with Scanning Ion Conductance Microscopy. *LANGMUIR* (2009).doi:10.1021/la8034227

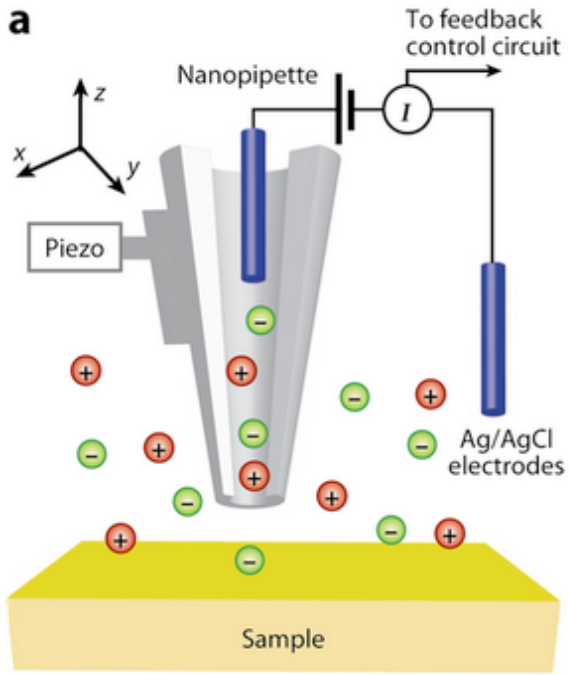

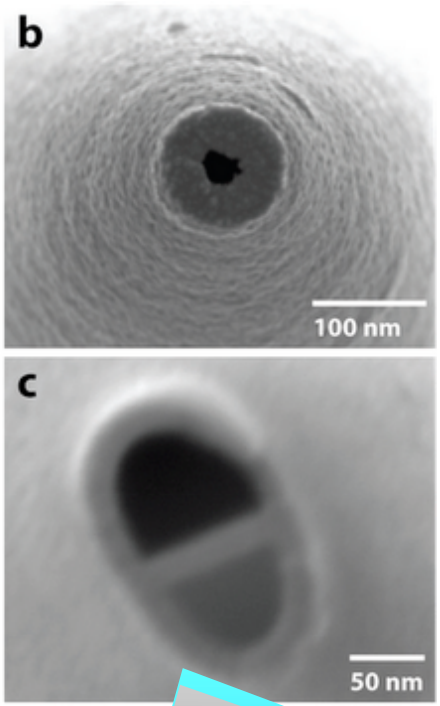

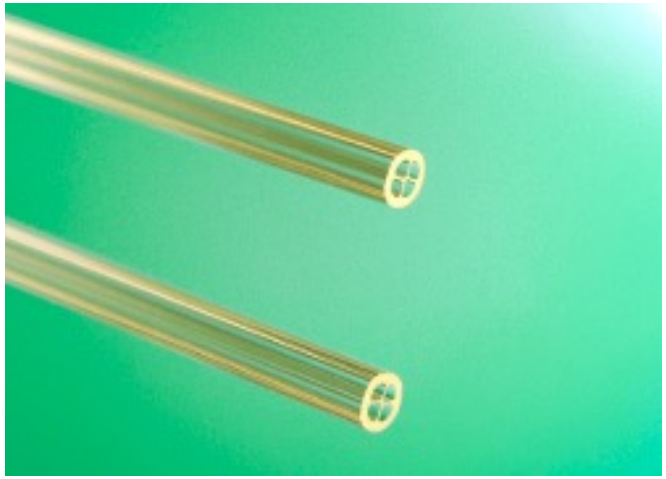

The ability of HPICM to image complex biological samples at nanoscale resolution can be combined with fluorescent imaging and/or other functional tests, such as local activation of individual receptors (ion channels) or single-channel patch-clamp recordings to enable structure-function studies at the surface of complex

Outer Injection

Neurotransmitters
(acetylcholine, dopamine)
channel blockers
(4AP/K+, Ni^{2+}/T-Ca^{2+})
neuropeptides or enzymes

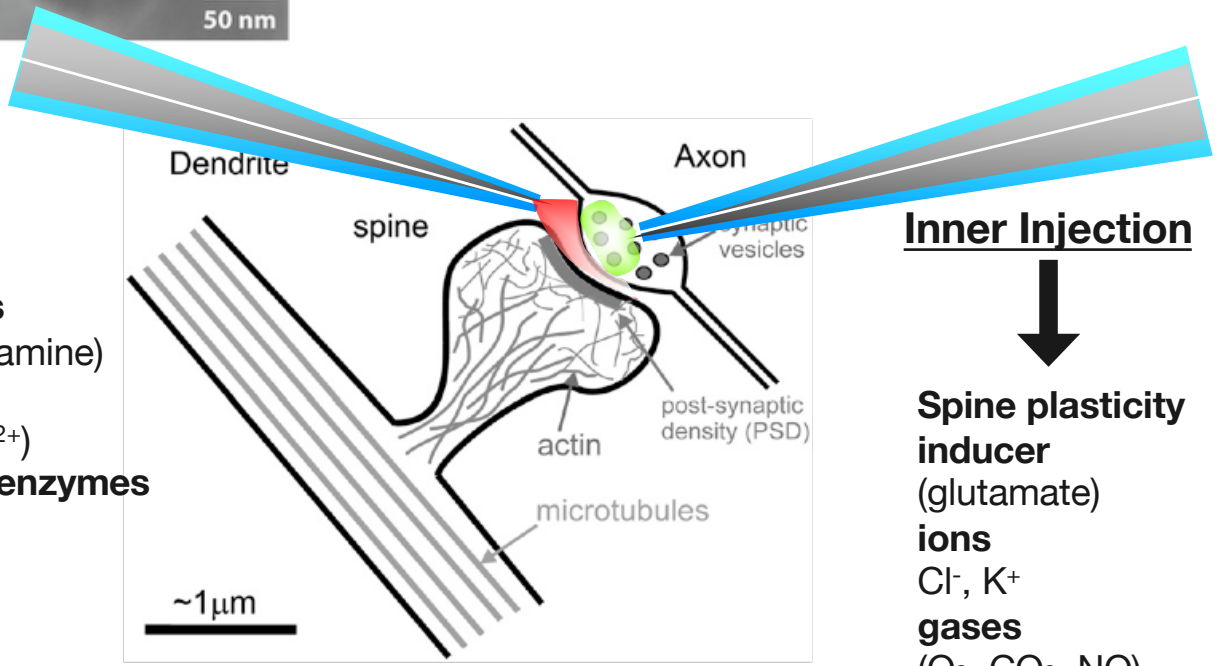

Inner Injection

Spine plasticity inducer
(glutamate)
ions
Cl^-, K^+
gases
(O_2, CO_2, NO)

Dissimilarly from whole culture chemical administration no wild endocrine effect will be induced!

Some critical points in SPM imaging (especially for living systems visualization):

Interaction: soft interaction (imaging) or strong (perturbation/measurement)?
Time: High Speed AFM (dynamics) or extremely slow speeds (resolution)?
Cell Immobilization: immobilized (surface studies) or free (cell dynamics)?
Environment: temperature, liquid, perfusion, incubation,...
Supplemental techniques: force (AFM), electrical (SICM), chemical (SECM)?

PRO	CONS
real living cells without any preparation	slow on corrugated samples
higher resolution possible (till now)	is a SURFACE technique
multi-environment	more complicated than (common) optical
multi-technique	no low and high resolution together
no destructive	expensive (?)